UNIVERSIDADE FEDERAL DE UBERLÂNDIA

FACULDADE DE ENGENHARIA QUÍMICA

PROGRAMA DE PÓS-GRADUAÇÃO EM ENGENHARIA QUÍMICA

PRODUCTION OF KAOLIN HOLLOW FIBER MEMBRANES TOWARDS DIFFERENT APPLICATIONS: BACTERIA REMOVAL AND PECTIN PURIFICATION

FLÁVIA DE SANTANA MAGALHÃES

Uberlândia

2022

UNIVERSIDADE FEDERAL DE UBERLÂNDIA

FACULDADE DE ENGENHARIA QUÍMICA

PROGRAMA DE PÓS-GRADUAÇÃO EM ENGENHARIA QUÍMICA

PRODUCTION OF KAOLIN HOLLOW FIBER MEMBRANES TOWARDS DIFFERENT APPLICATIONS: BACTERIA REMOVAL AND PECTIN PURIFICATION

FLÁVIA DE SANTANA MAGALHÃES

Orientadora: Dra. Miria Hespanhol Miranda Reis

Tese de doutorado apresentada ao Programa de Pós-Graduação em Engenharia Química da Universidade Federal de Uberlândia como parte dos requisitos necessários à obtenção do título de Doutora em Engenharia Química.

Uberlândia

2022

Ficha Catalográfica Online do Sistema de Bibliotecas da UFU
com dados informados pelo(a) próprio(a) autor(a).

M188
2022

Magalhães, Flávia de Santana, 1992-
Production of kaolin hollow fiber membranes towards different applications: bacteria removal and pectin purification [recurso eletrônico] / Flávia de Santana Magalhães. - 2022.

Orientadora: Miria Hespanhol Miranda Reis.
Tese (Doutorado) - Universidade Federal de Uberlândia, Pós-graduação em Engenharia Química.
Modo de acesso: Internet.
Disponível em: http://doi.org/10.14393/ufu.te.2022.118
Inclui bibliografia.
Inclui ilustrações.

1. Engenharia química. I. Reis, Miria Hespanhol Miranda,1978-, (Orient.). II. Universidade Federal de Uberlândia. Pós-graduação em Engenharia Química. III. Título.

CDU: 66.0

Bibliotecários responsáveis pela estrutura de acordo com o AACR2:

Gizele Cristine Nunes do Couto - CRB6/2091

UNIVERSIDADE FEDERAL DE UBERLÂNDIA
Coordenação do Programa de Pós-Graduação em Engenharia Química
Av. João Naves de Ávila, 2121, Bloco 1K, Sala 206 - Bairro Santa Mônica, Uberlândia-MG, CEP 38400-902
Telefone: (34)3239-4249 - www.ppgeq.feq.ufu.br - secppgeq@feq.ufu.br

ATA DE DEFESA - PÓS-GRADUAÇÃO

Programa de Pós-Graduação em:	Engenharia Química				
Defesa de:	Tese de Doutorado, 03/2022, PPGEQ				
Data:	24 de fevereiro de 2022	Hora de início:	09:30	Hora de encerramento:	12:30
Matrícula do Discente:	11813EQU006				
Nome do Discente:	Flávia de Santana Magalhães				
Título do Trabalho:	Production of kaolin hollow fiber membranes towards different applications: bacteria removal and pectin purification				
Área de concentração:	Desenvolvimento de Processos Químicos				
Linha de pesquisa:	Engenharia Bioquímica				
Projeto de Pesquisa de vinculação:	Processos de separação utilizando membranas				

Reuniu-se por meio de webconferência, a Banca Examinadora, designada pelo Colegiado do Programa de Pós-graduação em Engenharia Química, assim composta: Professores Doutores: Nádia Rosa Pereira - LTA/UENF; Suelen Siqueira dos Santos - PDJ/CNPq/UFU, UEMS; Marcos Antonio de Souza Barrozo - PPGEQ/UFU; Vicelma Luiz Cardoso - PPGEQ/UFU e Miria Hespanhol Miranda Reis - PPGEQ/UFU, orientadora da candidata.

Iniciando os trabalhos a presidente da mesa, Profa. Dra. Miria Hespanhol Miranda Reis, apresentou a Comissão Examinadora e a candidata, agradeceu a presença do público, e concedeu à Discente a palavra para a exposição do seu trabalho. A duração da apresentação da Discente e o tempo de arguição e resposta foram conforme as normas do Programa.

A seguir o senhor(a) presidente concedeu a palavra, pela ordem sucessivamente, aos(às) examinadores(as), que passaram a arguir o(a) candidato(a). Ultimada a arguição, que se desenvolveu dentro dos termos regimentais, a Banca, em sessão secreta, atribuiu o resultado final, considerando o(a) candidato(a):

Aprovada.

Esta defesa faz parte dos requisitos necessários à obtenção do título de Doutor.

O competente diploma será expedido após cumprimento dos demais requisitos, conforme as normas do Programa, a legislação pertinente e a regulamentação interna da UFU.

Nada mais havendo a tratar foram encerrados os trabalhos. Foi lavrada a presente ata que após lida e achada conforme foi assinada pela Banca Examinadora.

Documento assinado eletronicamente por **Miria Hespanhol Miranda Reis**, **Membro de Comissão**, em 24/02/2022, às 12:18, conforme horário oficial de Brasília, com fundamento no art. 6º, § 1º, do Decreto nº 8.539, de 8 de outubro de 2015.

Documento assinado eletronicamente por **Marcos Antonio de Souza Barrozo**, **Professor(a) do Magistério Superior**, em 24/02/2022, às 12:19, conforme horário oficial de Brasília, com fundamento no art. 6º, § 1º, do Decreto nº 8.539, de 8 de outubro de 2015.

Documento assinado eletronicamente por **Suelen Siqueira dos Santos**, **Usuário Externo**, em 24/02/2022, às 12:19, conforme horário oficial de Brasília, com fundamento no art. 6º, § 1º, do Decreto nº 8.539, de 8 de outubro de 2015.

Documento assinado eletronicamente por **Nádia Rosa Pereira**, **Usuário Externo**, em 24/02/2022, às 12:20, conforme horário oficial de Brasília, com fundamento no art. 6º, § 1º, do Decreto nº 8.539, de 8 de outubro de 2015.

Documento assinado eletronicamente por **Vicelma Luiz Cardoso**, **Professor(a) do Magistério Superior**, em 24/02/2022, às 12:35, conforme horário oficial de Brasília, com fundamento no art. 6º, § 1º, do Decreto nº 8.539, de 8 de outubro de 2015.

A autenticidade deste documento pode ser conferida no site https://www.sei.ufu.br/sei/controlador_externo.php?acao=documento_conferir&id_orgao_acesso_externo=0, informando o código verificador **3399209** e o código CRC **C5303E34**.

TESE DE DOUTORADO SUBMETIDA AO PROGRAMA DE PÓS-GRADUAÇÃO EM ENGENHARIA QUÍMICA DA UNIVERSIDADE FEDERAL DE UBERLÂNDIA COMO PARTE DOS REQUISITOS NECESSÁRIOS PARA O TÍTULO DE DOUTORA EM ENGENHARIA QUÍMICA, EM 24 DE FEVEREIRO DE 2022.

BANCA EXAMINADORA

Prof. Dra. Miria Hespanhol Miranda Reis

Orientadora (PPGEQ/UFU)

Prof. Dra. Vicelma Luiz Cardoso

PPGEQ/UFU

Prof. Dr. Marcos Antonio de Souza Barrozo

PPGEQ/UFU

Prof. Dra. Nadia Rosa Pereira

Engenharia de Alimentos/UENF

Dra. Suelen Siqueira dos Santos

Engenharia de Alimentos/UEMS

ACKNOWLEDGMENTS

My eternal gratitude to God, for everything.

I would like to thank my family, particularly my parents Cleide and Antônio for the support, love and patience during my whole academic life and to my brother Daniel and my uncle Evandro (*in memoriam*) for the friendship. Finally, to my lovely fiancé Thiago for his love, supporting and encouraging me throughout the all this process.

To my supervisor, Professor Miria Hespanhol Miranda Reis, for the support, encouragement, friendship and guidance given throughout my doctorate degree, which were crucial for my development as a researcher and as a person.

I would also like to express my special gratitude to Professor Daria Camilla Boffito, my supervisor during the internship, for receiving me so well in her research group in Polytechnique of Montreal and guidance and intellectual input given during the research developing.

I would also like to express my gratitude to all the professors of the Faculty of Chemical Engineering especially to Professor Vicelma Luiz Cardoso for the support and contribution to this research.

To the professors Dr. Marcos Antonio de Souza Barrozo, Prof. Dra. Nadia Rosa Pereira and Prof. Dra. Suelen Siqueira dos Santos for the suggestions and contributions to this study.

To the technicians for supporting the characterization of the membranes.

To my dear friends Ana Mota, Andressa Siqueira, Carla Sousa, Caroline Lacerda, Eduardo Ferreira, Lidiane Bessa, Sophia Mendes, Stella Ribeiro and Suelen Siqueira for all the days we had fun in the lab and to my “Canadian” friends Daniela Reis and Estela Hoffmann for all the fun we spent together and for all the unforgettable memories.

Finally, I acknowledge financial support from CAPES (Coordenação de Aperfeiçoamento de Pessoal de Nível Superior), CAPES-PRInt (Programa Institucional de Internacionalização), CNPq (Conselho Nacional de Desenvolvimento Científico e Tecnológico) and FAPEMIG (Fundação de Amparo à Pesquisa do Estado de Minas Gerais).

AGRADECIMENTOS

Minha eterna gratidão a Deus, por tudo.

Agradeço à minha família, principalmente aos meus pais Cleide e Antônio pelo apoio, amor e paciência durante toda a minha vida acadêmica e ao meu irmão Daniel e meu tio Evandro (*in memoriam*) pela amizade. Por fim, ao meu querido noivo Thiago pelo carinho, apoio e incentivo em todo este processo.

À minha orientadora, Professora Dra. Miria Hespanhol Miranda Reis, pelo apoio, incentivo, amizade e orientações ao longo do meu doutorado, que foram fundamentais para o meu desenvolvimento como pesquisadora e como pessoa.

Gostaria também de expressar minha gratidão à Professora Dra. Daria Camilla Boffito, minha supervisora durante o período sanduíche, por me receber tão bem em seu grupo de pesquisa na Polytechinique of Montreal e pela orientação e contribuição intelectual fornecida durante o desenvolvimento da pesquisa.

Gostaria também de expressar meus agradecimentos a todos os docentes da Faculdade de Engenharia Química em especial à Professora Dra. Vicelma Luiz Cardoso pelo apoio e contribuição a esta pesquisa.

Aos professores Dr. Marcos Antonio de Souza Barrozo, Dra. Nadia Rosa Pereira e Prof. Dra. Suelen Siqueira dos Santos pelas sugestões e contribuições a este estudo.

Aos técnicos pelo apoio na caracterização das membranas.

Aos meus queridos amigos Ana Mota, Andressa Siqueira, Carla Sousa, Caroline Lacerda, Eduardo Ferreira, Lidiane Bessa, Sophia Mendes, Stella Ribeiro e Suelen Siqueira por todos os dias que nos divertimos no laboratório e às minhas amigas “canadenses” Daniela Reis e Estela Hoffmann por toda a diversão que passamos juntas e por todas as memórias inesquecíveis.

Por fim, agradeço o apoio financeiro da CAPES (Coordenação de Aperfeiçoamento de Pessoal de Nível Superior), CAPES-PRInt (Programa Institucional de Internacionalização), CNPq (Conselho Nacional de Desenvolvimento Científico e Tecnológico) e FAPEMIG (Fundação de Amparo à Pesquisa do Estado de Minas Gerais).

"Segue o teu destino,
Rega as tuas plantas,
Ama as tuas rosas.
O resto é a sombra
De árvores alheias."

Fernando Pessoa

TABLE OF CONTENTS

LIST OF FIGURES

LIST OF TABLES

ABSTRACT

This work evaluated the use of kaolin, a low-cost ceramic material, for producing membranes with hollow fiber geometry and asymmetric pore size distribution. The produced membranes were used as a filtration barrier for bacterial retention. Also, the kaolin membranes were impregnated with silver nanoparticles (AgNPs) to improve bacterial removal. In another perspective, the produced kaolin membranes, with and without graphene oxide deposited on membrane surface are proposed to be used for pectin purification. For this application, pectin was extracted from orange peels using conventional extraction process. Regarding kaolin hollow fiber production, the membrane morphology and characteristics were influenced by the particle size, extrusion rate, type of solvent and sintering temperature. The increase in the sintering temperature up to 1250 °C caused crystallographic phase modifications in the crude kaolin, which were mainly assigned to transformations of quartz and kaolinite to mullite and cristobalite phases. AgNPs were successfully impregnated in the kaolin hollow fiber at a concentration of 0.51 ± 0.04 mg cm^{-1}. The pristine kaolin membrane enabled a log10 reduction value (LRV) of 2.47 ± 0.05 and 3.72 ± 0.13 for filtrations of aqueous solutions with *Enterobacter cloacae* and *Escherichia coli*, respectively. For the kaolin hollow fiber membrane impregnated with AgNPs, the LRV value increased to 4.38 ± 0.83 and 4.35 ± 0.25 for filtrations of aqueous solutions with *E. cloacae* and *E. coli*, respectively. Thus, the synergetic action of the kaolin membranes impregnated with AgNPs enabled a bacterial reduction greater than 99.9%. Thus, kaolin membranes were successfully applied for bacteria removal from aqueous solutions. Aimed to obtain an optimum condition to extract pectin from orange peels, a central composite design was applied to verify the influence of the temperature and irradiation time on pectin extraction from orange peels in a microwave assisted process. By using the desirability function approach, the optimal values of galacturonic acid content, degree of esterification, methoxyl content were achieved for microwave-assisted extractions at 140 °C and 5.6 min. However, the pectin yield was decreased to 22.73% at these conditions. Thus, pectin extractions under microwave heating at 134°C and 7.5 min are suggested to obtain the maximum pectin yield (33.31%), while optimum pectin quality parameters are achieved at 140 °C and 5.6 min. A conventional extraction process was applied for comparison, but even at longer extraction time (180 min) and lower temperature (90 °C), the conventionally extracted pectin presented inferior quality, with galacturonic acid content of 74.92 ± 0.14 % and methoxyl content of 7.35 ± 0.11 %. Therefore, the microwave assisted process enables to extract high quality pectin with considerable energy saving. As a next step, a purification of pectin was carried out using the

produced kaolin hollow fiber and graphene oxide coated kaolin hollow fibers After graphene oxide (GO) deposition on the membrane, the GO-coated membrane presented a GO layer with thickness of 143 nm. The pectin sample extracted conventionally from orange peels was predominantly constituted of galacturonic acid (68.69 ± 1.75%). The extracted pectin presented a degree of esterification lower than 50% and, thus, can be considered low-methoxylated pectin. Purification of this extract using the kaolin hollow fiber and the GO-coated membrane, gave rise to pectins with the highest amount of this acid monosaccharide (75.91 ± 0.43% and 82.12 ± 0.47%) respectively. Thus, this study evidenced the potential application of crossflow filtration processes to the purification of pectin using pristine and GO-coated kaolin hollow fiber membranes.

Keywords: kaolin, hollow fiber, AgNPs, bacteria removal, pectin, graphene oxide, pectin purification.

RESUMO

Este trabalho avaliou o uso do caulim, um material cerâmico de baixo custo, para a produção de membranas com geometria de fibra oca e distribuição assimétrica de tamanho dos poros. As membranas produzidas foram utilizadas como barreira de filtração para retenção bacteriana. Além disso, nanopartículas de prata (AgNPs) foram impregnadas nas membranas de caulim para melhorar a remoção bacteriana presente em solução aquosa. Em outra perspectiva, as membranas de caulim, com e sem óxido de grafeno (GO) depositado na superfície da membrana, foram propostas para serem utilizadas na purificação de pectina. Para esta aplicação, a pectina foi extraída a partir de cascas de laranja pelo processo convencional de extração. Em relação à produção de fibra oca de caulim, a morfologia e características da membrana foram influenciadas pelo tamanho de partícula, taxa de extrusão, tipo de solvente e temperatura de sinterização. O aumento da temperatura de sinterização até 1250 °C causou modificações na fase cristalográfica do caulim bruto, que foram atribuídas principalmente a transformações de quartzo e caulinita em fases de mulita e cristobalita. As AgNPs foram impregnadas com sucesso na fibra oca de caulim na concentração de 0,51 ± 0,04 mg cm^{-1}. A membrana de caulim permitiu um valor de redução log10 (LRV) de 2,47 ± 0,05 e 3,72 ± 0,13 para filtrações de soluções aquosas com *E. cloacae* e *E. coli*, respectivamente. Para a membrana de fibra oca de caulim impregnada com AgNPs, o valor de LRV aumentou para 4,38 ± 0,83 e 4,35 ± 0,25 para filtrações de soluções aquosas com *E. cloacae* e *E. coli*, respectivamente. Assim, a ação sinérgica das membranas de caulim impregnadas com AgNPs possibilitou uma redução bacteriana superior a 99,9%. Logo, membranas de caulim foram aplicadas com sucesso para remoção bacteriana de soluções aquosas. Com o objetivo de obter uma condição ótima para a extração de pectina a partir de casca laranja, foi aplicado um delineamento composto central para verificar a influência da temperatura e do tempo de irradiação na extração de pectina em um processo assistido por micro-ondas. Foi encontrado um ponto ótimo de extração (134°C e 7,5 min). Usando a abordagem da função de desejabilidade, os valores ótimos de teor de ácido galacturônico, grau de esterificação, teor de metoxila foram alcançados para extrações assistidas por micro-ondas a 140 °C e 5,6 min. No entanto, o rendimento de pectina foi reduzido para 22,73% nestas condições. Assim, extrações de pectina sob aquecimento de micro-ondas a 134°C e 7,5 min são sugeridas para obter o rendimento máximo de pectina, enquanto os parâmetros de qualidade de pectina ótimos são alcançados a 140°C e 5,6 min. Um processo de extração convencional foi aplicado para comparação, mas em maior tempo de extração (180 min) e menor temperatura (90 °C), a pectina extraída convencionalmente apresentou qualidade

inferior, com teor de ácido galacturônico de 74,92 ± 0,14% e teor de metoxila de 7,35 ± 0,11%. Portanto, o processo assistido por micro-ondas permite extrair pectina de alta qualidade com considerável economia de energia. Como próximo passo, foi realizada uma purificação da pectina utilizando a fibra oca de caulim produzida e fibras ocas de caulim revestidas com óxido de grafeno de espessura de 143 nm. A amostra de pectina extraída convencionalmente das cascas de laranja foi constituída predominantemente de ácido galacturônico (68,69 ± 1,75%). A pectina extraída apresentou grau de esterificação inferior a 50% e, portanto, pode ser considerada pectina de baixo teor de metoxila. A purificação deste extrato utilizando a fibra oca de caulim e a membrana revestida com GO, deu origem às pectinas com maior quantidade desse monossacarídeo (75,91 ± 0.43% and 82,12 ± 0,47%), respectivamente. Assim, este estudo evidenciou a potencial aplicação de processos de filtração de fluxo cruzado para a purificação de pectina usando membranas de fibra oca de caulim puras e revestidas com GO.

Palavras-chave: Caulim, fibra oca, AgNPs, remoção de bactéria, pectina, óxido de grafeno, purificação de pectina.

CHAPTER 1

1. INTRODUCTION

Membranes have been receiving increasing attention in a wide range of separation and purification applications, for example, water purification (Liu et al., 2019), clarification of plant extracts such as teas and juices (Bindes et al., 2020; Magalhães et al., 2019), purification of pectins (Muñoz-Almagro et al., 2020), bacteria removal (Magalhães et al., 2020; Shukla et al., 2019) and gas separations (Gil et al., 2015). Ceramic membranes present advantages compared to polymeric membranes. The main advantages of ceramic membrane are resistance to corrosion, in other words can be used to filter solutions with a wide pH range, high mechanical strength, they can be used to filter solution with high temperatures, and if, careful handling, can have a long-life time. However, ceramic membranes present the disadvantage of their high cost of production (Scott, 1995).

The most commonly material used in the production of ceramic materials are metal oxide like Al_2O_3, TiO_2, ZrO_2, etc. or the combination of those (K. Li, 2007). These kinds of materials are chosen due to its structural, chemical and thermal stabilities. However, ceramic membranes made of alumina need high sintering temperature (up to 1500ºC) to present a suitable mechanical strength (Li et al., 2016). This process at these high temperatures requires a large amount of heat and also the alumina powder is a high-cost material, thus making the ceramic membrane extremely expensive. Therefore, there has been significant emphasis toward the preparation of low cost ceramic membranes, using clay as the membrane material (Hubadillah et al., 2018a). Among all types of clay, kaolin ($Al_2Si_2O_5(OH)_4$) has received attention because of its unique physical properties, for example, this clay can promote low plasticity and high refractory properties to the ceramic membrane (Mittal et al., 2011). Furthermore, kaolin exhibits hydrophilic behavior (Mgbemena et al., 2013), which is desired in membranes used for water filtration (Hubadillah et al., 2018a). Hubadillah et al. (2017) produced kaolin hollow fiber membranes and applied to oily-wastewater separation. The results showed that the combination of hydrophilic characteristic of the membrane and its small pore size resulted in excellent oily wastewater separation. Due to the advantages offered by the ceramic membrane produced from kaolin, this membrane can be used in other kind of filtrations. As part of this phD thesis, Magalhães et al. (2020) produced kaolin hollow fiber membranes and applied for bacteria removal from an aqueous suspension. As results, the kaolin

hollow fiber membranes removed almost the total of bacteria aqueous suspension. The ceramic membranes can be modified with nanoparticles to provide enhanced bacteria removal efficiency (Vasanth et al., 2011). Silver nanoparticles (AgNPs) present considerable antibacterial activity (Cunha et al., 2016; Tang and Zheng, 2018). Cunha et al. (2016) evaluated antimicrobial activity of silver nanoparticles (AgNPs) against *Escherichia coli*.

In another perspective, pectin is a value-added chemical, which is largely used by food industries as stabilizing, thickening and emulsifying agent, in addition to be used as antioxidant agent and in encapsulation of drugs and as additive of cosmetic products. Also, pectin is related to some human health benefits, such as to prevent ulcer, cholesterol and cancer diseases and also to reduce lipase activity (Rahmani et al., 2020). Pectin can be extracted from several sources, but its extraction from citrus peels represents a lucrative opportunity to obtain a value-added chemical from an industrial waste. The microwave assisted extraction process is an eco-friendly alternative to extract pectin from different sources at lower extraction times and with lower energy demand than conventional processes (Sucheta et al., 2020). Also, pectin degradation caused by prolonged time exposure at high temperatures is minimized in microwave assisted processes (Arrutia et al., 2020). Some results are reported in the literature for optimal conditions to extract pectin from different sources under microwave heating (Košťálová et al. (2016) Rahmati et al. (2019), Maran et al. (2013) Hosseini et al. (2016), Su et al. (2019) Leão et al. (2018) Xu et al. (2018)). However, the relationships between extraction yield and pectin quality with the operation parameters of the microwave assisted process were not yet systematically presented.

After extraction of the pectin, the most commonly method for purification is the precipitation with ethanol (Yapo et al., 2007a). Although alcohol precipitation treatment is easy and quick, the lack of selectivity and its high alcohol consumption are the main problems for this kind of pectin purification (Kang et al., 2015; Yapo et al., 2007a). Therefore, techniques that replace the alcohol treatment which are more selective are required. In this context, membrane separation processes, represent alternatives to the conventional technology (Conidi et al., 2017). Muñoz-Almagro et al. (2020) purified pectin extracted from sunflower using alcohol precipitation, ultrafiltration and microfiltration with diafiltration. The best results of purification were obtained with the ultrafiltration with a pectin concentration higher than 90%.

1.1. Objectives

In this study, asymmetric hollow fiber membranes were produced using kaolin as the starting ceramic material. The produced hollow fibers were utilized in two different applications: (1) for bacterial removal with pristine and with kaolin hollow fibers impregnated with silver nanoparticles (AgNPs) and (2) for pectin extract purification with pristine and with graphene oxide coated kaolin hollow fibers, with attention for pectin extraction under microwave heating.

1.1.1. Specific objectives

- Characterization of kaolin powder;
- Investigation of the influence of kaolin powder particle size distribution and the influence of the solvents methyl sulfoxide and N-Methyl-2-pyrrolidone on the production of hollow fibers;
- Effect of the extrusion flow rates and sintering temperature on the membrane morphology, mechanical strength and water permeability;
- Synthesis and characterization of AgNPs;
- Impregnation of the AgNPs on the kaolin hollow fibers;
- Evaluation of both pristine and impregnate membranes for *Enterobacter spp*. bacteria removal from an aqueous solution;
- Investigation of the use of conventional extraction and microwave-assisted extraction, verifying the effect of temperature and irradiation time on pectin yield, galacturonic acid content (GA), degree of esterification (DE), methoxyl content (MC);
- Deposition of graphene oxide (GO) on the kaolin hollow fibers;
- Pectin purification by using pristine and graphene oxide coated kaolin hollow fibers.

1.2. Thesis structure and presentation

This thesis consists of 7 chapters, which includes introduction, literature review, experimental chapters, conclusions and future work. Chapters 3 to 6 are the experimental chapters:

Chapter 3 address to the fabrication of the kaolin hollow fiber membranes and the application on water sterilization.

Chapter 4 aproaches with the impregnation of silver nanoparticles (AgNPs) on a kaolin hollow fiber membrane and the application of the membranes (pristine and impregnated with AgNPs) on sterilization different bacteria solutions.

Chapter 5 address to the study of the influence of temperature and irradiation time on microwave-assisted extraction of pectin from orange peel powder.

Finally, Chapter 6, is about the deposition of graphene oxide on kaolin hollow fiber membrane surface and the application of the membranes (pristine and GO-coated membrane) to pectin purification.

1.3. REFERENCES

ARRUTIA, F. et al. Development of a continuous-flow system for microwave-assisted extraction of pectin-derived oligosaccharides from food waste. **Chemical Engineering Journal**, [s. l.], v. 395, n. April, p. 125056, 2020. Disponível em: https://doi.org/10.1016/j.cej.2020.125056.

BINDES, M. M. M. et al. Asymmetric Al2O3 and PES/Al2O3 hollow fiber membranes for green tea extract clarification. **Journal of Food Engineering**, [s. l.], v. 277, p. 109889, 2020. Disponível em: http://www.sciencedirect.com/science/article/pii/S0260877419305321.

CONIDI, C. et al. Separation and purification of phenolic compounds from pomegranate juice by ultrafiltration and nanofiltration membranes. **Journal of Food Engineering**, [s. l.], v. 195, p. 1–13, 2017.

CUNHA, F. A. et al. Silver nanoparticles-disk diff. **Revista do Instituto de Medicina Tropical de Sao Paulo**, [s. l.], v. 58, n. 1, p. 2–4, 2016.

GIL, A. G. et al. A highly permeable hollow fibre substrate for Pd/Al2O3 composite membranes in hydrogen permeation. **International Journal of Hydrogen Energy**, [s. l.], v. 40, n. 8, p. 3249–3258, 2015. Disponível em: https://www.sciencedirect.com/science/article/pii/S0360319915000580.

HOSSEINI, S. S.; KHODAIYAN, F.; YARMAND, M. S. Optimization of microwave assisted extraction of pectin from sour orange peel and its physicochemical properties. **Carbohydrate Polymers**, [s. l.], v. 140, p. 59–65, 2016. Disponível em: http://www.sciencedirect.com/science/article/pii/S0144861715012291.

HUBADILLAH, S. K. et al. Fabrications and applications of low cost ceramic membrane from kaolin: A comprehensive review. **Ceramics International**, [s. l.], v. 44, n. 5, p. 4538–4560, 2018. Disponível em: https://www.sciencedirect.com/science/article/pii/S0272884217329231.

HUBADILLAH, S. K. et al. Superhydrophilic, low cost kaolin-based hollow fibre membranes for efficient oily-wastewater separation. **Materials Letters**, [s. l.], v. 191, p. 119–122, 2017. Disponível em: http://dx.doi.org/10.1016/j.matlet.2016.12.099.

KANG, J. et al. Characterization of natural low-methoxyl pectin from sunflower head extracted by sodium citrate and purified by ultrafiltration. **Food Chemistry**, [s. l.], v. 180, p.

98–105, 2015. Disponível em: https://www.sciencedirect.com/science/article/pii/S0308814615002071.

KOŠŤÁLOVÁ, Z.; AGUEDO, M.; HROMÁDKOVÁ, Z. Microwave-assisted extraction of pectin from unutilized pumpkin biomass. **Chemical Engineering and Processing**: Process Intensification, [s. l.], v. 102, p. 9–15, 2016.

LEÃO, D. P. et al. Potential of pequi (Caryocar brasiliense Camb.) peels as sources of highly esterified pectins obtained by microwave assisted extraction. [S. l.: s. n.], 2018.

LI, L. et al. A low-cost alumina-mullite composite hollow fiber ceramic membrane fabricated via phase-inversion and sintering method. **Journal of the European Ceramic Society**, [s. l.], v. 36, n. 8, p. 2057–2066, 2016. Disponível em: http://dx.doi.org/10.1016/j.jeurceramsoc.2016.02.020.

LI, K. Ceramic Membranes for Separation and Reaction. [S. l.]: John Wiley & Sons Ltd, 2007.

LIU, T. et al. 2D kaolin ultrafiltration membrane with ultrahigh flux for water purification. **Water Research**, [s. l.], v. 156, p. 425–433, 2019. Disponível em: https://www.sciencedirect.com/science/article/pii/S0043135419302726.

MAGALHÃES, F. de S. et al. Fabrication of kaolin hollow fibre membranes for bacteria removal. **Processing and Application of Ceramics**, [s. l.], v. 14, n. 4, p. 303–313, 2020.

MAGALHÃES, F. de S. et al. Recovery of phenolic compounds from pequi (Caryocar brasiliense Camb.) fruit extract by membrane filtrations: Comparison of direct and sequential processes. **Journal of Food Engineering**, [s. l.], v. 257, p. 26–33, 2019. Disponível em: http://www.sciencedirect.com/science/article/pii/S0260877419301396.

MARAN, J. P. et al. Optimization of microwave assisted extraction of pectin from orange peel. **Carbohydrate Polymers**, [s. l.], v. 97, n. 2, p. 703–709, 2013. Disponível em: http://www.sciencedirect.com/science/article/pii/S0144861713005274.

MGBEMENA, C. O. et al. Characterization of kaolin intercalates of oleochemicals derived from rubber seed (Hevea brasiliensis) and tea seed (Camelia sinensis) oils. **Journal of King Saud University - Science**, [s. l.], v. 25, n. 2, p. 149–155, 2013. Disponível em: https://www.sciencedirect.com/science/article/pii/S1018364712000511.

MITTAL, P.; JANA, S.; MOHANTY, K. Synthesis of low-cost hydrophilic ceramic–polymeric composite membrane for treatment of oily wastewater. **Desalination**, [s. l.], v. 282,

p. 54–62, 2011. Disponível em: https://www.sciencedirect.com/science/article/pii/S0011916411006138.

MUÑOZ-ALMAGRO, N. et al. Obtainment and characterisation of pectin from sunflower heads purified by membrane separation techniques. Food Chemistry, [s. l.], v. 318, p. 126476, 2020. Disponível em: https://www.sciencedirect.com/science/article/pii/S0308814620303381.

RAHMANI, Z. et al. Optimization of microwave-assisted extraction and structural characterization of pectin from sweet lemon peel. **International Journal of Biological Macromolecules**, [s. l.], v. 147, p. 1107–1115, 2020. Disponível em: https://doi.org/10.1016/j.ijbiomac.2019.10.079.

RAHMATI, S.; ABDULLAH, A.; KANG, O. L. Effects of different microwave intensity on the extraction yield and physicochemical properties of pectin from dragon fruit (Hylocereus polyrhizus) peels. **Bioactive Carbohydrates and Dietary Fibre**, [s. l.], v. 18, n. May, p. 100186, 2019. Disponível em: https://doi.org/10.1016/j.bcdf.2019.100186.

SCOTT, K. Microfiltration. Handbook of Industrial Membranes. Amsterdam: Elsevier Science, 1995.

SHUKLA, A. K. et al. Selective ion removal and antibacterial activity of silver-doped multi-walled carbon nanotube / polyphenylsulfone nanocomposite membranes. **Materials Chemistry and Physics**, [s. l.], v. 233, p. 102–112, 2019. Disponível em: https://www.sciencedirect.com/science/article/pii/S0254058419304511.

SU, D. L. et al. Efficient extraction and characterization of pectin from orange peel by a combined surfactant and microwave assisted process. **Food Chemistry**, [s. l.], v. 286, n. February, p. 1–7, 2019. Disponível em: https://doi.org/10.1016/j.foodchem.2019.01.200.

SUCHETA; MISRA, N. N.; YADAV, S. K. Extraction of pectin from black carrot pomace using intermittent microwave, ultrasound and conventional heating: Kinetics, characterization and process economics. **Food Hydrocolloids**, [s. l.], v. 102, p. 105592, 2020. Disponível em: http://www.sciencedirect.com/science/article/pii/S0268005X19323720.

TANG, S.; ZHENG, J. Antibacterial Activity of Silver Nanoparticles: Structural Effects. **Advanced Healthcare Materials**, [s. l.], v. 7, n. 13, p. 1701503, 2018. Disponível em: https://doi.org/10.1002/adhm.201701503.

VASANTH, D.; PUGAZHENTHI, G.; UPPALURI, R. Fabrication and properties of low cost ceramic microfiltration membranes for separation of oil and bacteria from its solution. **Journal of Membrane Science**, [s. l.], v. 379, n. 1, p. 154–163, 2011. Disponível em: https://www.sciencedirect.com/science/article/pii/S0376738811004017.

XU, S. Y. et al. Ultrasonic-microwave assisted extraction, characterization and biological activity of pectin from jackfruit peel. **LWT - Food Science and Technology**, [s. l.], v. 90, n. September 2017, p. 577–582, 2018. Disponível em: https://doi.org/10.1016/j.lwt.2018.01.007.

YAPO, B. M. et al. Effect of extraction conditions on the yield, purity and surface properties of sugar beet pulp pectin extracts. **Food Chemistry**, [s. l.], v. 100, n. 4, p. 1356–1364, 2007.

CHAPTER 2

2. LITERATURE REVIEW

2.1. Membrane separation processes

A membrane is an interface between the two phases, which one is more concentrated in solute than the other. In membrane separation processes, these phases are together. Some species in solution pass more easily through the membrane than others, resulting in a concentrated solution on one side of the membrane and a permeate solution on the other. A membrane separation process can then be defined as the selective and controlled transfer of a species from one phase to another separated by a membrane subjected to an external force (Ho and Sirkar, 1992). Membranes can be classified according to geometry, structure, and material (Figure 2.1). For morphology, they can be symmetric or asymmetric along a transversal axis. Symmetrical membranes can be dense or porous and transport mostly occurs in a liquid phase. These membranes are widely used in microfiltration, ultrafiltration, and nanofiltration processes, and the choice of material is mainly determined by the tendency to fouling and by the thermal and chemical stability. Dense membranes present a transport that involves steps of dissolution and diffusion across the membrane and they are used mostly in gas separation processes. About the material membranes can be inorganic (ceramic or metallic) or organic. Organic membranes are less chemical and thermally stable when compared with inorganic membranes (Kang Li, 2007).

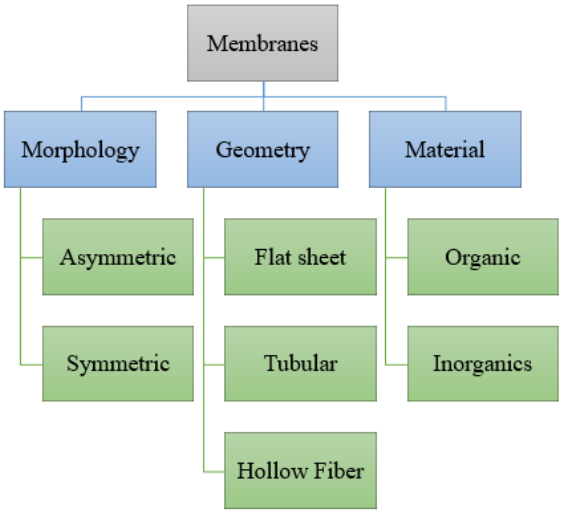

Figure 2.1 - Classification of membranes according to morphology, geometry and material

Ceramic hollow fiber membranes present a high surface area to volume ratio (Kingsbury et al., 2011). Asymmetric morphology of hollow fibers typically consists of micro-channels or micro-voids and one or multiple sponge-like layers with small pore size (Kingsbury et al., 2010). Figure 2.2 shows a ceramic membrane presenting a sponge like-layer and micro-voids. Therefore, hollow fibers with this morphology can be employed as porous membranes or as a matrix for deposition of others materials such as, graphite for hydrogen separation (Natália Mazzarioli Terra et al., 2018), titanium oxide for photoreduction of chromium (VI) (Costa et al., 2019), and other micro and nano sized materials.

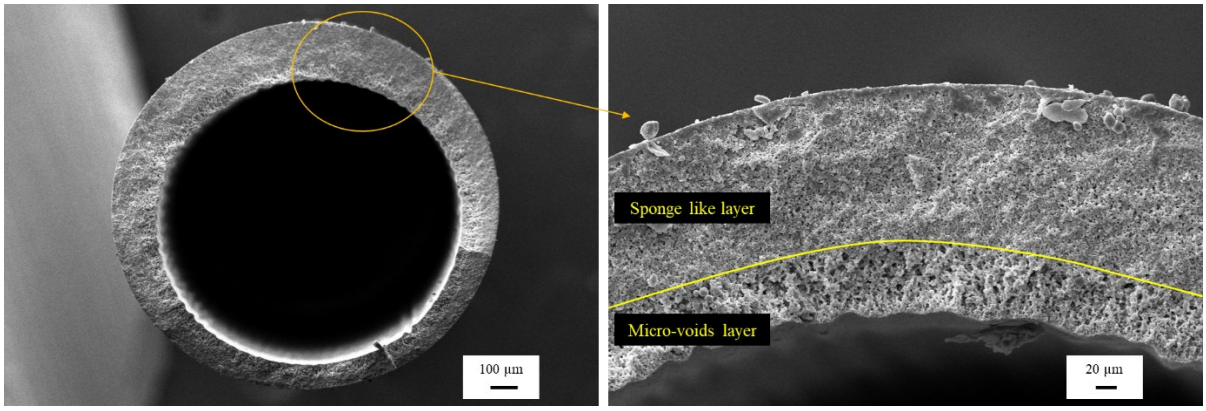

Figure 2.2 – Ceramic hollow fiber membrane.

2.1.1. Fabrication of ceramic hollow fibers

Hollow fiber ceramic membranes can be prepared by the phase-inversion and sintering technique(Kang Li, 2007). This method involves three main steps: preparation of ceramic suspension, spinning of hollow fiber precursors and sintering (Kingsbury et al., 2011; Kang Li, 2007). The first step is the production of the ceramic suspension that will later originate the membrane precursor, which after the sintering process, becomes the membrane of interest. For the production of the ceramic suspension, solvent and additives, such as polymers and dispersant agents, are added to the ceramic powder. The selection of the solvent aims a complete dissolution of the polymer and additives, resulting in a homogeneous suspension, and a high exchange rate with a non-solvent, which affects the final morphology and micro-structure of the hollow fiber. The main function of the dispersant in a ceramic suspension is improve its homogeneity by prevent and eliminate the formation of ceramic agglomerates. The polymer is to bind the ceramic particles and, it precipitates when in contact with a non-solvent bath immobilizing ceramic particles, forming the hollow fiber precursor during phase inversion. It

is important to consider that the complete degradation of the polymer during the sintering process (Kang Li, 2007; Tan et al., 2001).

As present in Figure 2.3, in spinning of hollow fiber, the ceramic suspension is extruded through a tube orifice and two individual pumps are used to control ceramic suspension and internal coagulant flows. Finally, the precursor of ceramic hollow fibers is discarded into a water coagulation bath.

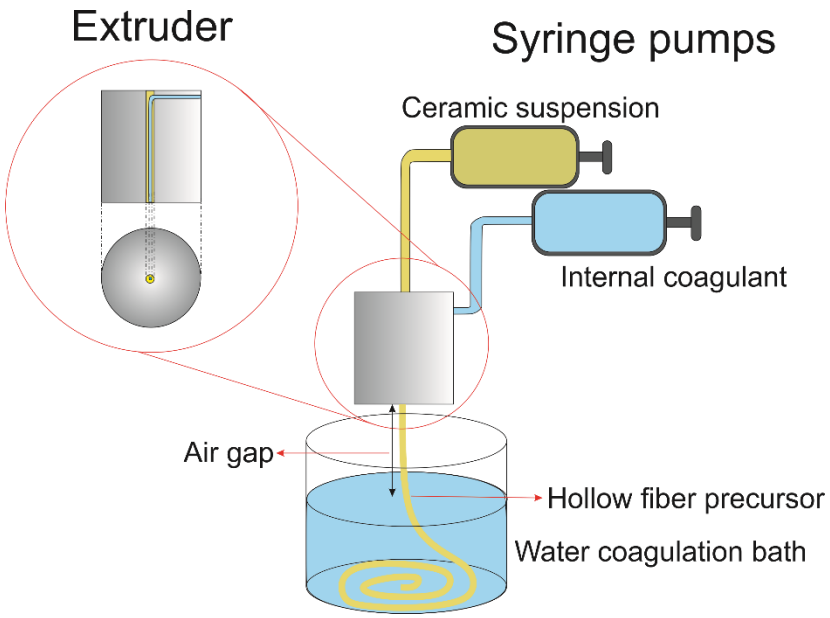

Figure 2.3 – Spinning of hollow fiber scheme.

The precursor membrane is the ceramic suspension in the desired geometry for the membrane, but without the heat treatment carried out by sintering. The mechanical strength of the hollow fiber precursor is low, and to increase this value, the sintering process is necessary. Finally, the precursor membrane is subjected to high temperatures (usually higher than 1500°C) in the sintering process, then there is the exit of the polymer and the molecular rearrangement of the ceramic particles allowing the membrane to gain mechanical resistance (Kang Li, 2007). This process varies according to the ceramic material and the polymer selected. According Tan et al. (2001), when the temperature of the sintering processes increases the pore size of the hollow fiber membrane decreases. The length and diameter of the hollow fiber is also reduced during the sintering procedure, since shrinkage occurs in all directions. The sintering process consists basically in three steps, a pre-sintering, a thermolysis and a final sintering. The remaining water present in the membrane precursor, is removed in the pre-sintering stage (Li, 2010). The polymer binder and dispersants from the precursor are removed during thermolysis process. The highest temperature is achieved in the final of sintering. This temperature aims to stimulate grain growth and coalescence.

Each stage of the temperature process has to be carried out under controlled conditions to avoid deformations, such as cracks of the hollow fibers due the expansions of the pores.

Tan et al. (2001) produced alumina hollow fiber membranes and then sintered them at elevated temperatures. The structure and performance of the membranes such as the sintering temperature were studied. The membranes showed an asymmetric structure. Results showed that a higher porosity and better mechanical strength could be achieved when smaller amount of alumina powder is used in ceramic suspension. Kingsbury et al. (2010) produced asymmetric ceramic hollow fiber membranes using the phase inversion and sintering. The asymmetric structure was achieved and the produced hollow fibers were used as a matrix for catalyst deposition and as a porous support for the coating of a gas separation layer. Terra et al. (2016) produced asymmetric alumina hollow fibers by the phase inversion/sintering method. The hollow fibers were prepared with different internal coagulants and at different sintering temperatures. The results showed that more fingers were obtained when a mixture of solvent with water was used as internal coagulant, instead of pure water. The decrease in the sintering temperature increased the water permeance through the fiber and decreased its mechanical strength. Bessa et al. (2017) produced ceramic hollow fibers from natural dolomite with different pore structures by the phase inversion method and applying different sintering temperatures (1250°C and 1350°C). The increase in the sintering temperature up to 1250 °C resulted in fragile hollow fibers due to dolomite transformations and the dolomite hollow fiber sintered at 1350 °C presented higher bending strength than the fibers sintered at lower temperatures. Ferreira et al. (2019) produced asymmetric niobium pentoxide hollow fiber membranes by the phase inversion and sintering process. The effects of extrusion parameters on the morphology and properties of the produced membranes were studied. Results showed that the hollow fibers sintered at temperatures greater than 1200°C presented modifications in the morphology of niobium pentoxide grains and presented suitable bending resistance and water permeability. Magalhães et al. (2020) studied the influence of the particle size, extrusion rate and sintering temperature on the characteristics of kaolin hollow fiber membranes. Results showed a decrease in water permeability with the increase of sintering temperature due the particle densification also with the increase of the sintering temperature the hollow fibers presented higher values of bending strength.

2.2. Silver nanoparticles and their antibacterial activity

The synthesis of AgNPs can be done by using several routes. Usually, AgNPs are synthetized based on the chemical reduction of Ag^+ ions (Dos Santos et al., 2014). Gallic acid (Martínez-Castañón et al., 2008), citrate, glucose, ascorbic acid, aldehydes and amines (Sharma et al., 2009) have been used as reducing agents. These reducing agents reduce Ag^+ and lead to the formation of metallic silver (Ag^0), which is followed by agglomeration of the nanoparticles. Thus, it is important to use protective agents aimed to stabilize dispersive NPs during the nanoparticle preparation, avoiding their agglomeration (Oliveira et al., 2005). The presence of thiols, amines, acids, and alcohols can stabilize particle growth, and protect particles from sedimentation or agglomeration (Iravani et al., 2014).

Metal nanoparticles are metal particles with a high specific surface area and sizes of 1−100 nm (Reddy et al., 2019). This small size of the nanoparticles provides a large surface area for the interaction with microorganisms (Reddy et al., 2008). The antibacterial activity of silver nanoparticles has been studied in literature (Cunha et al., 2016; Tang and Zheng, 2018). Cunha et al. (2016) evaluated antimicrobial activity of silver nanoparticles (AgNPs) against *Escherichia coli*. Antimicrobial activity was evaluated by the disk diffusion method against 10 strains of *E. coli* with a presence of an antibiotic. Results showed that the synthesized AgNPs increased the activity of the antibiotic by 40% and may represent an option for the treatment of bacterial infections. The antimicrobial effect of AgNPs depends on physic-chemical characteristics distribution and concentration, size and shape of the nanoparticle (Dos Santos et al., 2014). The AgNPs can cause damage to the cell membrane of bacteria that causes the loss of cellular components, breaking of the respiratory chain, which affects the cellular energy source causing death of the microorganism (Dos Santos et al., 2014; Durán et al., 2016; Rai et al., 2009; Wong and Liu, 2010).

2.3. Use of membranes to bacteria removal

The membrane filtration process for bacteria removal from water has been investigated by different research groups (Dobrowsky et al., 2015; Musico et al., 2014; Shukla et al., 2019). Membrane filtration delivers high-quality water compared to other conventional processes in terms of bacteria retention (Ottoson et al., 2006). Ceramic membranes with different compositions are being fabricated aimed to purify water until achieve zero bacteria in permeate (Goswami and Pugazhenthi, 2020). Surface modification was carried out by impregnating silver

nanoparticles on the surface of the membranes, as presented by Liu et al. (2017). Such modifications helped in reducing the biofilm formation on the membrane surface enhancing microorganism retention (Goswami and Pugazhenthi, 2020).

Literature study on the use of membrane filtration for bacteria removal from water revealed that both polymeric and ceramic membranes are being used for this purpose (Goswami and Pugazhenthi, 2020). Karim et al. (2008) utilized polysulfone hollow fiber membranes for the separation of the solids of *E. coli* lysate by a combined process of membrane filtration with flocculation for the separation. Results showed that the membrane filtration after flocculation pre-treatment succeeded in getting permeate with zero concentration of bacterial cells. Zodrow et al. (2009) utilized polysulfone ultrafiltration membranes impregnated with silver nanoparticles to improve biofouling resistance and removal of microorganisms from water. Zodrow et al. (2009) showed that AgNPs incorporated into polysulfone membranes exhibited antimicrobial properties towards a variety of bacteria, including *Escherichia coli* and *Pseudomonas mendocina*. AgNPs incorporation also increased membrane hydrophilicity, reducing the potential for other types of membrane fouling. Chaukura et al. (2020) evaluated a filtration using ceramic filters impregnated with silver nanoparticles as a viable method for water treatment, and to evaluate its capacity to remove *Escherichia coli* from water. Results showed that this filter impregnated with AgNPs removed 100% of *E. coli*.

2.4. Pectin extraction processes

2.4.1. Pectins

Pectins are polysaccharides occurring in the cell walls. D-galacturonic acid (D-GalA), is the basic constituent of all pectins. The most abundant pectic polysaccharide is the homogalacturonan (HG), that is a linear homopolymer of α-1,4-linked galacturonic acid that consist in about 65% of pectin (O' Neill et al., 1990). The other pectic polysaccharides are more complex in structure than HG and include the rhamnogalacturonan II (RG-II), that corresponds about 10% of pectin. Its structure consists of an HG backbone of at least 8 or probably more 1,4-linked α-D-GalA residues with side branches consisting of 12 different types of sugars in over 20 different linkages (O'Neill et al., 2004). Rhamnogalacturonan I (RG-I) that represents 20–35% of pectin contains a repetition of the disaccharide [-α-D-GalA-1,2-α-L-Rha-1-4-]$_n$ and exhibits a high dependence of cell type and number of sugars, oligosaccharides, and branched oligosaccharides attached to its backbone (Ridley et al., 2001). Two other galacturonans are xylogalacturonan (XGA) and apiogalacturonan (AP). XGA is an HG substituted at *O*-3 with a

β-linked xylose and is most prevalent in reproductive tissues. Apiogalacturonan (AP) is HG substituted at O-2 or O-3 with d-apiofuraose, and is commonly found in aquatic monocots (Mohnen, 2008; Zandleven et al., 2007, 2006). Figure 2.4 shows a schematic representation of pectin structure.

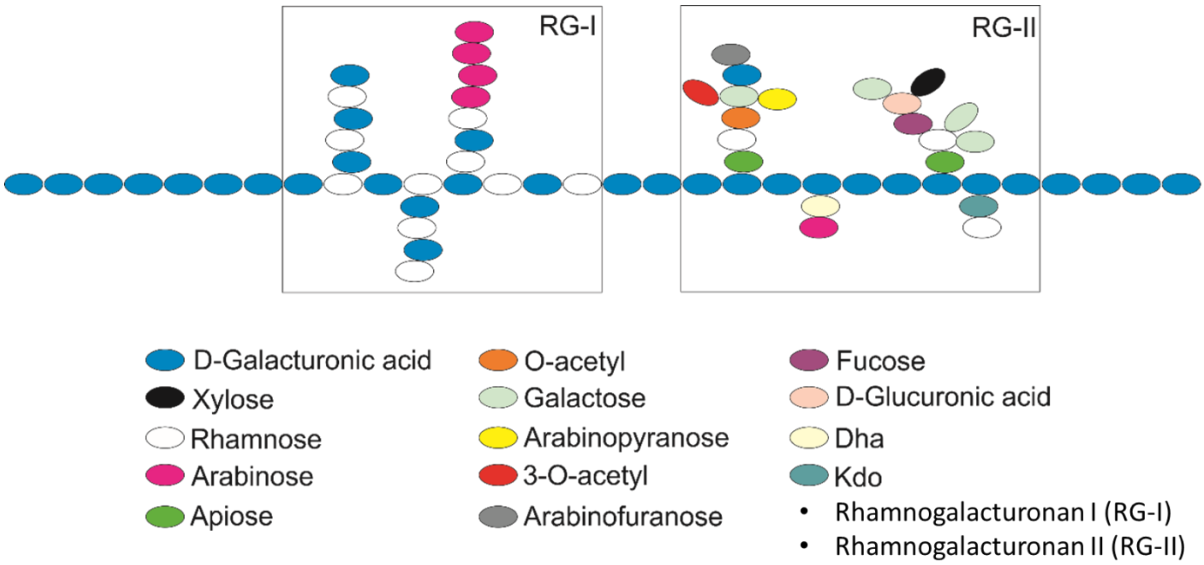

Figure 2.4 - Schematic structure of pectin.

Adapted from Noreen et al. (2017).

2.4.2. Conventional extraction of pectins

Extraction of pectin is a physical and chemical operation, comprising of multiple hydrolysis steps causing a sequential extraction of pectin macromolecules from vegetable tissues (Kumar et al., 2020). Solid liquid conventional extraction depends on factors such as temperature, pH value, solvent properties, solid-to-solvent ratio, dry solids, particle size of the material and diffusion rate (Kulkarni and Vijayanand, 2010). Extraction of pectins traditionally are made using water acidified with different acids, such sulfuric, hydrochloric, nitric, phosphoric, acetic or citric (0.05-2 M), and using a temperature between 60 and 100 °C for 0.5-6 h (Georgiev et al., 2012; Koubala et al., 2008).

The increase in acid strength is an important parameter to increase the galacturonic acid content in the extracted pectin. Furthermore, acid type and its concentration has influence in the process yield and in the physiochemical and functional properties of pectin (Yapo, 2009). Higher ionic strength acids have an capability to precipitate pectin due to their higher affinity for cations such as Ca^{2+}, which stabilizes the pectin molecule and the presence of high concentration of hydrogen ions turns easily the hydrolysis of pectin from proto pectin

(Sandarani, 2017). Higher values of process yield for pectin extraction are achieved when hydrochloric acid is used to acidify water instead of sulphuric, nitric and citric acids (Banu et al., 2012; Castillo-Israel et al., 2015). Banu et al. (2012) extracted pectin from fruits (orange, apple, guava and grapes) using different acids (hydrochloric acid, sulphuric acid and nitric acid) and results indicated that the pectin yield was found to be high using hydrochloric acid for all fruits studied. Castillo-Israel et al. (2015) extracted pectin from Saba banana (*Musa acuminata x Musa balbisiana*) peel under two different extraction conditions. Pectin extraction was carried out using hydrochloric acid and citric acid. Results showed that higher pectin yield was obtained when the extraction was carried out using hydrochloric acid.

However, the conventional extraction requires huge amounts of solvents and prolonged time of extraction. An option to this kind of extraction can be the use of non-conventional options, such as ultrasound-assisted and microwave-assisted extraction (MAE), which both present a decrease in the time of extraction, significant increase in yield, lower energy consumption and the decreased usage of solvents if compared to conventional extractions. Thus, these non-conventional processes can be considered an environmental friendly solution in pectin extraction (Chemat et al., 2011).

2.4.3. Microwave-assisted extraction

Microwave consists of two perpendicular and oscillating fields: magnetic and electric fields. A frequency range from 300 MHz to 300 GHz is covered by microwaves on the electromagnetic spectrum. Generally, microwaves are used as energy carriers using a frequency range from 0.915 to 2.450 GHz (Kumar et al., 2020). At this frequency, the polar molecules in solution rotate in a disorganized manner producing thermal energy, and this phenomenon is termed as dielectric heating (H. Wang et al., 2016). In order to apply microwaves as a heating process, it is essential that at least one component in the sample is polarizable or ionic, thus showing the ability to reorient in response to changes in the electromagnetic field (Guenin, 2016). Transfer of electromagnetic energy in thermal energy in microwave heating occurs by the change of dipoles of polar molecules and the motion of charged ions in the solvent (H. Wang et al., 2016).

The efficiency of pectin extraction using microwaves depends on solvent properties, for example, dielectric constant and volume, temperature, moisture content of the material and microwave power. In biological materials, water is the most absorber of microwave energy, therefore, materials with a high moisture content, exhibit a more rapid response to microwave

heating. Acidified water, makes an ideal solvent with a high energy absorption capacity because of the use of polar solvent with a fast dipole rotation and a superior ionic conductivity of the acid. This can effectively be used for pectin extraction (Kumar et al., 2020). When occurs a quick heating of plant materials in acidified water, losses in the plant tissues are observed due to the presence of water vapor in the porous plant structure. Increases in microwave energy increases the rupture of the plant tissue, facilitating the transport of pectins into the solvent (Maran and Prakash, 2015). However, when the power of the microwave increases, there is a decrease of pectin yield due its degradation and depolymerization (Kumar et al., 2020).

Rahmani et al. (2020) extracted pectin from sweet lemon peel using microwave-assisted extraction. The highest pectin yield (pectin extracted weight/sweet lemon peel weight) (25.31%) was observed under optimal condition (microwave power of 700 W, irradiation time of 3 min and pH of 1.5). The pectin obtained at the option condition was rich in galacturonic acid and galactose (87.2 mol%), high in molecular weight (615.836 kDa) and low in degree of esterification (1.2 –35.1%). Dranca et al. (2020) studied non-conventional techniques (microwave-assisted extraction, ultrasound-assisted extraction, enzyme-assisted extraction ultrasound-assisted extraction with heating treatment, and enzyme-assisted extraction with ultrasound treatment) and conventional citric acid to extract pectin from *Malus domestica* 'Fălticeni' apple pomace. Microwave-assisted extraction led to the highest extraction yield. Pectin samples obtained by microwave extraction had high galacturonic acid content, increased equivalent weight and high degree of esterification and molecular weight. Rahmati et al. (2019) evaluated the microwave-assisted extraction optimized using a central composite experimental design to extracted pectin from dragon fruit. The optimal extraction condition was established at pH 2.07, extraction time of 65 s, and solid-to-liquid ratio of 66.57. Microwave-assisted extraction process is effective in obtaining high-quality dragon fruit peel pectin with a galacturonic acid content of 59.73 – 69.68%. Bagherian et al. (2011) investigated the effect of microwave power and heating time on the yield and quality of extracted pectin from grapefruit. As results, the highest amount of pectin yield was 27.81% (w/w) for 6 min of extraction at 900 W. The authors observed that yield, the galacturonic acid content, and degree of esterification increased with an increase in microwave power and heating time.

2.4.4. Pectin purification by membranes filtration

After the extraction, currently, the method for purification of pectin is the precipitation with ethanol, and it results in higher operating costs (Cho et al., 2003; Muñoz-Almagro et al.,

2020; Yapo et al., 2007). The disadvantages of using alcohol to purify pectin are the lack of selectivity and the high consumption during the production in large scale (da Silva et al., 2012; Muñoz-Almagro et al., 2020; Yapo et al., 2007) . Thus, it is necessary the use of more selective techniques that replace the alcohol treatment. Membrane separation processes, such as microfiltration and ultrafiltration combined with diafiltration, represent an alternative to conventional purification. Also these processes are easy to control (Conidi et al., 2017; Galanakis, 2015).

Cho et al. (2003) used a crossflow microfiltration process to concentrate and purify soluble pectin extracted from citrus peel. The extracted pectin solution was concentrated with the crossflow microfiltration using a 0.2 μm regenerated cellulose membrane. The purification of the pectin was using ethanol. In addition, the results showed that the volume of ethanol used for the recovery of pectin could be reduced to 25%. To purify pectin further, the authors used a diafiltration system. The diafiltration process was effective to remove flavonoids, polyphenols and carotenoids, which were impurities in pectin products.

Yapo et al. (2007) purified pectin from sugar beet pulp by two different procedures, alcohol precipitation with washing and a 10 kDa MWCO membrane ultrafiltration with diafiltration. The results showed that the yield, purity, chemical, and physicochemical features of isolated pectins depended upon the type of procedure used. The purified pectin with alcohol technique gave a higher pectin yield, and the isolated pectin contained more neutral sugars, more proteins, and more ash but less galacturonic acids than the pectin obtained by the ultrafiltration. The weight-average molar mass of the pectin obtained by alcohol precipitation was lower and its emulsifying properties slightly better than those of the ultrafiltration.

Qiu et al. (2009) used to obtain different relative molecular weights for apple. Five kinds of ultrafiltration membranes with different molecular weight cut-offs (5, 10, 30, 100, and 300 kDa) are used to separate apple pectin. As results was verified that the molecular weight of apple pectin is correspondingly related to its physicochemical properties. The galacturonic acid contents, esterification and gelatination degrees and monosaccharide composition increase relatively with an increase in molecular weight.

Muñoz-Almagro et al. (2020) extracted pectin from sunflower and used different procedures of purification including alcohol precipitation, microfiltration and ultrafiltration, both followed by diafiltration. The best results obtained was using the membrane processes, especially the ultrafiltration followed by diafiltration with a pectin concentration higher than 90%. In all the procedures, pectins presented very low amount of glucose and mannose (1%), indicating the great selectivity of the method applied.

2.4.5. Graphene oxide coated membranes in filtration of liquid solutions

Graphene oxide (GO), is a derivative of graphene, has been considered in the literature as a promising material to realize functional thin films because of its two-dimensional structure (Aba et al., 2015). Graphene oxide (GO) coated membranes have demonstrated great potential in liquid filtration. With the aim of applications, such as water purification (Han et al., 2013; Hu and Mi, 2013), GO-coated membranes in a hollow fiber shape are of particular interest because of the high-efficiency and easy-assembly features (Aba et al., 2015).

Aba et al. (2015) produced graphene oxide membranes and reported that GO hollow fiber membranes showed higher permeation fluxes of acetone and methanol than most commercial membranes, and reject molecules larger than 300 Da, showing a great potential in the use of value-added organic solvent nanofiltration processes.

Han et al. (2013) fabricated ultrathin graphene nanofiltration membranes for water purification. The flux presented for a dead-end filtration for pure water was 21.8 L $h^{-1}m^{-2}$ bar -1. The membrane presented a high retention (> 99%) for organic dyes and moderate retention (approximately 20–60%) for ion salts.

Hu & Mi (2013) reported a procedure to synthesize membrane using graphene oxide (GO) nanosheets to water purification. The GO membrane was made via layer-by-layer deposition of GO nanosheets, which were cross-linked by 1,3,5-benzenetricarbonyl trichloride, on a polydopamine-coated polysulfone support. When the membranes synthesized with different numbers of GO layers were tested to demonstrate their efficiency in water separation. GO membrane presented low rejection (6−46%) of monovalent and divalent salts, exhibited a moderate rejection (46−66%) of methylene blue and a high rejection (93−95%) of rhodamine.

2.5. REFERENCES

ABA, N. F. D. et al. Graphene oxide membranes on ceramic hollow fibers – Microstructural stability and nanofiltration performance. **Journal of Membrane Science**, [s. l.], v. 484, p. 87–94, 2015. Disponível em: https://www.sciencedirect.com/science/article/pii/S0376738815001672.

BAGHERIAN, H. et al. Comparisons between conventional, microwave- and ultrasound-assisted methods for extraction of pectin from grapefruit. **Chemical Engineering and Processing: Process Intensification**, [s. l.], v. 50, n. 11–12, p. 1237–1243, 2011. Disponível em: http://dx.doi.org/10.1016/j.cep.2011.08.002.

BANU, M. S. et al. Emerging trends in pectin extraction and its anti-microbial f. [s. l.], v. 42, p. 6349–6351, 2012.

BESSA, L. P. et al. Macro-porous dolomite hollow fibers sintered at different temperatures toward widened applications. **Ceramics International**, [s. l.], v. 43, n. 18, p. 16283–16291, 2017. Disponível em: http://dx.doi.org/10.1016/j.ceramint.2017.08.214.

CASTILLO-ISRAEL, K. A. T. et al. Extraction and characterization of pectin from Saba banana [Musa 'saba'(Musa acuminata x Musa balbisiana)] peel wastes: A preliminary study. **International Food Research Journal**, [s. l.], v. 22, n. 1, p. 202–207, 2015.

CHAUKURA, N. et al. Development and evaluation of a low-cost ceramic filter for the removal of methyl orange, hexavalent chromium, and Escherichia coli from water. **Materials Chemistry and Physics**, [s. l.], v. 249, p. 122965, 2020. Disponível em: https://www.sciencedirect.com/science/article/pii/S0254058420303412.

CHEMAT, F.; ZILL-E-HUMA; KHAN, M. K. Applications of ultrasound in food technology: Processing, preservation and extraction. **Ultrasonics Sonochemistry**, [s. l.], v. 18, n. 4, p. 813–835, 2011. Disponível em: http://dx.doi.org/10.1016/j.ultsonch.2010.11.023.

CHO, C. W.; LEE, D. Y.; KIM, C. W. Concentration and purification of soluble pectin from mandarin peels using crossflow microfiltration system. **Carbohydrate Polymers**, [s. l.], v. 54, n. 1, p. 21–26, 2003.

CONIDI, C. et al. Separation and purification of phenolic compounds from pomegranate juice by ultrafiltration and nanofiltration membranes. **Journal of Food Engineering**, [s. l.], v. 195, p. 1–13, 2017.

COSTA, I. G. F. et al. Photoreduction of chromium(VI) in microstructured ceramic hollow fibers impregnated with titanium dioxide and coated with green algae Chlorella vulgaris. **Journal of Hazardous Materials**, [s. l.], v. 379, n. June, 2019.

CUNHA, F. A. et al. Silver nanoparticles-disk diff. **Revista do Instituto de Medicina Tropical de Sao Paulo**, [s. l.], v. 58, n. 1, p. 2–4, 2016.

DA SILVA, V. R.; HAMERSKI, F.; SCHEER, A. P. Pretreatment of aqueous pectin solution by cross-flow microfiltration: Analysis of operational parameters, degree of concentration and pectin losses. **International Journal of Food Science and Technology**, [s. l.], v. 47, n. 6, p. 1246–1252, 2012.

DOBROWSKY, P. et al. Efficiency of Microfiltration Systems for the Removal of Bacterial and Viral Contaminants from Surface and Rainwater. **Water, Air, & Soil Pollution**, [s. l.], v. 226, 2015.

DOS SANTOS, C. A. et al. Silver nanoparticles: Therapeutical uses, toxicity, and safety issues. **Journal of Pharmaceutical Sciences**, [s. l.], v. 103, n. 7, p. 1931–1944, 2014.

DRANCA, F.; VARGAS, M.; OROIAN, M. Physicochemical properties of pectin from Malus domestica ‘ F ă lticeni ’ apple pomace as a ff ected by non-conventional extraction techniques. **Food Hydrocolloids**, [s. l.], v. 100, n. May 2019, p. 105383, 2020. Disponível em: https://doi.org/10.1016/j.foodhyd.2019.105383.

DURÁN, N. et al. Silver nanoparticles: A new view on mechanistic aspects on antimicrobial activity. **Nanomedicine: Nanotechnology, Biology and Medicine**, [s. l.], v. 12, n. 3, p. 789–799, 2016. Disponível em: https://www.sciencedirect.com/science/article/pii/S1549963415006000.

FERREIRA, E. de P. et al. Improved Microstructure of Asymmetric Niobium Pentoxide Hollow Fiber Membranes. **Journal of the European Ceramic Society**, [s. l.], 2019. Disponível em: https://linkinghub.elsevier.com/retrieve/pii/S0955221919301360.

GALANAKIS, C. M. Separation of functional macromolecules and micromolecules: From ultrafiltration to the border of nanofiltration. **Trends in Food Science & Technology**, [s. l.], v. 42, n. 1, p. 44–63, 2015. Disponível em: https://www.sciencedirect.com/science/article/pii/S092422441400260X.

GEORGIEV, Y. et al. Isolation , characterization and modification of citrus pectins Isolation , characterization and modification of citrus pectins. **Journal of Bioscience and Biotechnology**, [s. l.], v. 1, n. October, p. 223–233, 2012.

GOSWAMI, K. P.; PUGAZHENTHI, G. Credibility of polymeric and ceramic membrane filtration in the removal of bacteria and virus from water: A review. **Journal of environmental management**, [s. l.], v. 268, n. March, p. 110583, 2020. Disponível em: https://doi.org/10.1016/j.jenvman.2020.110583.

GUENIN, E. Microwave Engineering of Nanomaterials: From Mesoscale to Nanoscale. 1. ed. New York: Jenny Stanford Publishing, 2016.

HAN, Y.; XU, Z.; GAO, C. Ultrathin graphene nanofiltration membrane for water purification. **Advanced Functional Materials**, [s. l.], v. 23, n. 29, p. 3693–3700, 2013.

HO, W. S. W.; SIRKAR, K. K. Overview. In: MEMBRANE HANDBOOK. New York: Chapman & Hall, 1992. p. 954.

HU, M.; MI, B. Enabling graphene oxide nanosheets as water separation membranes. **Environmental Science and Technology**, [s. l.], v. 47, n. 8, p. 3715–3723, 2013.

IRAVANI, S. et al. Synthesis of silver nanoparticles: chemical, physical and biological methods. **Research in pharmaceutical sciences**, [s. l.], v. 9, n. 6, p. 385–406, 2014. Disponível em: https://pubmed.ncbi.nlm.nih.gov/26339255.

KARIM, M. N. et al. Flocculation enhanced microfiltration of Escherichia coli lysate. **Biochemical Engineering Journal**, [s. l.], v. 40, n. 3, p. 512–519, 2008. Disponível em: https://www.sciencedirect.com/science/article/pii/S1369703X08000636.

KINGSBURY, B. F. K.; WU, Z.; LI, K. A morphological study of ceramic hollow fibre membranes: A perspective on multifunctional catalytic membrane reactors. **Catalysis Today**, [s. l.], v. 156, n. 3, p. 306–315, 2010. Disponível em: https://www.sciencedirect.com/science/article/pii/S0920586110001240.

KINGSBURY, B. F. K.; WU, Z.; LI, K. Inorganic Hollow Fibre Membranes for Chemical Reaction. [S. l.: s. n.], 2011. Disponível em: https://doi.org/10.1002/9780470977569.ch3.

KOUBALA, B. B. et al. Effect of extraction conditions on some physicochemical characteristics of pectins from “Améliorée” and “Mango” mango peels. **Food Hydrocolloids**, [s. l.], v. 22, n. 7, p. 1345–1351, 2008.

KULKARNI, S. G.; VIJAYANAND, P. Effect of extraction conditions on the quality characteristics of pectin from passion fruit peel (Passiflora edulis f. flavicarpa L.). **LWT - Food Science and Technology**, [s. l.], v. 43, n. 7, p. 1026–1031, 2010. Disponível em: http://dx.doi.org/10.1016/j.lwt.2009.11.006.

KUMAR, M. et al. Emerging trends in pectin extraction and its anti-microbial functionalization using natural bioactives for application in food packaging. **Trends in Food Science & Technology**, [s. l.], v. 105, p. 223–237, 2020. Disponível em: https://www.sciencedirect.com/science/article/pii/S0924224420305999.

LI, K. Ceramic Hollow Fiber Membranes and Their Applications. **Comprehensive Membrane Science and Engineering**, [s. l.], v. 1, p. 253–273, 2010.

LI, Kang. **Ceramic Membranes for Separation and Reaction**. Londres: Wiley, 2007.

LIU, C. et al. Mitigation of Biofilm Development on Thin-Film Composite Membranes Functionalized with Zwitterionic Polymers and Silver Nanoparticles. **Environmental Science & Technology**, [s. l.], v. 51, n. 1, p. 182–191, 2017. Disponível em: https://doi.org/10.1021/acs.est.6b03795.

MAGALHÃES, F. de S. et al. Fabrication of kaolin hollow fibre membranes for bacteria removal. **Processing and Application of Ceramics**, [s. l.], v. 14, n. 4, p. 303–313, 2020.

MARAN, J. P.; PRAKASH, K. A. Process variables influence on microwave assisted extraction of pectin from waste Carcia papaya L. peel. **International Journal of Biological Macromolecules**, [s. l.], v. 73, p. 202–206, 2015. Disponível em: http://dx.doi.org/10.1016/j.ijbiomac.2014.11.008.

MARTÍNEZ-CASTAÑÓN, G. A. et al. Synthesis and antibacterial activity of silver nanoparticles with different sizes. **Journal of Nanoparticle Research**, [s. l.], v. 10, n. 8, p. 1343–1348, 2008.

MOHNEN, D. Pectin structure and biosynthesis. **Current Opinion in Plant Biology**, [s. l.], v. 11, n. 3, p. 266–277, 2008. Disponível em: https://www.sciencedirect.com/science/article/pii/S1369526608000630.

MUÑOZ-ALMAGRO, N. et al. Obtainment and characterisation of pectin from sunflower heads purified by membrane separation techniques. **Food Chemistry**, [s. l.], v. 318, p.

126476, 2020. Disponível em: https://www.sciencedirect.com/science/article/pii/S0308814620303381.

MUSICO, Y. L. F. et al. Surface modification of membrane filters using graphene and graphene oxide-based nanomaterials for bacterial inactivation and removal. **ACS Sustainable Chemistry and Engineering**, [s. l.], v. 2, n. 7, p. 1559–1565, 2014.

NOREEN, A. et al. Pectins functionalized biomaterials; a new viable approach for biomedical applications: A review. **International Journal of Biological Macromolecules**, [s. l.], v. 101, p. 254–272, 2017. Disponível em: https://www.sciencedirect.com/science/article/pii/S0141813017305391.

O' NEILL, M.; ALBERSHEIM, P.; DARVILL, A. 12 - The Pectic Polysaccharides of Primary Cell Walls. In: DEY, P. M. B. T.-M. in P. B. (org.). **Carbohydrates**. [S. l.]: Academic Press, 1990. v. 2, p. 415–441. E-book. Disponível em: https://www.sciencedirect.com/science/article/pii/B9780124610125500185.

O'NEILL, M. A. et al. Rhamnogalacturonan II: Structure and function of a borate cross-linked cell wall pectic polysaccharide. **Annual Review of Plant Biology**, [s. l.], v. 55, p. 109–139, 2004.

OLIVEIRA, M. M. et al. Influence of synthetic parameters on the size, structure, and stability of dodecanethiol-stabilized silver nanoparticles. **Journal of Colloid and Interface Science**, [s. l.], v. 292, n. 2, p. 429–435, 2005. Disponível em: https://www.sciencedirect.com/science/article/pii/S0021979705006430.

OTTOSON, J. et al. Removal of viruses, parasitic protozoa and microbial indicators in conventional and membrane processes in a wastewater pilot plant. **Water Research**, [s. l.], v. 40, n. 7, p. 1449–1457, 2006. Disponível em: https://www.sciencedirect.com/science/article/pii/S0043135406000789.

QIU, N. xue et al. Apple Pectin Behavior Separated by Ultrafiltration. **Agricultural Sciences in China**, [s. l.], v. 8, n. 10, p. 1193–1202, 2009. Disponível em: http://dx.doi.org/10.1016/S1671-2927(08)60329-6.

RAHMANI, Z. et al. Optimization of microwave-assisted extraction and structural characterization of pectin from sweet lemon peel. **International Journal of Biological Macromolecules**, [s. l.], v. 147, p. 1107–1115, 2020. Disponível em: https://doi.org/10.1016/j.ijbiomac.2019.10.079.

RAHMATI, S.; ABDULLAH, A.; KANG, O. L. Effects of different microwave intensity on the extraction yield and physicochemical properties of pectin from dragon fruit (Hylocereus polyrhizus) peels. **Bioactive Carbohydrates and Dietary Fibre**, [s. l.], v. 18, n. May, p. 100186, 2019. Disponível em: https://doi.org/10.1016/j.bcdf.2019.100186.

RAI, M.; YADAV, A.; GADE, A. Silver nanoparticles as a new generation of antimicrobials. **Biotechnology Advances**, [s. l.], v. 27, n. 1, p. 76–83, 2009. Disponível em: https://www.sciencedirect.com/science/article/pii/S0734975008000918.

REDDY, K. R. et al. Chapter 10 - Functionalized magnetic nanoparticles/biopolymer hybrids: Synthesis methods, properties and biomedical applications. In: GURTLER, V.; BALL, A. S.; SONI, S. B. T.-M. in M. (org.). **Nanotechnology**. [S. l.]: Academic Press, 2019. v. 46, p. 227–254. E-book. Disponível em: https://www.sciencedirect.com/science/article/pii/S058095171930011X.

REDDY, K. R. et al. Facile synthesis of conducting polymer–metal hybrid nanocomposite by in situ chemical oxidative polymerization with negatively charged metal nanoparticles. **Materials Letters**, [s. l.], v. 62, n. 12, p. 1815–1818, 2008. Disponível em: https://www.sciencedirect.com/science/article/pii/S0167577X07010154.

RIDLEY, B. L.; O'NEILL, M. A.; MOHNEN, D. Pectins: structure, biosynthesis, and oligogalacturonide-related signaling. **Phytochemistry**, [s. l.], v. 57, n. 6, p. 929–967, 2001. Disponível em: https://www.sciencedirect.com/science/article/pii/S0031942201001133.

SANDARANI, M. A Review: Different Extraction Techniques of Pectin. **Journal of Pharmacognosy & Natural Products**, [s. l.], v. 03, n. 03, p. 1–5, 2017.

SHARMA, V. K.; YNGARD, R. A.; LIN, Y. Silver nanoparticles: Green synthesis and their antimicrobial activities. **Advances in Colloid and Interface Science**, [s. l.], v. 145, n. 1, p. 83–96, 2009. Disponível em: https://www.sciencedirect.com/science/article/pii/S0001868608001449.

SHUKLA, A. K. et al. Selective ion removal and antibacterial activity of silver-doped multi-walled carbon nanotube / polyphenylsulfone nanocomposite membranes. **Materials Chemistry and Physics**, [s. l.], v. 233, p. 102–112, 2019. Disponível em: https://www.sciencedirect.com/science/article/pii/S0254058419304511.

TAN, X.; LIU, S.; LI, K. Preparation and characterization of inorganic hollow fiber membranes. **Journal of Membrane Science**, [s. l.], v. 188, n. 1, p. 87–95, 2001. Disponível em: https://www.sciencedirect.com/science/article/pii/S0376738801003696.

TANG, S.; ZHENG, J. Antibacterial Activity of Silver Nanoparticles: Structural Effects. **Advanced Healthcare Materials**, [s. l.], v. 7, n. 13, p. 1701503, 2018. Disponível em: https://doi.org/10.1002/adhm.201701503.

TERRA, N. et al. Characterisation of asymmetric alumina hollow fibres: Application for hydrogen permeation in composite membranes. **Brazilian Journal of Chemical Engineering**, [s. l.], v. 33, p. 567–576, 2016.

TERRA, N. M. et al. Graphite coating on alumina substrate for the fabrication of hydrogen selective membranes. **International Journal of Hydrogen Energy**, [s. l.], v. 43, n. 3, p. 1534–1544, 2018.

WANG, H.; DING, J.; REN, N. Recent advances in microwave-assisted extraction of trace organic pollutants from food and environmental samples. **TrAC Trends in Analytical Chemistry**, [s. l.], v. 75, p. 197–208, 2016. Disponível em: https://www.sciencedirect.com/science/article/pii/S0165993615002125.

WONG, K.; LIU, X. Silver nanoparticles - The real “silver bullet” in clinical medicine? Medchemcomm, [s. l.], v. 1, 2010.

YAPO, B. M. Biochemical characteristics and gelling capacity of pectin from yellow passion fruit rind as affected by acid extractant nature. **Journal of Agricultural and Food Chemistry**, [s. l.], v. 57, n. 4, p. 1572–1578, 2009.

YAPO, B. M.; WATHELET, B.; PAQUOT, M. Comparison of alcohol precipitation and membrane filtration effects on sugar beet pulp pectin chemical features and surface properties. **Food Hydrocolloids**, [s. l.], v. 21, n. 2, p. 245–255, 2007.

ZANDLEVEN, J. et al. Enzymatic degradation studies of xylogalacturonans from apple and potato, using xylogalacturonan hydrolase. **Carbohydrate Polymers**, [s. l.], v. 65, n. 4, p. 495–503, 2006. Disponível em: https://www.sciencedirect.com/science/article/pii/S0144861706000944.

ZANDLEVEN, J. et al. Xylogalacturonan exists in cell walls from various tissues of Arabidopsis thaliana. **Phytochemistry**, [s. l.], v. 68, n. 8, p. 1219–1226, 2007. Disponível em: https://www.sciencedirect.com/science/article/pii/S0031942207000556.

ZODROW, K. et al. Polysulfone ultrafiltration membranes impregnated with silver nanoparticles show improved biofouling resistance and virus removal. **Water Research**, [s. l.], v. 43, n. 3, p. 715–723, 2009. Disponível em: https://www.sciencedirect.com/science/article/pii/S0043135408005290.

CHAPTER 3

3. FABRICATION OF KAOLIN HOLLOW FIBER MEMBRANES FOR BACTERIA REMOVAL

ABSTRACT

This study examines the influence of the particle size, extrusion rate and sintering temperature on the characteristics of kaolin hollow fiber membranes. In addition, the produced membranes were applied for bacteria removal from an aqueous suspension. The milling process reduced the size of kaolin particles from 8.7 to 5.1 μm and greatly enhanced the morphology and mechanical resistance of the produced membranes. The increase in the sintering temperature up to 1250 °C caused crystallographic phase modifications in the crude kaolin, which were mainly assigned to transformations of quartz and kaolinite to mullite and cristobalite phases. The fibers sintered at 1250 °C have bending strength of 145 MPa, but this relatively high sintering temperature caused a substantial particle densification and drastic decrease of the membrane water permeability. The kaolin hollow fiber membranes enabled almost total removal of the *Enterobacter cloacae* bacteria from an aqueous suspension.

Keywords: ceramic membrane, kaolin, asymmetric hollow fiber, phase inversion, bacteria removal.

3.1. INTRODUCTION

Membrane separation processes have been applied in several areas, including chemical, food and biotechnology industries (Jedidi et al., 2011). Related to the material, ceramic membranes usually present greater resistance to harsh environment, microbiological degradation and high-pressure conditions than polymeric membranes (Sharma et al., 2017). The phase inversion method is commonly applied for producing polymeric membranes and, since the beginning of the 21st century, this method has been modified and combined with a single sintering step in order to produce asymmetric ceramic membranes (Liu et al., 2003). Fabrication of ceramic membranes involves the adjustment of several parameters, such as ceramic suspension and bore fluid compositions, extrusion flow rates and sintering temperatures (Bessa et al., 2019). The powder particle size also influences the membrane morphology, and materials

with particle sizes smaller than 1 μm are usually used to produce ceramic membranes (Ferreira et al., 2019). The choice of the ceramic powder is also crucial to develop a membrane with positive characteristics related to permeability, selectivity and cost. Actually, the cost of ceramic membranes, which is related to the material cost itself and the required sintering temperature, is a great obstacle for its widespread use (Sahnoun and Baklouti, 2013).

Alumina (Al2O3) is the material most commonly used for producing ceramic membranes (Lee et al., 2016). In addition to the relatively high cost of this high purity oxide, alumina membranes require sintering temperatures greater than 1500 °C in order to achieve suitable mechanical strength values. Thus, some studies have been carried out to evaluate low cost materials for membrane production (Prekajski et al., 2014). The literature presents applications of several ceramic materials for producing membranes, such as kaolin (Hubadillah et al., 2019), silica (Hubadillah et al., 2018b), dolomite (Bessa et al., 2017), niobium pentoxide (Ferreira et al., 2019) and others. These mineral based materials are largely available and they usually require lower sintering temperatures than pure alumina.

Kaolin ($Al_2Si_2O_5(OH)_4$) is a clay mineral found in great abundance in many countries and it has been recently used as the starting material for producing ceramic membranes (Hubadillah et al., 2017). Zhou et al. (2010) proposed the application of a ceramic mixture of kaolin and dolomite to produce low cost macroporous ceramic supports. Kaur et al. (2016) produced kaolin based ceramic supports by using different amounts of calcium and sodium carbonates. Hubadillah et al. (2017) applied the phase inversion method to produce a low cost kaolin-based ceramic hollow fiber membrane with asymmetric pore size distribution. Abdulhameed et al. (2017) produced hollow fiber membranes from a powder mixture of alumina and kaolin. Chakraborty et al. (2018) applied statistical tools to optimize the ceramic composition for producing kaolin membranes. Hubadillah et al. (2019) modified kaolin membranes via grafting with fluoroalkylsilane in order to improve the membrane hydrophobicity. However, the relatively low mechanical resistance of the produced mineral membranes is still a drawback to be overcome. In general, the increase in the sintering temperature increases the mechanical properties. Nevertheless, mineral membranes are composed of mixture of oxide materials which are often converted into other phases during sintering. Thus, better understanding of the crystallographic transformations as function of the sintering process is crucial to produce ceramic membranes with reliable properties. Also, the applied extrusion conditions certainly dictate the characteristics of the produced membranes.

(Hubadillah et al. (2018) suggested applying the phase inversion method to produce kaolin hollow fibers with enhanced mechanical strength and surface/volume ratio.

In this study, low cost asymmetric hollow fiber membranes were produced by using kaolin as the starting material. The influence of the powder particle size distribution, ceramic suspension composition, extrusion flow rate and sintering temperature on the membrane morphology, mechanical strength and water permeability was for the first time systematically investigated. Additionally, crystallographic transformations of the kaolin powder as a function of the sintering temperature were related to the membrane characteristics. Finally, the produced kaolin hollow fiber membranes were applied to remove the *Enterobacter cloacae* bacteria from an aqueous suspension.

3.2. MATERIAL AND METHODS

3.2.1. Material

Kaolin powder was supplied by Kalamazon Estudos Geológicos LTDA (Brazil). Dimethyl sulfoxide (DMSO, Vetec, Brazil) and N-Methyl-2-pyrrolidone (NMP Vetec, Brazil) were used as solvents. PEG-30 Dipolyhydroxy stearate (ArlacelTM P135, Croda) and polyether sulfone (PES, Veradel 3000P, Solvay) were used as additive and polymer binder, respectively.

3.2.2. Preparation of kaolin hollow fibers

The kaolin powder was wet ball milled in order to reduce its particle size distribution. A porcelain vessel was filled with 1/3 of balls, 2/3 of distilled water and 125 g of kaolin powder. Porcelain balls of two different diameters (1.0 and 2.5 cm) were used to increase the milling efficiency. The wet ball-milling process was continuously carried out for 170 h without interruption. The powder material was removed from the liquid medium by decanting and evaporating at 105 °C.

The milled and un-milled kaolin powders were then individually used to prepare the ceramic suspensions and NMP and DMSO were evaluated as solvents (Table 3.1).

Table 3.1 - Ceramic suspension and extrusion parameters for producing kaolin hollow fiber membranes.

Hollow fiber denomination	Kaolin poder	Solvent	Flow rates (mL min^{-1})	
			Ceramic suspension	Internal coagulant
K-NMP-7/15	Non-milled	NMP	7	15
MK-NMP-7/15	Milled	NMP	7	15
MK-NMP-15/25	Milled	NMP	15	25
MK-DMSO-7/15	Milled	DMSO	7	15
MK-DMSO-15/25	Milled	DMSO	15	25

The ceramic suspension composition (0.37 wt.% additive, 55.17 wt.% solvent, 34.58 wt.% kaolin powder and 9.88 wt.% polymer) was based on the values suggested by Hubadillah et al. (2016). The additive (Arlacel) was firstly dissolved in the solvent (NMP or DMSO) followed by the addition of the kaolin powder and stirring in a ball mill for 48 h. Then, the polymer (PES) was added to the mixture and the final ceramic suspensions were stirred for another 48 h.

Hollow fibers were produced by the phase inversion/sintering technique following the methodology described by Kingsbury & Li (2009). After homogenization, the ceramic suspension was extruded through a tube orifice spinneret (outer and inner diameters of 3 and 1.2 mm, respectively). Two individual pumps (Harvard Apparatus, model XHF) were used to control ceramic suspension and internal coagulant flows. Distilled water was used as internal coagulant. The ceramic suspension and internal coagulant flow rates are presented in Table 3.1. The ceramic hollow as-prepared fibers were discarded into a water coagulation bath with an air gap of 5 cm and they were left in the coagulating bath for 48 h. Then, the as-prepared hollow fibers were washed with water to complete solvent removal. After that, the fibers were manually cut to the desired length, straighten and dried at room temperature (approximately 25 °C) for at least 48 h.

The fibers were sintered in a tubular furnace (Carbolite, model TZF 15) at different temperatures (1100, 1150, 1200 and 1250 °C) using a rate of 2 °C/min in the range from room temperature to 300 °C, a rate of 1 °C/min in the range from 300 to 600 °C with dwell time of 60 min and a rate of 10 °C/min up to the maximal temperature with a dwell of 5 h (Natália Mazzarioli Terra et al., 2018). Finally, the samples were cooled to room temperature at a rate of 2 °C/min. Figure 3.1 presents a scheme of the set up used for producing ceramic hollow fibers.

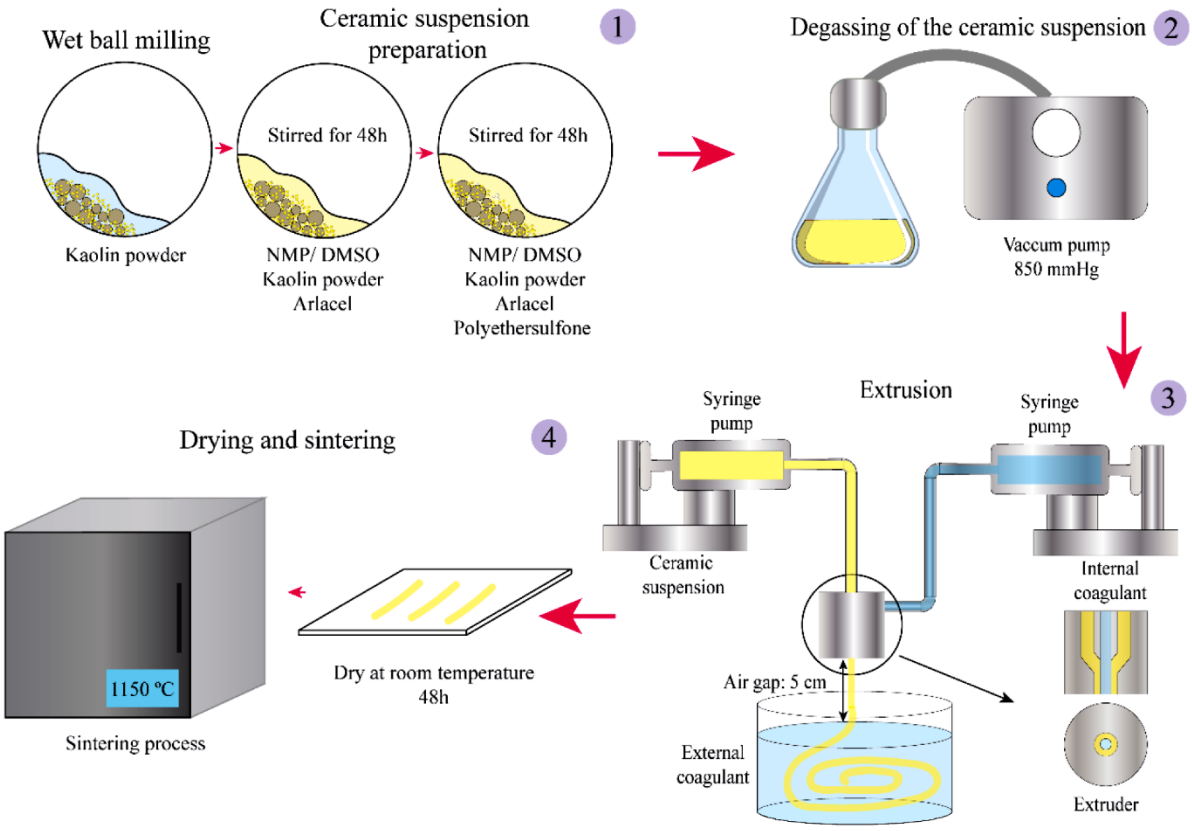

Figure 3.1 - Scheme of the extrusion process.

3.2.3. Characterizations

Particle size distributions of the kaolin powders before and after the wet ball-milling process were obtained using a laser particle size analyzer (Mastersizer 2000, Malvern). Thermogravimetric analyses (TG-DTA) were performed in a thermobalance (Shimadzu, model DTG-60H) under a nitrogen atmosphere (50 ml min^{-1}) at a heating rate of 10 °C min^{-1} from 30 to 1200 °C. Infrared absorption bands of the kaolin powders before and after sintering at 1100 and 1200 °C were verified using a Fourier transform infrared spectrophotometer (FTIR, Perkin Elmer, Spectrum two) coupled with attenuated total reflectance (ATR) at the frequency range of 4000 to 400 cm^{-1} with a resolution of 4 cm^{-1}.

Crystalline phases of the kaolin powders before and after sintering were characterized by X-ray diffraction (XRD) in a Shimadzu diffractometer (model XDR600) with an X-ray tube containing a copper anode (Cu-Ka wavelength) at a rate of 2 °min^{-1}, 2θ ranging from 10° to 80° with a step of 0.02°, a voltage of 40 kV and a current of 30 mA. The phases were identified using the ICDD Powder Diffraction File (PDF) database.

Morphological analyses of the powder samples and ceramic hollow fibers were performed using scanning electron microscopy (SEM, Carl Zeiss, model EVO MA10). The samples were first fixed in stubs with a double carbon tape and covered with a thin layer of gold in a metallizer equipment (Leica - EM SCD050). The pore structure and porosity of the kaolin hollow fiber MK-DMSO-15/25 sintered at 1150 °C were investigated by mercury intrusion porosimetry (MIP, Autopore IV 9500, Micrometrics) at a pressure range between 35 and 414000 kPa to ensure maximum mercury penetration into pores of diameters down to 0.003 μm.

The hollow fibers were also characterized in terms of mechanical strength and water permeability. The water permeability through the produced hollow fibers was measured at room temperature (approximately 25 °C) and at different transmembrane pressures. For these water flow measurements, the fibers were glued in a plastic tube and the lumen side of the fiber was kept open. The end of the fiber was closed with epoxy resin glue. The plastic tube was then connected to an automatic pumping system (Convergence Inspector Minus equipment, Netherlands) and Milli-Q® water was flowed through the fibers from lumen to shell side. Water flow was recorded at several transmembrane pressures (from 20 to 100 kPa) and the water flow permeability was calculated as the angular coefficient of the straight line which related water flux and transmembrane pressure according to the Darcy law (Terra et al., 2018). For mechanical strength evaluations, the three-point bending test was performed using an Instron Model 9600 attached to a 5 kN cell and using hollow fibers with a length of 30 mm.

3.2.4. Filtrations of aqueous bacteria suspension

Dead-end filtrations experiments were carried out in order to sterilize a synthetic bacteria suspension. A bacteria suspension with the *E. cloacae* bacteria was prepared in a 0.9% NaCl solution at 4.0×10^8 CFU mL^{-1} (colony forming units per mL). The use of NaCl solution for bacteria suspensions allows the maintenance of bacteria size and viability over the filtration.

The prepared kaolin hollow fibers MK-DMSO-15/25 sintered at 1200 and 1250 °C were evaluated for this filtration. Three pieces of each fiber (filtration area of 1.7×10-5 m^2) were glued in a plastic tube which was connected to a pressurized system and permeation was from lumen to shell side. Filtrations were carried out at room temperature (25 °C) and at transmembrane pressure of 20 kPa.

The permeate flow was recorded according to the filtration time. Experimental flux decay data were then adjusted to the mathematical model proposed by Hermia (1982) (Eq. 3.1) in order to describe fouling mechanisms. The parameter n in Eq. 3.1 dictates the fouling mechanism as follow: n = 0 for cake filtration; n = 2 for complete pore blocking; n = 1 for partial pore blocking and n = 1.5 for internal pore blocking.

$$-\frac{dJ}{dt} = K_n A^{2-n} J^{3-n} \quad (3.1)$$

where J is the permeate flux, t is the filtration time, A is the membrane area and Kn is an adjusted parameter.

Equation 3.1 was numerically adjusted to experimental data using the Levenberg-Marquardt method at an integration step of 10^{-3} with a precision of 10^{-8}. The accuracy of Equation 3.1 was evaluated according to the values of sum of square of the relative error (SSRE) between experimental and calculated flux data at each n index (Terra et al., 2018).

Bacteria concentrations in permeate and feed solutions were determined by enumeration of CFU. The spread-plate method was used to determinate the concentration of cells. A volume of 0.1 ml of the samples were pipetted aseptically on the different agar plates and overnight incubated at 37 °C (Boczek et al., 2014).

3.3. RESULTS AND DISCUSSION

3.3.1. Kaolin powder characteristics

Figure 3.2 presents SEM images and the particle size distributions of the kaolin powders before and after the milling process. According to the SEM image (Figure 3.2a) the kaolin powder presents particles with irregular shape and sizes. This wide particle size distribution was also verified by the laser particle size analysis (Figure 3.2a), with D50 of 8.7 μm and particles in the range of 0.37–34.2 μm (D10-D90). As it is evidenced by SEM images (Figures 3.2a and 3.2b), the milling process reduced the kaolin particle size. The milled kaolin powder has D50 of 5.1 μm with particles in the range of 0.51–23.4 μm (D10-D90).

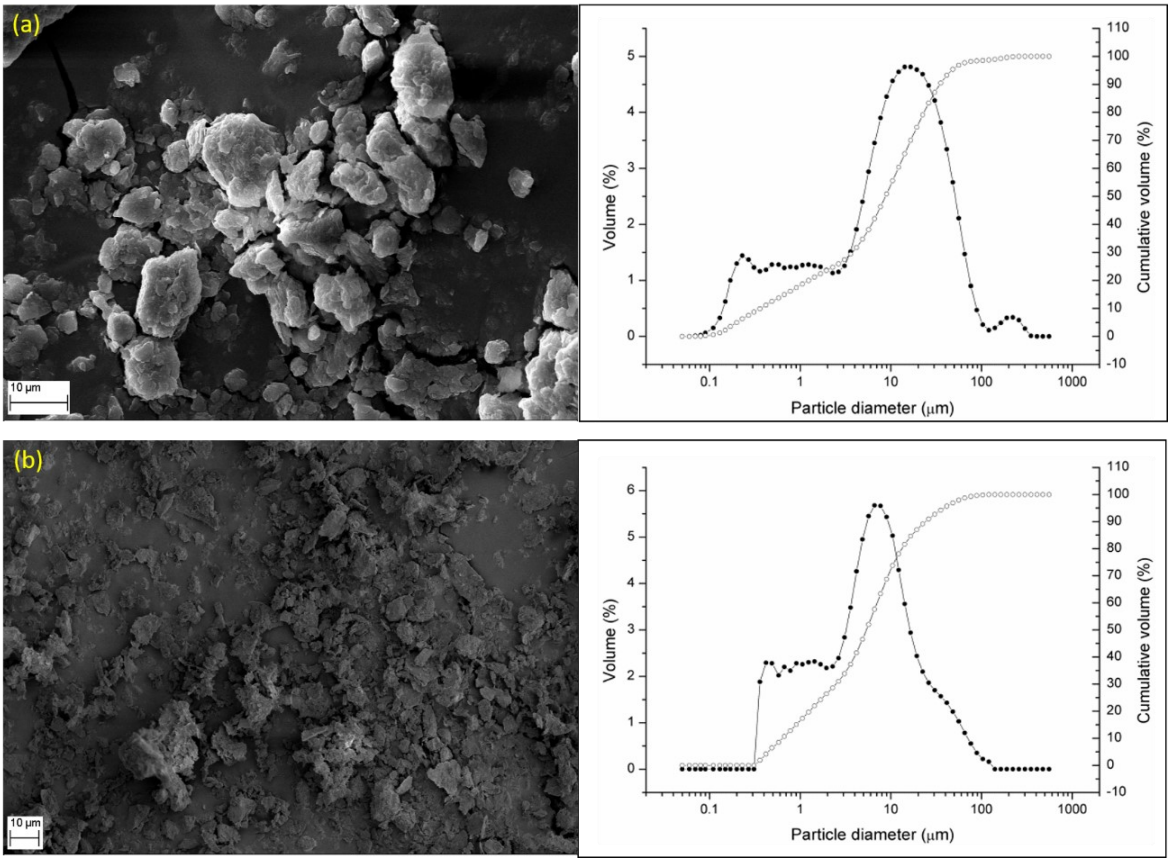

Figure 3.2 - SEM images and particle size distributions of kaolin powder samples before (a) and after (b) the milling process.

The crystalline phases of the kaolin powder and sintered samples at different temperatures were evaluated by XRD (Figure 3.3a). According to the ICDD Powder Diffraction File (PDF) database, the crude kaolin sample (before sintering) was associated with a mixture of quartz (SiO2), PDF card No. 85-865 (unit-cell parameters: a = 26.71 Å, b = 36.64 Å, c =39.84 Å, d=50.04 Å, e=59.97 Å and f=68.06 Å) and kaolinite ($Al_2SiO_2(OH)_4$), PDF card No. 1-527 (unit-cell parameter a = 20.48 Å).

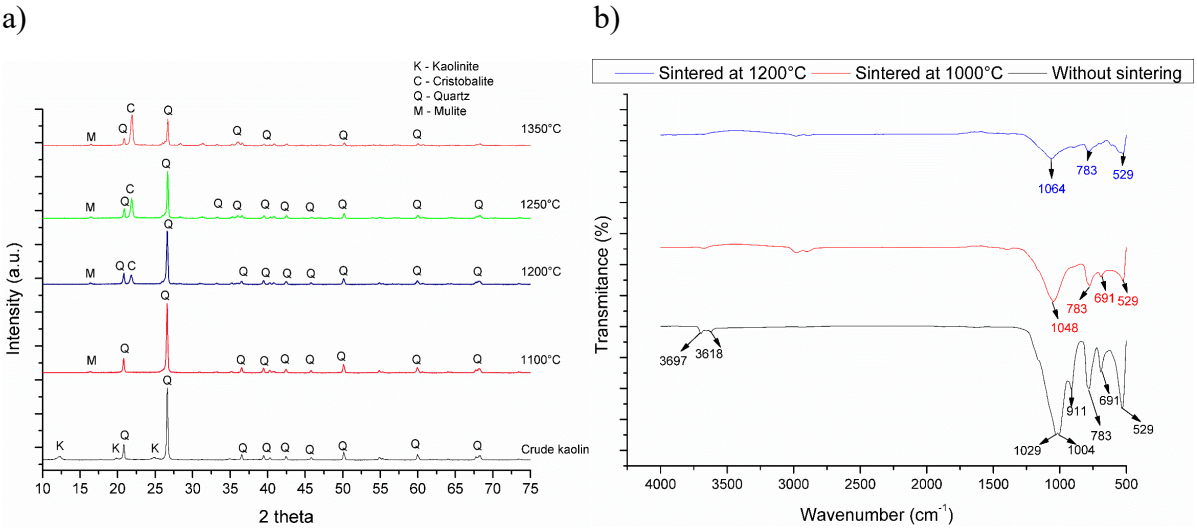

Figure 3.3 - XRD patterns (a) and FTIR spectra (b) of kaolin samples sintered at different temperatures.

The sintering of the kaolin sample at 1100 °C caused the formation of a mullite phase (PDF card No. 89-2813, unit-cell parameter: a = 16.35 Å). According to Ptáček et al. (2012), kaolinite is transformed into amorphous metakaolinite when it is heated to temperatures of 500 to 700 °C (Equation 3.2). The further increase in the sintering temperature up to 1050 °C causes the transformation of metakaolinite to spinel (Equation 3.3). Spinel is then transformed to mullite at sintering temperatures greater than 1050 °C (Equation 3.4). Finally, at sintering temperatures greater than 1050 °C, mullite is transformed to cristobalite, as presented in Equation 3.5. The cristobalite phase (PDF card No. 79-936, unit-cell parameter a = 21.97 Å) was detected in the sample sintered at 1200 °C, as shown in Figure 3.3a. Additionally, the intensity of the quartz peaks presented in Figure 3.3a was decreased with the increase in the sintering temperature. According to Wang et al. (2016), there is an isomeric transformation of the quartz towards cristobalite at sintering temperatures above 1100 °C.

$$Al_2O_3{\cdot}2SiO_2{\cdot}2H_2O \text{ (kaolinite)} \rightarrow Al_2O_3{\cdot}2SiO_2 \text{ (metakaolinite)} + 2H_2O \quad (3.2)$$

$$2\ (Al_2O_3{\cdot}2SiO_2) \text{ (metakaolinite)} \rightarrow 2Al_2O_3{\cdot}3SiO_2 \text{ (Al-Si-spinel)} + SiO_2 \text{ (amorphous)} \quad (3.3)$$

$$3\ (2Al_2O_3{\cdot}3SiO_2) \text{ (Al-Si-spinel)} \rightarrow 2\ (3Al_2O_3{\cdot}2SiO_2) \text{ (mullite)} + 5SiO_2 \text{ (amorphous)} \quad (3.4)$$

$$SiO_2 \text{ (amorphous)} \rightarrow SiO_2 \text{ (cristobalite)} \quad (3.5)$$

FTIR spectra of the kaolin samples before sintering and those sintered at 1000 and 1200 °C are presented in Figure 3.3b. Before sintering, the kaolin sample presented typical bands related to its kaolinite structure (Fitos et al., 2015). The bands observed between 4000 and 3000

cm^{-1} are related to OH^- stretching vibrations, which are typical for kaolinite. These bands were not observed for the sintered samples, probably due to the dehydroxylation of kaolinite. The bands between 1200 and 500 cm^{-1} correspond to the Si–O stretching and bending vibrations. The bands at 1029 and 1004 cm^{-1} arise from the Si–O–Si and Si–O–Al vibrations, respectively. The band at approximately 911 cm^{-1} arises from the vibrations of inner OH^- groups, and the bands at 691 and 529 cm^{-1} originate from Si–O–Al vibrations (Al in octahedral coordination). However, as the sintering temperature increased, the intensity of these bands was decreased, indicating a complete dehydroxylation of kaolinite and its transformation into metakaolinite (Fitos et al., 2015).

The TG curve of the kaolin powder (Figure 3.4) showed that there was a mass loss of 5% in the temperature range of 400 to 600 °C. This mass loss was probably caused by a dehydroxylation reaction (Balek and Murat, 1996). The thermal behaviour of the kaolin sample (Figure 3.4) is similar to those reported by Fitos et al. (2015) for kaolin samples of hydrothermal origin. The thermal stability of the kaolin powder is a positive aspect for the membrane production. The DTA curve showed that kaolin decomposition occurred at a temperature of approximately 200 °C due to the loss of physisorbed water, followed by the dehydroxylation of coordinated and structural water at approximately 400 °C and the condensation of hydroxyl groups at higher temperatures (ElDeeb et al., 2019).

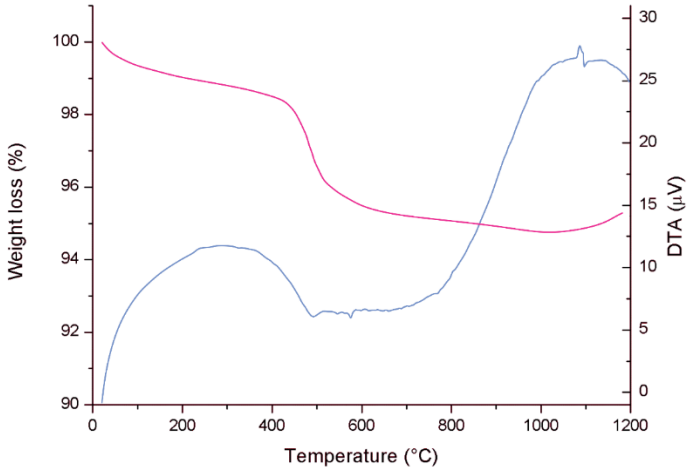

Figure 3.4 - TG/DTA curves of kaolin powder sample.

3.3.2. Characteristics of fiber membranes

Figure 3.5 presents SEM images of the as-prepared hollow fibers (before sintering), which were produced at different extrusion rates and with different solvents (Table 3.1). The

membrane produced with the un-milled kaolin powder (K-NMP-7/15) presented irregular cavities throughout the fiber. Relatively large particle size of the un-milled kaolin powder mitigated the formation of micro-voids during the phase inversion process, since the ceramic powder was surrounded by the coagulated polymer. The fibers produced with the milled kaolin powder presented finger like regions at the inner and outer surfaces of the fiber. The micro-voids at the finger like regions were formed due to the interfacial instabilities at the interfaces between the ceramic dispersion and the internal and external coagulant fluids. These instabilities were caused due to the density, viscosity and composition differences between the ceramic suspension and the internal and external coagulant fluids. Thus, there was a solvent mass transfer from the ceramic dispersion to the coagulant fluid (water), and the solvent output caused the polymer precipitation (Lee et al., 2015).

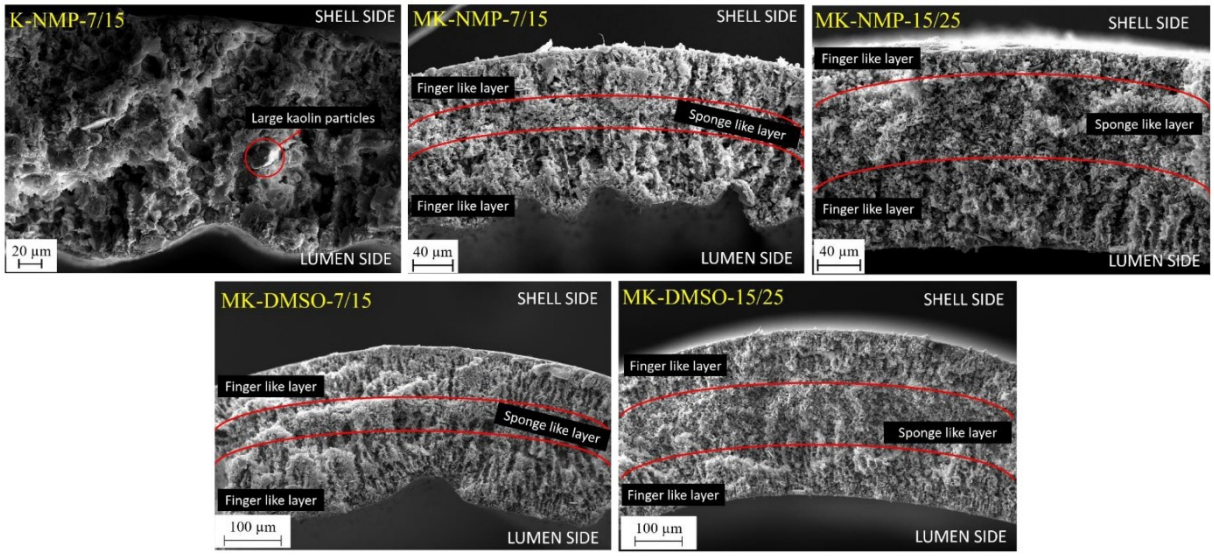

Figure 3.5 - Cross-section SEM images of the kaolin hollow fibers produced at different conditions.

The micro-voids were formed on the shell and lumen sides of the fiber and a sponge like layer remained in the central region of the fiber. The observed asymmetric pore size distribution is similar to those reported by Terra et al. (2018) for alumina hollow fiber membranes. However, the micro-void shapes observed in the kaolin hollow fibers were more irregular than those of the alumina hollow fibers, probably due to the larger particle size of the used kaolin powder. The inner surfaces of the fibers produced at the lowest evaluated extrusion rates (7 and 15 ml min^{-1}) for the ceramic suspension and internal coagulant, respectively) were irregular. This irregular structure was probably formed because the internal coagulant flow rate at 15 ml min^{-1} was not enough to produce a hydrodynamic force against the ceramic suspension during

the spinning process (Li et al., 2017). The increase in the internal coagulant flow rate to 25 ml min^{-1} resulted in a fiber with a regular internal contour, as observed in the SEM image of the MK-NMP-15/25 hollow fiber. However, the increase in the extrusion rates decreased the extent of the finger like regions, since it increased the phase inversion phenomenon. The use of DMSO as solvent produced long, straight, cylindrical and densely packed micro-voids. Lee et al. (2015) evaluated different solvents for producing alumina hollow fibers and observed that cylindrical micro-channels were formed when DMSO was the solvent, while conical structures were formed when NMP was the solvent.

The fibers sintered at different temperatures showed slight modifications in their morphological characteristics, as it is shown in Figure 3.6 for the MK-DMSO-15/25 fiber. The effect of the sintering temperature on the morphological characteristics was similar for all other produced hollow fibers.

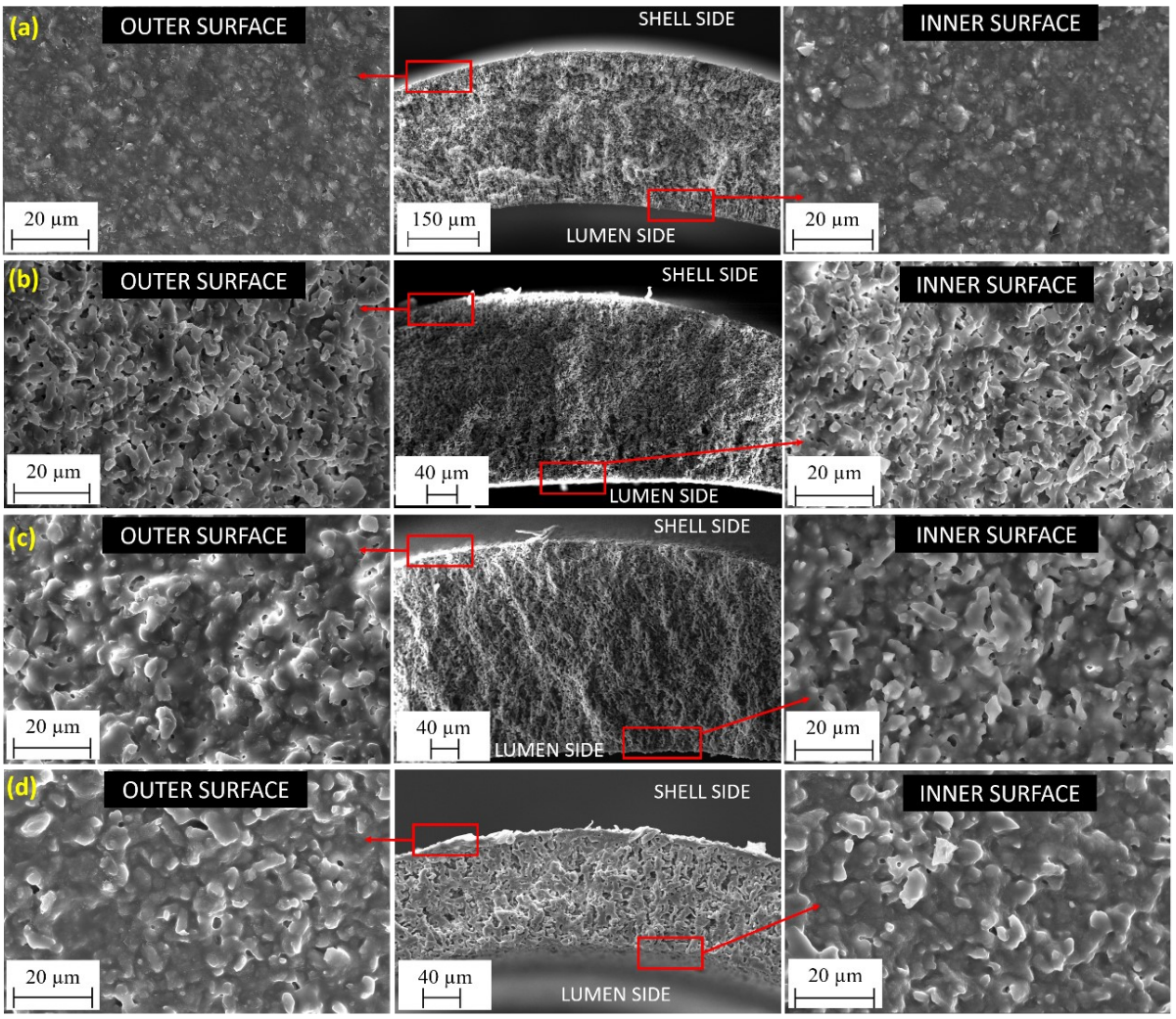

Figure 3.6 - SEM images (cross-section and inner and outer surfaces) of the hollow fiber MK-DMSO-15/25 - a) as-prepared samples and samples sintered at different temperatures: b) 1150°C, c) 1200°C, and d) 1250°C.

Figure 3.6a shows that inner and outer surfaces of the as-prepared membranes were covered by the precipitated polymer, as a result of the phase inversion process during the extrusion. The relatively large particle size of the used kaolin powder compared to other conventionally used ceramic materials (alumina of 1 µm, for instance) promoted the polymer coagulation at the hollow fiber surface instead of inside the formed micro-voids structures. When the hollow fiber was sintered at 1150 °C (Figure 3.6b), a porous structure was formed due to the complete elimination of the polymer. The increase in the sintering temperature from 1150 to 1200 °C caused the coalescence of kaolin particles (Figure 3.6c). The particle coalescence is more evident on the outer and inner surfaces of the hollow fiber sintered at 1200 °C. However, a particle coalescence process was evidenced in the whole cross-section region of the fiber sintered at 1250 °C (Figure 3.6d).

The pore structure of the kaolin hollow fiber MK-DMSO-15/25 sintered at 1200 °C was evaluated by the mercury intrusion technique, as shown in Figure 3.7.

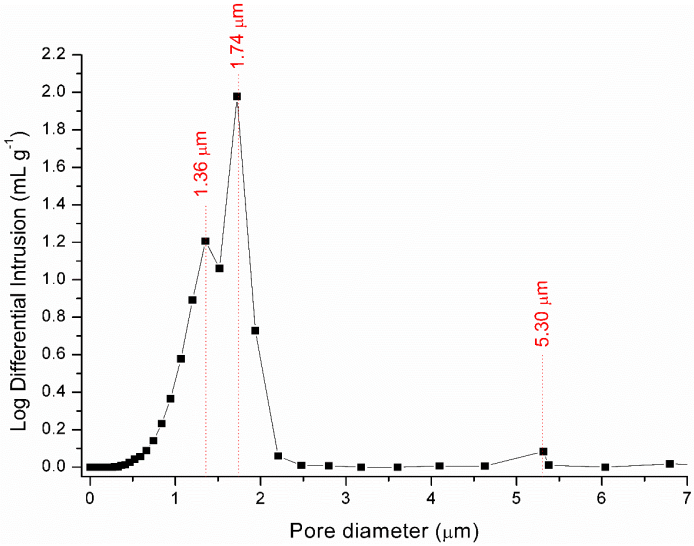

Figure 3.7 - Pore size distribution of the fiber MK-DMSO-15/25 sintered at 1150°C.

The pore size distribution of the fiber MK-DMSO-15/25 sintered at 1150 °C presented 3 major peaks. The peaks at 1.36 and 1.74 µm correspond to the pore size of the packed pore-network at the sponge-like layer region. The last peak at 5.30 µm designates the pore size of the opened micro-channels. Lee et al. (2016) reported that alumina hollow fiber membranes presented a sponge like-layer with pore sizes between 0.25 and 0.30 µm and micro-voids of 3.2 µm. Thus, the application of kaolin powder resulted in a loosely packed structure at the sponge-like layer region than conventional asymmetric alumina hollow fibers. However, the size of the micro-voids formed with kaolin is similar to those with alumina. The porosity of the MK-DMSO-15/25 fiber sintered at 1150 °C was evaluated to be 46% according to the mercury intrusion technique. Gil et al. (2015) reported that pure alumina hollow fibers presented porosities of 64 and 54% when sintered at 1300 and 1400 °C, respectively. Obada et al. (2017) reported a porosity of 62% for disk kaolin membrane sintered at 1150 °C, which was produced by the pressing method.

The porosity of the membrane critically influences its application and, in general, membranes with high porosity are suggested to be applied as a substrate for the deposition of a selective layer while denser membranes are used for proper separations. However, the mechanical resistance of the membrane should not be negatively affected by its porosity. The

pore distribution of the membrane and the sintering temperature are the main factors affecting the mechanical resistance of the membrane, as presented in Table 3.2.

Table 3.2 - Bending strength values (MPa) of the kaolin hollow fibers sintered at different temperatures.

Hollow fiber membrane	Sintering temperature	
	1150 °C	1250 °C
K-NMP-7/15	-	$20.74^{a} \pm 1.90$
MK-NMP-7/15	$26.57^{a} \pm 1.69$	$75.34^{b} \pm 2.94$
MK-NMP-15/25	$30.70^{a} \pm 3.68$	$81.99^{b} \pm 3.62$
MK-DMSO-7/15	$31.60^{a} \pm 2.85$	$81.09^{b} \pm 5.86$
MK-DMSO-15/25	$41.98^{b} \pm 2.61$	$145.64^{c} \pm 9.88$

[a, b, c] Mean values denoted by different letters at the same column are significantly different at $p \leq 0.05$

Due to the larger particle size of the un-milled kaolin powder, the hollow K-NMP-7/15 fiber sintered at 1150 °C was fragile and its mechanical resistance could not be evaluated. The mechanical resistance of the MK-NMP-7/15 fiber is 3.6 times greater than for the K-NMP-7/15 fiber, both sintered at 1250 °C. Thus, the milling of the kaolin powder was strictly necessary to produce hollow fiber membranes with reliable mechanical resistance. The change in the extrusion rates had no significant effect on the bending strength values of the fibers produced with NMP as solvent at both evaluated sintering temperatures (1150 and 1250 °C). However, the mechanical resistances of the fibers produced with DMSO increased with the increase in the extrusion rates. Actually, as presented in Figure 3.5 for the fibers produced with DMSO as solvent, a larger sponge like layer was formed at higher extrusion rates, which contributed to the increase in the mechanical resistance of the fiber. The use of DMSO or NMP as solvent resulted in fibers with similar bending strength values if compared at the extrusion rates of 7 and 15 ml min^{-1} for ceramic suspension and bore fluid, respectively. However, at the highest extrusion rates of 15 and 25 ml min^{-1} for ceramic suspension and bore fluid, respectively, the mechanical resistance of the fibers produced with DMSO was higher than with NMP. The use of DMSO as solvent produced more organized micro-voids and, thus, the fibers produced with DMSO presented higher mechanical resistance. Chakraborty et al. [17] highlighted the importance of optimizing the conditions for producing kaolin membranes in order to have suitable mechanical resistances.

The increase in the sintering temperature from 1150 to 1250 °C increased the mechanical resistance of all the produced kaolin hollow fibers for approximately 3 times. The

sample MK-DMSO-15/25 sintered at 1200 °C presented bending strength of 95.27 ± 4.38 MPa. The increase in mechanical strength with the increase in the sintering temperature may be associated with the enhanced densification of the ceramic particles, as observed in the SEM images (Figure 3.6). Hubadillah et al. (2020) verified that the mechanical resistances of kaolin fibers were increased from almost 5 to 60 MPa when the sintering temperatures were increased from 1200 to 1500 °C. Terra et al. (2016) reported that the increase in the sintering temperature of asymmetric alumina hollow fibers from 1300 to 1400 °C increased the bending strength of the fibers from 41.2 to 74.5 MPa. Thus, the fibers produced with kaolin as starting material and sintered at temperatures lower than 1250 °C presented suitable values of mechanical strength. Rekik et al. (2019) related kaolin as reinforcing agent for polymeric membranes.

The water permeabilities of the MK-DMSO-15/25 fibers sintered at 1150, 1200 and 1250 °C were 23.38, 14.64 and 3.46 L $h^{-1} \cdot m^{-2} \cdot kPa^{-1}$, respectively. All other produced hollow fibers presented similar behavior. The increase in the sintering temperature caused a pore densification which resulted in the increase in the mechanical resistance of the membrane, but also the decrease in its water permeability. The water permeability of the produced hollow fibers is quite similar to the values reported in the literature (Hubadillah et al., 2017). Sharma et al. (2017) reported the use of a low cost kaolin-based membrane sintered at 950 °C for antibiotic removal from an aqueous solution, which presented water permeability of 12.96 L $h^{-1} \cdot m^{-2} \cdot kPa^{-1}$ and mechanical resistance of 28 MPa. Liu et al. (2019) produced a layered kaolin membrane which was supported on a polymeric substrate and presented water permeability of 40.00 L $h^{-1} \cdot m^{-2} \cdot kPa^{-1}$.

3.3.3. Retention of bacteria by membrane filtration

The hollow MK-DMSO-15/25 fibers sintered at 1200 and 1250 °C presented suitable characteristics for filtration applications. The use of DMSO and extrusion rates of 15 and 25 ml/min resulted in a fiber with positive morphological characteristics: regular contours and asymmetric pore size distribution. The hollow MK-DMSO-15/25 fibers sintered at 1200 and 1250 °C presented suitable mechanical resistance. Figures 3.8a and 3.8b show the permeate flux of the bacteria solution through the hollow MK-DMSO-15/25 fiber sintered at 1200 and 1250 °C, respectively.

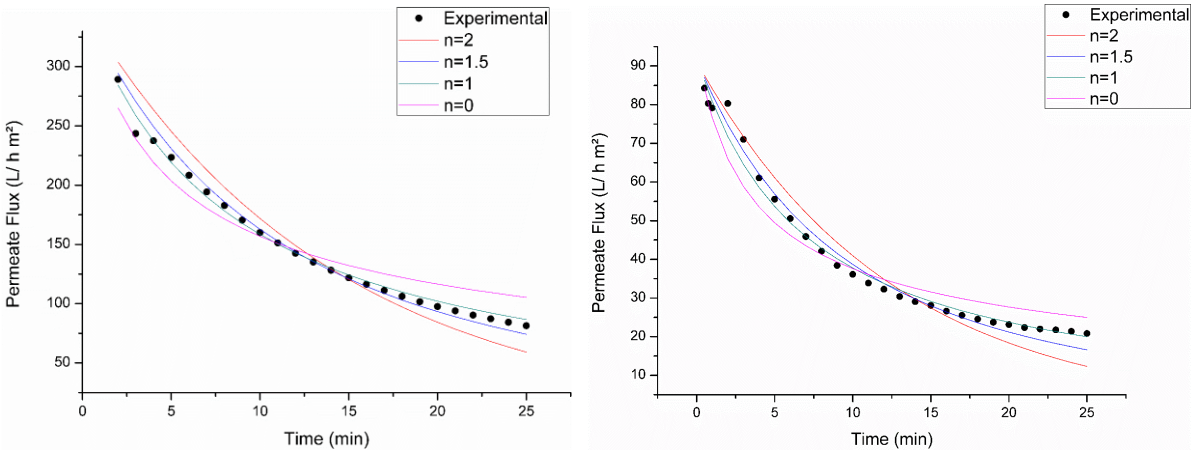

Figure 3.8 - Permeate flux of bacteria solution through the hollow fibreMK-DMSO-15/25 sintered at: a) 1200 °C and b) 1250 °C.

There was a pronounced flux decline during the first 15 min of filtration with both evaluated fibers. The permeate fluxes through the fiber sintered at 1200 °C were at least 3 times greater than through the fiber sintered at 1250 °C. Thus, the increase in the sintering temperature decreased the membrane porosity and reduced its permeability. The initial fluxes of the bacteria solution through both membranes were quite similar to the pure water flux at 20 kPa, but after 25 min of filtration, the initial fluxes through both membranes were decreased for approximately 3 times. This decrease was probably due to the membrane fouling occurrences during the filtration process.

The modelling of experimental data according to the differential equations proposed by Hermia 1982) for dead-end filtration showed that the main fouling occurrences were due to the partial and internal pore blocking mechanisms (Table 3.3). These mechanisms were probably more pronounced than total pore blocking and cake formation because the evaluated membranes presented larger pore sizes than the size of the filtered bacteria. According to the literature (Gaston, 1988), *E. cloacae* is a rod-shaped bacterium that measures 0.6–1.0 µm wide by 1.2–3.0 µm long.

Table 3.3 - Values of the sum of squares of the relative error (SSRE) between calculated and experimental flux data for each fouling mechanism.

Sintering temperature [°C]	Complete pore blocking ($n = 2$)	Internal pore blocking ($n = 1.5$)	Partial pore blocking ($n = 1$)	Cake formation ($n = 0$)
1200	0.4304	0.0988	0.0862	0.5712
1250	0.8020	0.1838	0.0540	0.5155

Notwithstanding, the hollow fiber membranes were quite efficient in removal of the *E. cloacae* bacteria from the feed solution. The bacteria retention values were 99.8% and 99.9% for the hollow fibers sintered at 1200 and 1250 C°, respectively. Kumar et al., (2019) reported removal of 90% of Escherichia coli from an aqueous solution by using a ceramic membrane.

3.4. CONCLUSIONS

The potential use of kaolin as the starting material for producing ceramic hollow fiber membranes was demonstrated. The milling of the ceramic powder was crucial to achieve the asymmetric pore size distribution in the membrane. The flow rate of the internal coagulant fluid (water) during the extrusion process was adjusted to 25 ml min^{-1} in order to produce enough hydrodynamic force against the ceramic suspension and, thus, produce a hollow fiber with regular internal contour. The fibers sintered at 1150 °C presented a high porosity, but their mechanical resistance was not enough to guarantee its applicability in separation processes. The crystallographic transformations of the ceramic material at temperatures greater than 1100 °C also caused modifications in the morphology of the produced hollow fiber membranes. The fibers sintered at 1200 and 1250 °C facilitated a pore densification process which increased the mechanical resistance of the fibers. Moreover, they showed excellent potential for bacteria removal from water by demonstrating retention values of almost 100% of bacteria in water. The presented systematic analysis revealed proper conditions for producing kaolin-based hollow fiber membranes which can be extrapolated for using other mineral based ceramic materials.

3.5. REFERENCES

ABDULHAMEED, M. A. et al. Fabrication and characterization of affordable hydrophobic ceramic hollow fibre membrane for contacting processes. **Journal of Advanced Ceramics**, [s. l.], v. 6, n. 4, p. 330–340, 2017. Disponível em: https://doi.org/10.1007/s40145-017-0245-1.

BALEK, V.; MURAT, M. The emanation thermal analysis of kaolinite clay minerals. **Thermochimica Acta**, [s. l.], v. 282–283, p. 385–397, 1996. Disponível em: https://www.sciencedirect.com/science/article/pii/0040603196028869.

BESSA, L. P. et al. Macro-porous dolomite hollow fibers sintered at different temperatures toward widened applications. **Ceramics International**, [s. l.], v. 43, n. 18, p. 16283–16291, 2017. Disponível em: http://dx.doi.org/10.1016/j.ceramint.2017.08.214.

BESSA, L. P. et al. Micro-structured and reinforced spinel hollow fiber membranes: Influence of sintering temperature and ceramic powder composition. **Ceramics International**, [s. l.], v. 45, n. 17, Part B, p. 23632–23642, 2019. Disponível em: https://www.sciencedirect.com/science/article/pii/S0272884219322722.

BOCZEK, L. A.; RICE, E. W.; JOHNSON, C. H. Total Viable Counts: Spread Plate Technique. Second Edied. [S. l.]: Elsevier, 2014. v. 3 E-book. Disponível em: http://dx.doi.org/10.1016/B978-0-12-384730-0.00331-1.

CHAKRABORTY, S.; UPPALURI, R.; DAS, C. Optimal fabrication of carbonate free kaolin based low cost ceramic membranes using mixture model response surface methodology. **Applied Clay Science**, [s. l.], v. 162, p. 101–112, 2018. Disponível em: https://www.sciencedirect.com/science/article/pii/S0169131718302564.

ELDEEB, A. B. et al. Extraction of alumina from kaolin by a combination of pyro- and hydro-metallurgical processes. **Applied Clay Science**, [s. l.], v. 172, p. 146–154, 2019. Disponível em: https://www.sciencedirect.com/science/article/pii/S0169131719300729.

FERREIRA, E. de P. et al. Improved Microstructure of Asymmetric Niobium Pentoxide Hollow Fiber Membranes. **Journal of the European Ceramic Society**, [s. l.], 2019. Disponível em: https://linkinghub.elsevier.com/retrieve/pii/S0955221919301360.

FITOS, M. et al. Pozzolanic activity of thermally and mechanically treated kaolins of hydrothermal origin. **Applied Clay Science**, [s. l.], v. 116–117, p. 182–192, 2015. Disponível em: http://dx.doi.org/10.1016/j.clay.2015.08.028.

GASTON, M. A. Enterobacter: an emerging nosocomial pathogen. J Hosp Infect., [s. l.], v. 11, n. 3, p. 197–208, 1988.

GIL, A. G. et al. A highly permeable hollow fibre substrate for Pd/Al2O3 composite membranes in hydrogen permeation. **International Journal of Hydrogen Energy**, [s. l.], v. 40, n. 8, p. 3249–3258, 2015. Disponível em: https://www.sciencedirect.com/science/article/pii/S0360319915000580.

HERMIA, J. Constant Pressure Blocking Filtration Laws - Application to Power-Law Non-Newtonian Fluids. Icheme, [s. l.], v. 60, p. 183–187, 1982.

HUBADILLAH, S. K. et al. A low cost hydrophobic kaolin hollow fiber membrane (h-KHFM) for arsenic removal from aqueous solution via direct contact membrane distillation. **Separation and Purification Technology**, [s. l.], v. 214, p. 31–39, 2019.

HUBADILLAH, S. K. et al. Fabrications and applications of low cost ceramic membrane from kaolin: A comprehensive review. **Ceramics International**, [s. l.], v. 44, n. 5, p. 4538–4560, 2018. Disponível em: https://www.sciencedirect.com/science/article/pii/S0272884217329231.

HUBADILLAH, S. K. et al. Green silica-based ceramic hollow fiber membrane for seawater desalination via direct contact membrane distillation. **Separation and Purification Technology**, [s. l.], v. 205, n. February, p. 22–31, 2018.

HUBADILLAH, S. K. et al. Preparation and characterization of inexpensive kaolin hollow fibre membrane (KHFM) prepared using phase inversion/sintering technique for the efficient separation of real oily wastewater. **Arabian Journal of Chemistry**, [s. l.], v. 13, n. 1, p. 2349–2367, 2020. Disponível em: https://www.sciencedirect.com/science/article/pii/S1878535218301072.

HUBADILLAH, S. K. et al. Preparation and characterization of low cost porous ceramic membrane support from kaolin using phase inversion/sintering technique for gas separation: Effect of kaolin content and non-solvent coagulant bath. **Chemical Engineering Research and Design**, [s. l.], v. 112, p. 24–35, 2016. Disponível em: http://dx.doi.org/10.1016/j.cherd.2016.06.007.

HUBADILLAH, S. K. et al. Superhydrophilic, low cost kaolin-based hollow fibre membranes for efficient oily-wastewater separation. **Materials Letters**, [s. l.], v. 191, p. 119–122, 2017. Disponível em: http://dx.doi.org/10.1016/j.matlet.2016.12.099.

JEDIDI, I. et al. Preparation of a new ceramic microfiltration membrane from mineral coal fly ash: Application to the treatment of the textile dying effluents. **Powder Technology**, [s. l.], v. 208, n. 2, p. 427–432, 2011. Disponível em: https://www.sciencedirect.com/science/article/pii/S0032591010004316.

KAUR, H.; BULASARA, V. K.; GUPTA, R. K. Effect of carbonates composition on the permeation characteristics of low-cost ceramic membrane supports. **Journal of Industrial**

and Engineering Chemistry, [s. l.], v. 44, p. 185–194, 2016. Disponível em: http://dx.doi.org/10.1016/j.jiec.2016.08.026.

KINGSBURY, B. F. K.; LI, K. A morphological study of ceramic hollow fibre membranes. **Journal of Membrane Science**, [s. l.], v. 328, n. 1–2, p. 134–140, 2009.

KUMAR, C. M.; ROSHNI, M.; VASANTH, D. Treatment of aqueous bacterial solution using ceramic membrane prepared from cheaper clays : A detailed investigation of fouling and cleaning. **Journal of Water Process Engineering**, [s. l.], v. 29, n. February, p. 100797, 2019. Disponível em: https://doi.org/10.1016/j.jwpe.2019.100797.

LEE, M. et al. Formation of micro-channels in ceramic membranes - Spatial structure, simulation, and potential use in water treatment. **Journal of Membrane Science**, [s. l.], v. 483, p. 1–14, 2015.

LEE, M.; WANG, B.; LI, K. New designs of ceramic hollow fibres toward broadened applications. **Journal of Membrane Science**, [s. l.], v. 503, p. 48–58, 2016.

LI, T. et al. X-ray tomography-assisted study of a phase inversion process in ceramic hollow fiber systems – Towards practical structural design. **Journal of Membrane Science**, [s. l.], v. 528, n. December 2016, p. 24–33, 2017. Disponível em: http://dx.doi.org/10.1016/j.memsci.2017.01.004.

LIU, T. et al. 2D kaolin ultrafiltration membrane with ultrahigh flux for water purification. **Water Research**, [s. l.], v. 156, p. 425–433, 2019. Disponível em: https://www.sciencedirect.com/science/article/pii/S0043135419302726.

LIU, H. H.; LI, K.; HUGHES, R. Preparation of porous aluminium oxide (Al2O3) hollow fibre membranes by a combined phase-inversion and sintering method. **Ceramics International**, [s. l.], v. 29, p. 875–881, 2003.

OBADA, D. O. et al. Physico-mechanical and gas permeability characteristics of kaolin based ceramic membranes prepared with a new pore-forming agent. **Applied Clay Science**, [s. l.], v. 150, p. 175–183, 2017. Disponível em: https://www.sciencedirect.com/science/article/pii/S0169131717304143.

PREKAJSKI, M. et al. Synthesis and characterization of biomorphic CeO2 obtained by using egg shell membrane as template. **Processing and Application of Ceramics**, [s. l.], v. 8, p. 81–85, 2014.

PTÁČEK, P. et al. The kinetics and mechanism of kaolin powder sintering I. The dilatometric CRH study of sinter-crystallization of mullite and cristobalite. **Powder Technology**, [s. l.], v. 232, p. 24–30, 2012. Disponível em: https://www.sciencedirect.com/science/article/pii/S0032591012005426.

REKIK, S. B. et al. Enhancing hydrophilicity and permeation flux of chitosan/kaolin composite membranes by using polyethylene glycol as porogen. **Applied Clay Science**, [s. l.], v. 168, p. 312–323, 2019. Disponível em: https://www.sciencedirect.com/science/article/pii/S0169131718305015.

SAHNOUN, R. D.; BAKLOUTI, S. Characterization of flat ceramic membrane supports prepared with kaolin-phosphoric acid-starch. **Applied Clay Science**, [s. l.], v. 83–84, p. 399–404, 2013. Disponível em: https://www.sciencedirect.com/science/article/pii/S0169131713002202.

SHARMA, V. et al. Integrated adsorption-membrane filtration process for antibiotic removal from aqueous solution. **Powder Technology**, [s. l.], v. 321, p. 259–269, 2017. Disponível em: https://www.sciencedirect.com/science/article/pii/S0032591017306836.

TERRA, N. et al. Characterisation of asymmetric alumina hollow fibres: Application for hydrogen permeation in composite membranes. **Brazilian Journal of Chemical Engineering**, [s. l.], v. 33, p. 567–576, 2016.

TERRA, Natália Mazzarioli et al. Graphite coating on alumina substrate for the fabrication of hydrogen selective membranes. International **Journal of Hydrogen Energy**, [s. l.], v. 43, n. 3, p. 1534–1544, 2018.

TERRA, N.M. et al. High Performance of Asymmetric Alumina Hollow Fiber Membranes for the Clarification of Genipap (Genipa americana L.) Fruit Extract. **Food and Bioprocess Technology**, [s. l.], 2018.

WANG, W. et al. The phase transformation and thermal expansion properties of cordierite ceramics prepared using drift sands to replace pure quartz. **Ceramics International**, [s. l.], v. 42, n. 3, p. 4477–4485, 2016.

ZHOU, J. et al. Elaboration and characterization of tubular macroporous ceramic support for membranes from kaolin and dolomite. [s. l.], p. 1–9, 2010.

CHAPTER 4

4. INCORPORATION OF SILVER NANOPARTICLES IN A KAOLIN HOLLOW FIBER MEMBRANE FOR EFFICIENT REMOVAL OF *Enterobacter cloacae* AND *Escherichia coli* FROM AQUEOUS SOLUTIONS

ABSTRACT

Kaolin hollow fiber membranes were produced by the phase inversion method and silver nanoparticles (AgNPs) were sequentially impregnated in the fiber lumen side. The composite membranes were applied to treat aqueous solutions contaminated with Enterobacter cloacae and Escherichia coli. The prepared pristine kaolin hollow fibers presented an asymmetric pore size distribution. According to mercury intrusion analyses, the sponge like layer presented pore sizes between 1.14 and 2.16 μm, while the micro-voids in the finger like layer presented pore sizes between 7.86 and 9.17 μm. The kaolin hollow fibers presented water permeability of 8.46 ± 0.17 L h-1·m-2·kPa-1 and mechanical resistance of 103.58 ± 14.41 MPa. The AgNPs were properly synthetized and, according to spectroscopic analyses, the AgNP solution presented a single broad peak centered at 400 nm, which indicates a uniform dispersion of the synthetized AgNPs. The synthetized AgNPs presented a spherical and pseudospherical geometry, with average hydrodynamic size of 81.71 ± 8.05 nm, polydispersity index of 0.262 ± 0.012 and zeta potential of -20.7 ± 2.6 mV, which indicate a suitable AgNP stability in the aqueous suspension. The AgNPs were successfully impregnated in the lumen side of kaolin hollow fibers at a concentration of 0.51 ± 0.04 mg cm-1. Energy dispersive spectroscopy images showed that the AgNPs were more concentrated in the hollow fiber inner layer and a homogenous distribution of AgNPs were observed through the fiber cross-section. After AgNP impregnation, the composite hollow fiber membranes presented water permeability of 5.22 ± 0.32 L h-1 m-2 kPa-1. The pristine kaolin membrane enabled a log10 reduction value (LRV) of 2.47 ± 0.05 and 3.72 ± 0.13 for filtrations of aqueous solutions with E. cloacae and E. coli, respectively. For the kaolin hollow fiber membrane impregnated with AgNPs, the LRV value increased to 4.38 ± 0.83 and 4.35 ± 0.25 for filtrations of aqueous solutions with E. cloacae and E. coli, respectively. Thus, the synergetic action of the kaolin membranes impregnated with AgNPs enabled a bacterial reduction greater than 99.9%. The AgNPs decreased the permeate flux through the membrane but, for the filtration of the E. cloacae suspension, mitigated the cake formation on the membrane surface.

Keywords: Kaolin; Hollow fibers; Membranes; *Enterobacter cloacae*; *Escherichia coli.*

4.1. INTRODUCTION

The major causes of water pollution are the growth of human population and industrial and agricultural practices (Goswami and Pugazhenthi, 2020). Improper disposal of sewage and animal wastes are some of the main sources of water contamination, which cause a substantial drop in the amount of dissolved oxygen caused by the action of bacteria on organic matter decompositions (Owa, 2014). The consumption of contaminated water is associated to several diseases, such diarrhea, cholera, dysentery, typhoid, and polio. About 829 000 people are estimated to die each year from diarrhea as a result of unsafe drinking-water consumption and poor hygiene (WHO, 2019).

Several technologies are proposed for water purification, including chemical (ultraviolet irradiation, ozonation, chlorination, pasteurization, flocculation, etc.) and physical (sand filters, adsorption on activated carbon, membrane technology, etc.) processes. Membrane filtration is a promising alternative for water purification due to its ability to simultaneously reduce or eliminate several contaminants, such as heavy metals and microorganisms (Kaniganti et al., 2014). (Praveena and Aris, 2015)Praveena and Aris (2015) presented an important review about the application of membranes produced from low-cost materials for water treatment. In our previous work (Magalhães et al., 2020), we showed that membranes produced from kaolin, a low cost ceramic material, were able to achieve almost total removal of *Enterobacter* from aqueous suspensions. Low-cost ceramic membranes are produced from traditional ceramic materials, such as kaolin, dolomite, etc., and are used sintered at reduced temperatures. Thus, the cost reduction is mainly associated to the material cost itself and the costs of the production in the membrane sintering. A membrane produced from a ceramic material based on a kaolin-quartz-feldspar composition, which is sintered at 1300°C, presents a cost reduction in 50% if compared to an alumina membrane, which is sintered at 1600°C (Harabi et al., 2014; Mestre et al., 2019). However, low-cost ceramic materials are usually wet-grinded in ball mills, with milling times ranging from 2 to 48 h, in order to obtain particle sizes lower than 10 μm. The cost of this milling process should be considered, although it is believed it does not suppress the total cost reduction.

Ceramic filters can be coated with silver nanoparticles (AgNPs) to enhance the removal of pathogens from water (Murugesan et al., 2021). Uz et al. (2020) reported that membrane functionalization with antimicrobial particles, such as silver, reduced of biofouling caused by the deposition of bacterial cells on the membrane surface and, thus, enhanced the membrane

performance for producing pathogen free water. Qi et al. (2018) showed that polysulfone ultrafiltration membranes impregnated with silver nanoparticles presented antibacterial efficiency of 90% against the *Escherichia coli* and *Staphylococcus aureus* bacteria. Musico et al. (2014) reported that the presence of nanomaterials improved the antibacterial properties of membrane filters for *E. coli* and *Bacillus subtilis* removal. Behboudi et al. (2018) produced polyvinyl chloride/polycarbonate hollow fiber membranes incorporated with modified silver nanoparticles, which were applied for the treatment of pharmaceutical wastewater. Chaukura et al. (2020) produced ceramic filters impregnated with silver nanoparticles for water purification and showed the filter was able to remove 100% of *E. coli*.

Despite the number of publications about AgNP-impregnated membranes for water purification, there are some critical challenges to the still overcome, such as the cost of the ceramic membrane, the membrane pore size distribution for a precise nanoparticle deposition, and a reliable method for nanoparticle deposition. Thus, the main objective of this work was to evaluate the performance of kaolin hollow fibers impregnated with AgNPs for water purification. The kaolin hollow fiber membranes were produced by the phase inversion method followed by a single sintering step to achieve the desired asymmetric pore size distribution. Then, the synthetized AgNPs were impregnated in the fiber lumen side by a simple filtration assisted dip-coating method. Thus, the AgNP-kaolin hollow fiber membranes were evaluated for bacteria removal from aqueous solutions. The individual *Enterobacter cloacae* and *E. coli* bacteria were selected as model strains, since these bacteria are two major pathogens causing human diseases, such as urinary tract infection (Xu and He, 2019). The main novelties of our study are: 1) use of kaolin hollow fibers for the deposition of silver nanoparticles, and 2) application of the asymmetric pore distribution to favor the adhesion of the silver nanoparticles to the membrane.

4.2. MATERIAL AND METHODS

4.2.1. Material

Silver nitrate Silver nitrate (AgNO3, 99%, Isofar, Brazil,), sodium benzoate (99.5%, Dinâmica, Brazil), gallic acid (99.5%, Vetec, Brazil), n-methyl-2-pyrrolidone (NMP, Vetec, Brazil), sodium hydroxide (NaOH, 98%, Vetec, Brazil), kaolin (Kalamazon Estudos Geológicos LTDA, Brazil), PEG-30 Dipolyhydroxy stearate (ArlacelTM P135, Croda), polyether sulfone (PES, Veradel 3000P, Solvay) and sodium chloride (NaCl, 99%, Vetec) were used for syntheses and analyses.

4.2.2. Synthesis of silver nanoparticles

AgNPs were produced according to the procedure described by Mocanu et al. (2019). First of all, a silver benzoate ($C_7H_5AgO_2$) solution was obtained by mixing aqueous solutions of silver nitrate ($AgNO_3$) and sodium benzoate ($C_7H_5NaO_2$) at individual concentrations of 0.04 and 0.034 g mL^{-1}, respectively. The final solution, containing the precipitated silver benzoate, was sequentially filtrated through a 6 μm paper filter (Unifil, Brazil). The silver benzoate powder was dried at 50°C in an oven (Biomact, Brazil) for at least 24 h. Afterward, 0.09 g silver benzoate powder was dissolved in 9 mL of n-methyl-2-pyrrolidone to form a silver benzoate solution at 10 g L^{-1}. Also, a gallic acid solution at 50 g L^{-1} was prepared by dissolving 0.05 g of gallic acid in 1 mL n-methyl-2-pyrrolidone. Then, the silver benzoate solution was slowly added to the gallic acid solution at a volumetric ratio of 9:1. The pH value of the mixed solution was adjusted to 11 by using a NaOH aqueous solution at 0.1 M. This final solution with silver nanoparticles at a theoretical concentration of 4.24 g L^{-1} was used for further impregnations in kaolin hollow fibers.

4.2.3. Production of hollow fiber ceramic membranes

The ceramic suspension was prepared according to the procedure described by Hubadillah et al. (2017). The additive (Arlacel) (1 wt%) was dissolved in the of solvent (n-methyl-2-pyrrolidone (NMP)) (57 wt%) followed by the addition of the kaolin powder (36 wt%). The ceramic suspension was stirred in a ball mill (QUIMIS, model Q298-2) for 48 h at a rotation speed of 150 rpm. Then, the polymer (PESf) (6 wt%) was added to the ceramic suspension, which was ball milled for another 48 h at a rotation speed of 150 rpm.

Hollow fibers were produced by the phase inversion/sintering technique following the methodology described by Kingsbury and Li (2009). Before extrusion, the ceramic suspension was degassed using a vacuum pump (Prismatec, 122 BCP, Brazil) at 850 mmHg for approximately 2 h for air removal. The ceramic suspension was then extruded through a home-made stainless steel spinneret (outer diameter of 3 mm, inner diameter of 1.2 mm, Figure 1), falling into a tap water bath with an air gap distance of 5 cm. Flow rates of 15 and 25 mL min^{-1} were applied for the ceramic suspension and the internal coagulant (deionized water), respectively. Flow rates were controlled using two individual pumps (Harvard Apparatus, model XHF). Figure 1 presents a scheme of the extrusion process for hollow fiber production.

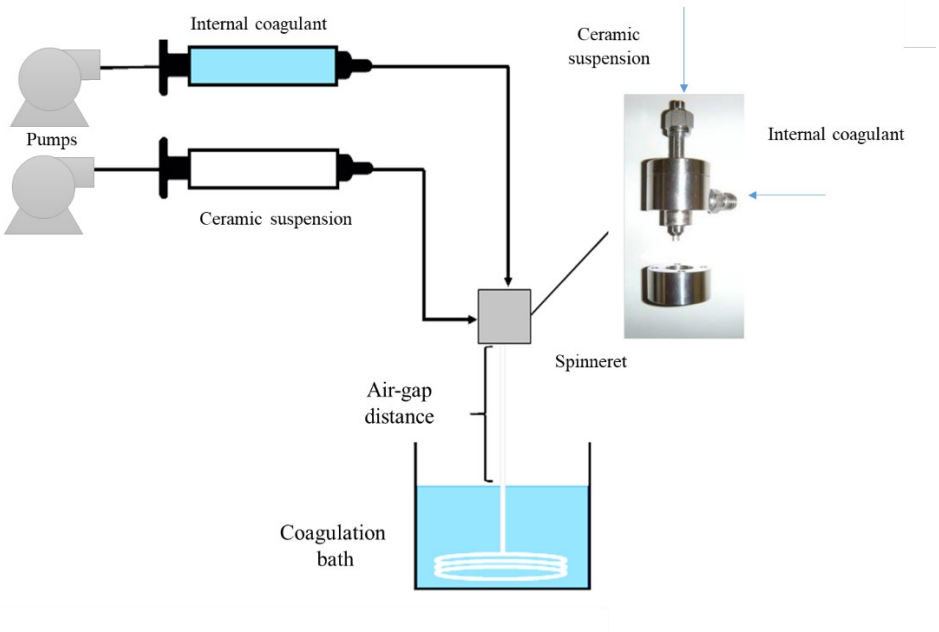

Figure 1. Flow scheme of the extrusion process to produce ceramic hollow fibers.

The precursor hollow fibers were left in the coagulating bath for 48 h to complete the phase inversion, and were then manually cut to the desired length. The fibers were dried at room temperature (approximately 25°C) for 48 h followed by a sintering process in a tubular furnace (Carbolite, model TZF 15) at 1150 °C (Magalhães et al., 2020). The temperature ramp was programmed according to the values presented by Bessa et al. (2017). The temperature was first increased from room temperature (25 °C) a rate of 2 °C/min to 300 °C. A second temperature ramp was programmed from 300 to 600 °C a rate of 1 °C/min with dwell time of 60 min. At this stage, the polymer is removed from the fiber precursor. The fiber is sintered at the third temperature ramp, from 600 to 1150 °C a rate of 10 °C/min with dwell time of 5 h Finally, the samples were cooled to room temperature at a rate of 2 °C/min.

4.2.4. Impregnation of AgNPs in the kaolin hollow fibers

AgNPs were impregnated in the lumen side of the produced asymmetric kaolin hollow fibers according to the methodology proposed by Costa et al. (2019). Figure 2 presents a flow scheme of the impregnation process. The individual fiber of 5 cm length was connected to a flexible plastic tube, which was coupled to a syringe. The fiber end side was sealed with PTFE tape. Then, 10 mL of the AgNP dispersion was manually injected to the fiber lumen side. The injection was repeated for approximately 10 times. After AgNP impregnation, the fiber was

dried at 50 °C for 12 h. The loading of AgNPs in the fiber was obtained by measuring the mass of the dried fiber before and after impregnation.

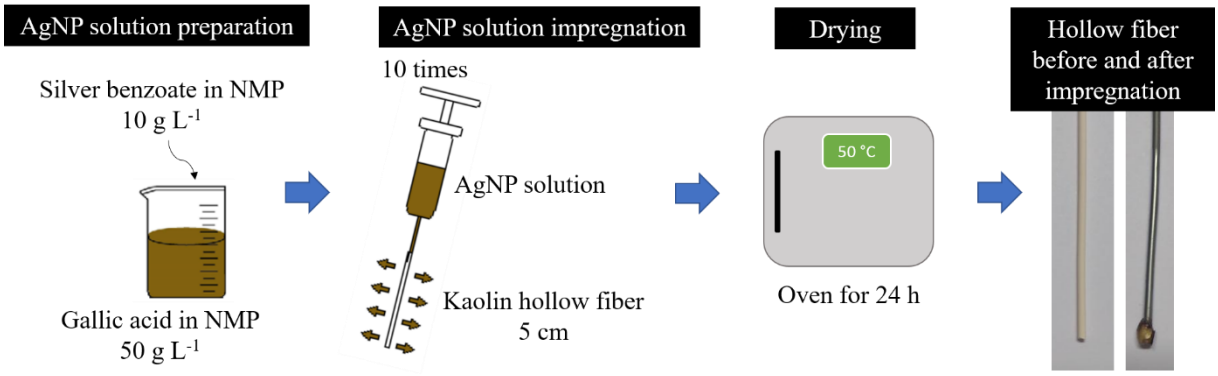

Figure 2. Flow scheme of the AgNPs impregnation in kaolin hollow fibers.

4.2.5. Membrane filtrations of bacteria suspensions

Individual bacterial suspensions with *E. cloacae* and *E. coli* were prepared at concentrations of $7.72 \times 10^7 \pm 1.78 \times 10^7$ and $4.8 \times 10^8 \pm 2.83 \times 10^6$ CFU mL^{-1} (colony forming units per mL), respectively. Both bacterial suspensions were prepared in aqueous NaCl solutions at 0.9 vol%. The bacterial suspensions were then filtered through pristine and AgNP-impregnated kaolin hollow fibers. Filtration experiments were carried out in triplicate and results are presented with standard deviations. For dead-end filtrations, the ceramic membranes with a filtration area of 1.68×10^{-5} m^2 were glued in a plastic tube, which as connected to a nitrogen gas cylinder for the pressurization of the membrane module. The bacterial suspension was flowed from the feed tank to the membrane lumen side at a transmembrane pressure of 100 kPa. A manometer was used for pressure verifications. Filtrations were carried out at room temperature (approximately 25°C).

Bacterial concentrations in permeate and feed suspensions were determined by enumeration of CFU. Sample volumes of 0.1 mL were aseptically pipetted on agar plates and overnight incubated at 37 °C (Boczek et al., 2014). The average percent of bacterial rejection (R) was estimated according to Equation 1.

$$R = \left(1 - \frac{C_p}{C_f}\right) 100 \qquad (1)$$

where C_f is the bacterial concentration in the feed stream (CFU mL^{-1}) and C_p is the bacterial concentration in the permeate stream (CFU mL^{-1}).

The log_{10} reduction value (LRV) was calculated according to Equation 2.

$$LRV = log_{10}(C_f) - log_{10}(C_p) \quad (2)$$

During filtrations, the permeate flow was recorded according to the filtration time. Experimental flux data were then adjusted to model proposed by Hermia (1982) (Equation 3) in order to describe fouling mechanisms.

$$-\frac{dJ}{dt} = k\ A^{2-n}\ J^{3-n} \quad (3)$$

where J is the permeate flux (L h^{-1} m^{-2}), t is the filtration time (h), A is the membrane area (m^2) and k is an adjusted parameter. The parameter "n" indicates the fouling mechanism, as follows: n = 0 for cake filtration, n = 1 for partial pore blocking, n = 1.5 for internal pore blocking and n = 2 for complete pore blocking.

Equations (4) to (7) represent the ingratiated form of Equation 3 for each fouling mechanism.

Cake filtration (n=0): $J = \frac{J_0}{(1+J_0 kt)^{1/2}}$ (4)

Partial pore blocking (n = 1): $J = \frac{J_0}{1+J_0 kt}$ (5)

Internal pore blocking (n = 1.5): $J = \frac{J_0}{(1+J_0^{0.5} kt)^2}$ (6)

Complete pore blocking (n = 2): $J = J_0 \exp(-kt)$ (7)

where J_0 is the initial permeate flux (L h^{-1} m^{-2}).

The Levenberg-Marquart algorithm was applied to solve the non-linear equations. Values of correlation coefficient (R^2) were considered to verify the adjustment of experimental flux data to the proposed equations.

4.2.6. Characterizations

4.2.6.1. Silver nanoparticles

Ultraviolet-Visible Spectroscopy (UV–vis) method was used to verify the stability of the produced AgNPs (de Oliveira et al., 2019). An UV–vis Shimadzu UV-1280

spectrophotometer was used at a wavelength range of 300–600 nm. The synthetized AgNPs were also characterized by transmission electron microscopy (TEM). A transmission electron microscope (TEM, Hitachi model HT7700) was used to obtain TEM images and the AgNP samples were deposited on Copper 200 mesh grids which were coated with carbon or silicon monoxide films. The hydrodynamic diameter (size), the polydispersity index (PDI) and the zeta potential of the synthetized nanoparticles were measured in a DLS-based instrument (Litesizer 500, Anton Paar).

4.2.6.2. Kaolin hollow fibers

The produced hollow fibers were characterized in terms of their morphology, porosity, water permeability and mechanical resistance. Morphological analyses of pristine and AgNP-impregnated kaolin hollow fibers were performed using a scanning electron microscope (SEM, Carl Zeiss, model EVO MA10, Carl Zeiss). Qualitative elemental composition of the produced fibers was analyzed by energy dispersive spectroscopy (EDS, Oxford, model 51 - ADD0048). The pore structure and porosity of the kaolin hollow fiber were investigated by mercury intrusion porosimetry (MIP, Autopore IV 9500, Micrometrics) at a pressure range between 1.41 and 225221.51 kPa. The water permeability through the produced hollow fibers was measured at different transmembrane pressures and at room temperature (approximately 25 °C). For mechanical strength, the three-point bending test was performed using an Instron Model 9600 attached to a 5 kN cell and using hollow fibers with a length of 3 cm (Magalhães et al., 2020).

4.3. RESULTS AND DISCUSSION

4.3.1. Characterisitics of the synthetized AgNP suspensions

The antimicrobial activity of AgNPs is greatly influenced by the particle sizes, shapes and zeta potentials and, thus, a proper physicochemical characterization of the synthesized AgNPs are required (Panáček et al., 2006). The AgNP particles were synthetized by the chemical route with gallic acid, which caused the production of a ketoenol-system. This ketoenol-system is adsorbed on the silver nanoparticle surface and provides the stabilization of the particles in the suspension (Wang et al., 2007). The UV/Vis spectra of the AgNP suspension (Figure 3a) presents a broad and centered peak at 400 nm, which is an indicative of the formation of silver nanoparticles (Shen et al., 2021).

The AgNP particles presented a spherical and pseudospherical geometry, with sizes ranging from 28 to 380 nm, as presented in Figure 3b. Prihandana et al. (2022) compared the bacterial efficiency of polymeric membranes impregnated with silver nanoparticles of sizes varying from 20 to 210 nm and suggested the use of the smallest silver particles in order to maximize the contact of the silver particle with the bacteria. Thus, additional improvements in the synthesis of silver nanoparticles should be suggest to obtain particles of reduced sizes. According to DLS analyses (Figure 3c), the average hydrodynamic size of the AgNPs was determined as 81.71 ± 8.05 nm, which is quite equivalent to the size estimated from the TEM image. Similar values of hydrodynamic diameters are reported in the literature for AgNPs produced from different chemical routes (Guzmán et al., 2019; Khan et al., 2020; Lunkov et al., 2020; Szerencsés et al., 2020). Based on the particle size distribution, the polydispersity index (PDI) is a measure of the sample heterogeneity and, according to International Standards Organizations (ISOs), monodisperse samples present PDI values lower than 0.05, while polydisperse samples, with a broad size distribution of particles, present PDI values greater than 0.7 (Mudalige et al., 2019). The polydispersity index of the AgNPs was determined as 0.262 ± 0.012, which indicates the sample has a reasonable dispersion. The observed broad peak in the UV/Vis spectra (Figure 3a) is also an indicative that the nanoparticles are polydisperse (Barbhuiya et al., 2022). The zeta potential of the AgNP suspension (Figure 3d) was measured in order to indicate the surface charge potential and the AgNP stability in the aqueous suspension. The produced nanoparticles presented a negatively charged surface with zeta potential of -20.7 ± 2.6 mV. Thus, carboxyl groups with negative charges were attached to the nanoparticle surface, which guarantees the electrostatic repulsion of NPs in the solution and the consequent suspension stability.

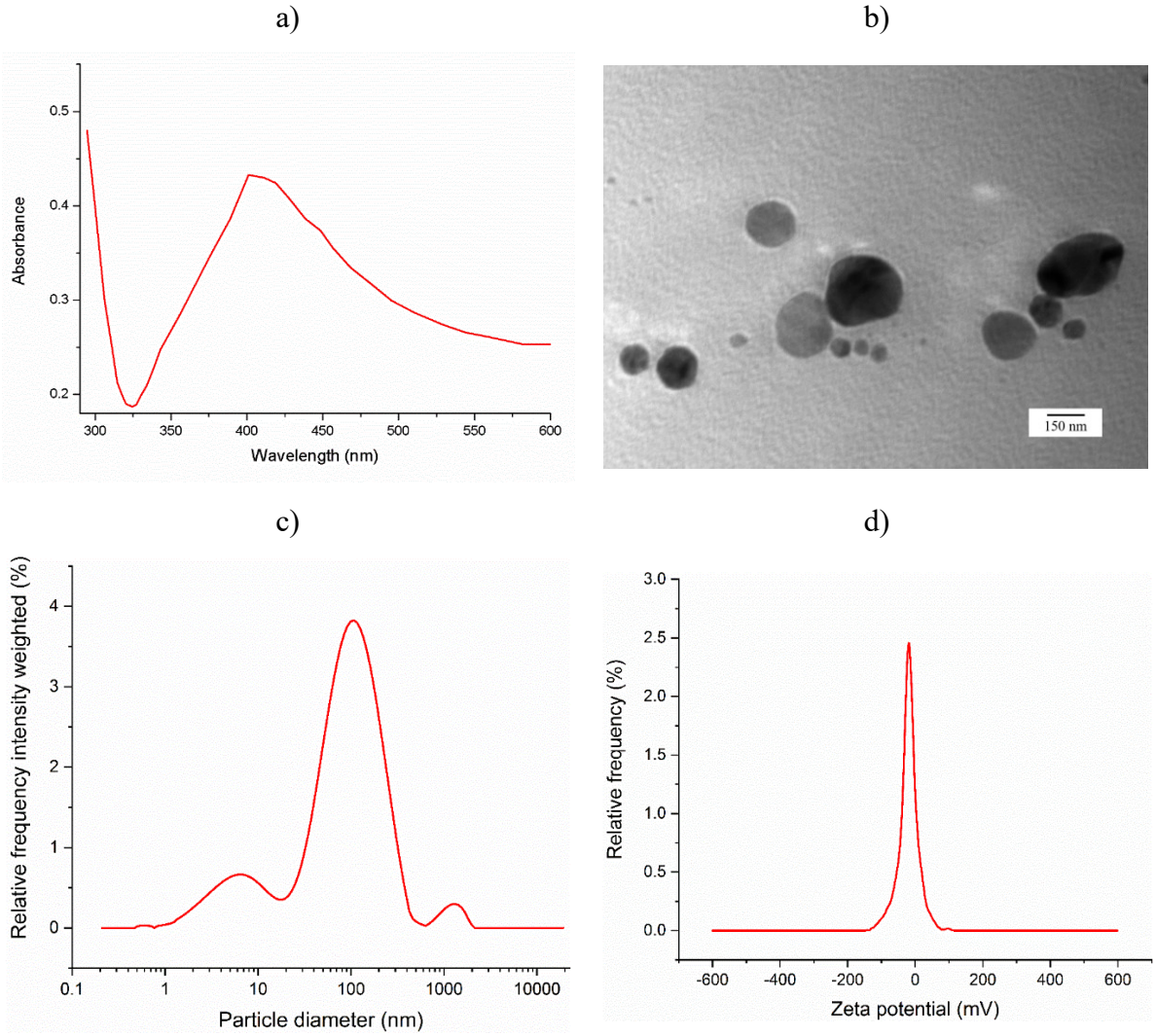

Figure 3 – (a) UV/Vis spectra, (b) TEM image, (c) size distribution and (d) zeta potential distribution of the synthesized AgNPs.

4.3.2. Characteristics of the kaolin hollow fiber membrane

Figure 4 presents SEM images of the produced kaolin hollow fiber. The produced kaolin hollow fiber presented a finger like region at the lumen side. The formation of micro-voids at the finger like region is caused by interfacial instabilities due to the density, viscosity and composition differences between the ceramic suspension and the internal coagulant fluid (Lee et al., 2015). Thus, the contact of the ceramic suspension with the internal coagulation caused the polymer precipitation, and micro-voids were formed to compose the finger like region. These micro-voids presented the desired morphology for the impregnation of silver nanoparticles. On the other hand, the air-gap of 5 cm between the spinneret and the external

coagulation bath promoted the densification of the ceramic suspension, so that a sponge like layer was observed in the outer layer of the hollow fiber. The sponge like layer accounts for approximately 60% of the fiber extension. The sponge like layer is mainly responsible for the fiber mechanical strength and also for the membrane selectivity. The coagulant flow rate at 25 mL min^{-1} resulted in a fiber with a regular internal contour, as observed in the SEM image. Similar results were reported by Magalhães et al. (2020) for kaolin hollow fibers produced at different extrusion conditions.

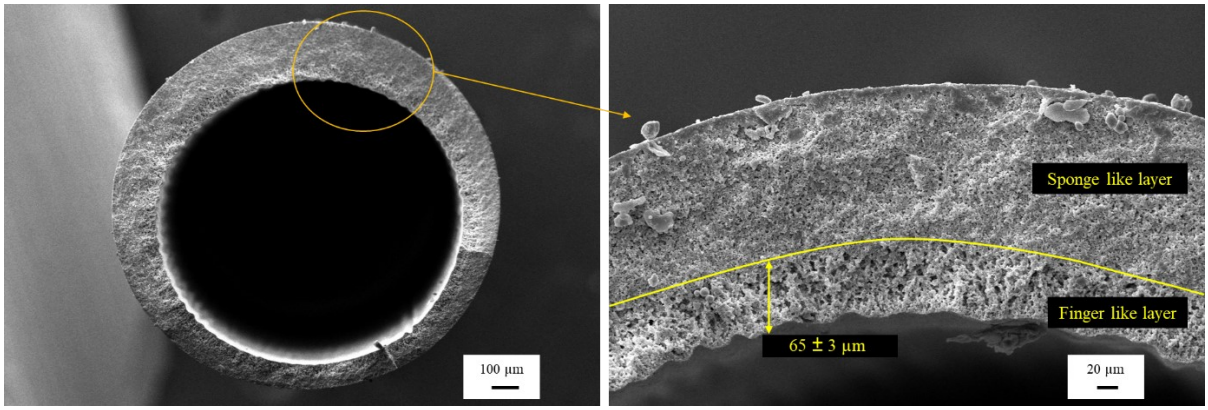

Figure 4 – Cross-section SEM images of the kaolin hollow fiber sintered at 1150 °C.

The pore structure of the kaolin hollow fiber was evaluated by the mercury intrusion technique, as shown in Figure 5. The pore size distribution of the kaolin fiber presented 3 major peaks, which correspond to the pore sizes in the finger- and in the sponge-like layers. As presented in SEM images (Figure 4), the opened micro-channels in the finger like layer presented larger pore sizes than the packed pore-network in the sponge like layer. According to the mercury intrusion analysis, the lowest pore sizes were measured between 1.14 and 2.16 µm (Figure 5), which correspond to the packed pore-network at the sponge like layer region. The peaks centered at 7.86 and 9.17 µm designates the pore size of the opened micro-channels (Figure 5). Similar behavior was reported in the literature for the pore size distribution of ceramic hollow fibers (Bindes et al., 2020; Kingsbury and Li, 2009). Magalhães et al. (2020) produced kaolin hollow fibers that presented a sponge like layer with pore sizes of approximately 1.5 µm and a finger like layer with micro-voids of 5.3 µm. The alumina hollow fiber produced by Gil et al. (2015) presented a peak of the packed-pore network located between 0.1 and 0.3 µm, while the peak related to the micro-voids was located between 6 and 10 µm.

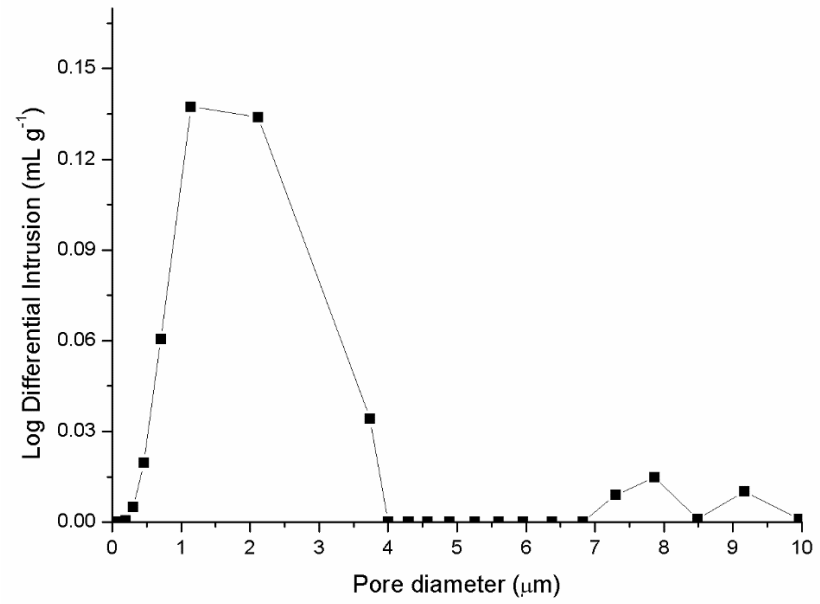

Figure 5 - Pore size distribution of the kaolin fiber sintered at 1150 °C.

The water permeability of the produced kaolin fiber was 8.459± 0.170 L $h^{-1} \cdot m^{-2} \cdot kPa^{-1}$, as presented in Figure 6. According to the Darcy's low, the hydraulic permeability is taken as the angular coefficient of the linear adjustment between water flux and transmembrane pressure, with linear intercept equals to zero (Terra et al., 2018). The water permeability of the produced kaolin hollow fibers is quite similar to the values reported by Sharma et al. (Sharma et al., 2017) for a kaolin-based membrane sintered at 950 °C, which presented water permeability of 12.96 L $h^{-1} \cdot m^{-2} \cdot kPa^{-1}$. The kaolin hollow fiber presented bending strength of 103.58 ± 14.41 MPa, indicating that the kaolin fibers have suitable mechanical resistance for pressure driven filtrations. Terra et al. (2016) reported that the mechanical resistance of asymmetric alumina hollow fibers sintered at 1400 °C was 74.5 MPa.

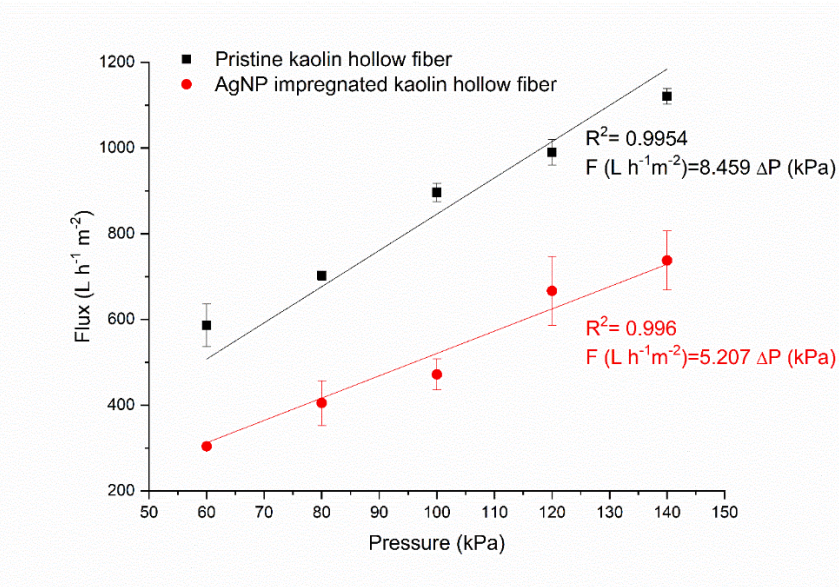

Figure 6. Water fluxes through the pristine and AgNP impregnated kaolin hollow fibers according to the transmembrane pressure.

4.3.3. Characteristics of the kaolin hollow fibers impregnated with AgNPs

According to EDS images (Figure 7), the pristine kaolin hollow fibers are composed by oxygen, aluminum and silicon compounds, which are related to the kaolin material ($Al_2Si_2O_5(OH)_4$). After impregnation, AgNPs were mainly observed in the fiber inner surface, although some silver particles were also verified throughout all the fiber extension at a regular distribution (Figure 8). The small particle size of the AgNPs promoted their impregnation in the fiber micro-voids and in the sponge like layer. After 10 injections of 10 mL of the AgNP suspension through a 5 cm length hollow fiber, the measured mass of impregnated AgNPs was 0.51 ± 0.04 mg cm^{-1}. Theoretically, the silver concentration in the AgNP suspension is 4.24 mg mL^{-1}. Thus, based on the ratio between the impregnated silver mass and the actual silver mass in the suspension, the impregnation efficiency was of 6.01%. There is a limit for the loading amount of silver because the nanoparticles need to penetrate into the pores of the substrate. Also, other automatic pressure driven injection methods may be suggested to improve the impregnation efficiency. Xia et al. (2015) evaluated the impregnation of calcium carbonate nanoparticles in kenaf fibers and reported an impregnation efficiency of 15.7%.

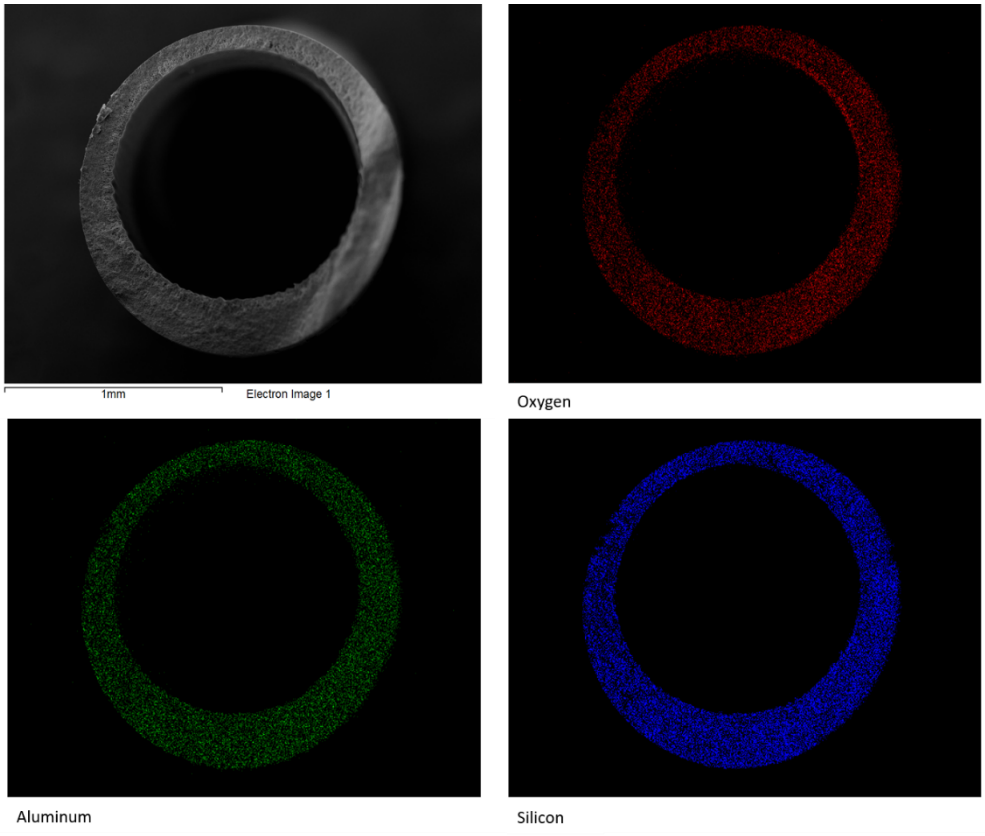

Figure 7 - EDS images of the kaolin hollow fiber before AgNP impregnation.

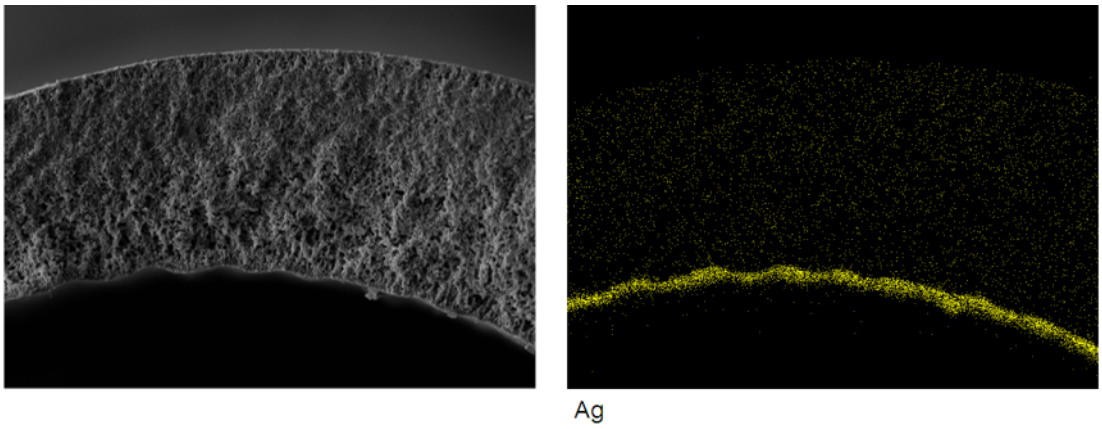

Figure 8 - EDS images of the kaolin hollow fiber after AgNP impregnation.

The water permeability of the kaolin hollow fiber after AgNP impregnation was 5.207 ± 0.320 L $h^{-1} \cdot m^{-2} \cdot kPa^{-1}$, as presented in Figure 6. Thus, the water permeability of the pristine kaolin hollow fiber was reduced in 38.30% after AgNP impregnation. This reduction was

probably related to the formation of a selective layer of AgNPs in the fiber lumen side in addition to the decrease in the fiber porosity after AgNP impregnations.

4.3.4. Bacteria removal by membrane filtration

Bacteria suspensions with *E. cloacae* and *E. coli* were subjected to filtrations using kaolin hollow fiber membranes with and without AgNPs. Table 1 presents the bacterial concentrations (CFU mL^{-1}) of feed and permeate samples.

Table 4.1 – Bacterial concentration, average percent bacterial rejection (R) and $\log_{10}$ reduction value (LRV) of feed and permeate samples.

Bacteria	Kaolin membrane	Bacterial concentration (CFU mL^{-1})		R (%)	LRV
		Feed	Permeate		
E. cloacae	Without AgNPs	$7.72x10^7 \pm 1.78x10^5$	$2.64x10^5 \pm 3.11x10^4$	99.66 ± 0.04	2.47 ± 0.05
	With AgNPs		$3.20x10^3 \pm 3.13x10^4$	99.99 ± 0.04	4.38 ± 0.83
E. coli	Without AgNPs	$4.80x10^8 \pm 2.83x10^6$	$9.11x10^4 \pm 2.26x10^4$	99.98 ± 0.00	3.72 ± 0.13
	With AgNPs		$2.10x10^4 \pm 8.27x10^3$	99.99 ± 0.00	4.35 ± 0.25

The kaolin hollow fiber membranes with and without AgNPs were efficient for *E. cloacae* and *E. coli* removals from aqueous solutions. Size-exclusion and sorption were probably the main mechanisms for the bacterial removal by the pristine kaolin hollow fibers (Kallman et al., 2011). Both *E. cloacae* and *E. coli* bacteria are gram-negative, rod-shaped with peritrichous and present sizes of 1.1–1.5 μm wide by 2–6 μm long. Thus, values of average percent bacteria rejection were similar for both bacteria. Simonis and Basson (2011) used lithium alumina-silicate ceramic membranes and showed that the membrane provided a $\log_{10}$ reduction value (LRV) of 5.5, 4.2, and 3.6 for *E. coli*, *Streptococcus feacalis* and *Bacillus cereus*, respectively. Magalhães et al. (2020) also showed that ceramic membranes were efficient to remove the *E. cloacae* bacteria from an aqueous suspension.

The addition of AgNPs in the kaolin hollow fibers improved the membrane performance for bacterial removal. The $\log_{10}$ reduction values for both bacteria are almost twice higher with the AgNPs than with the pristine kaolin hollow fibers (Table 1). The pristine kaolin hollow fibers reached bacterial removals of 99%, and the kaolin membranes with AgNPs were able to improve the bacterial removal to 99.99%. This improvement is significant since the primary drinking water standards and other health-based standards establish that the concentration of

bacteria in water should be absence. The AgNPs have electrostatic interactions to the negatively charged cells of the bacteria, causing oxidative stress and bacteria death (Vohra et al., 2006). The AgNPs impair the key functions of the bacterium cells, such as enzymatic regulation, respiratory processes and its metabolic reactions (Dimapilis et al., 2018; Feng et al., 2018; Xiang et al., 2017). Chaukura et al. (2020) also showed that ceramic filters impregnated with silver nanoparticles removed 100% of *E. coli from aqueous suspensions*. Also, the membrane hydraulic permeability was reduced after AgNP impregnations, as presented in Figure 6, which suggests the porosity of the fiber was probably reduced after AgNP impregnations. Thus, the improvement in the bacterial retention by the membrane after AgNP impregnations is probably related to the synergistic effects of electrostatic interaction of silver and reduction in the membrane pore size.

The impair of AgNPs on the fouling mechanisms during membrane filtration is an important feature to be evaluated, since the addition of a bacteriostatic skin layer deactivates the growth of the bacterial film on the membrane surface and blockages the bacteria passage to the permeate stream (Kaniganti et al., 2014). Figures 9 and 10 present the flux declines through pristine and AgNP-impregnated kaolin hollow fibers for filtrations of *E. cloacae* and *E. coli* aqueous suspensions, respectively. Experimental flux values were also adjusted to the model proposed by Hermia (1982) in order to investigate the fouling mechanisms.

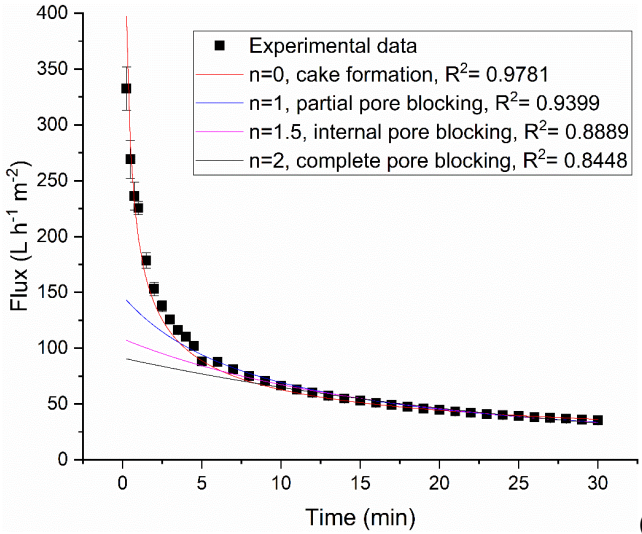

(a)

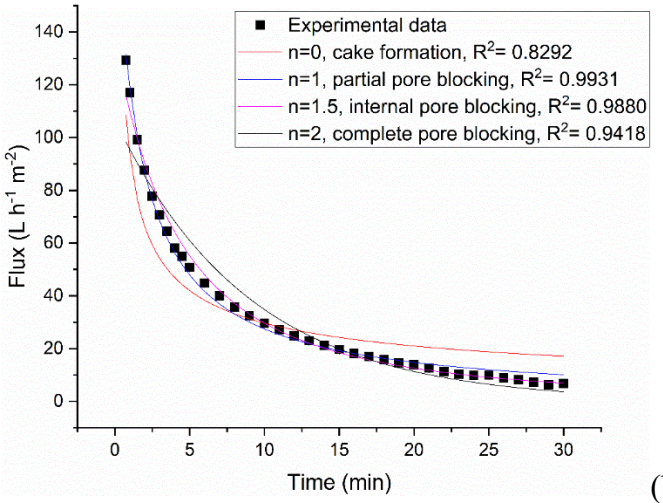

(b)

Figure 9 - Permeate fluxes of *E. cloacae* bacteria suspensions through (a) pristine and (b) AgNP-impregnated kaolin hollow fibers.

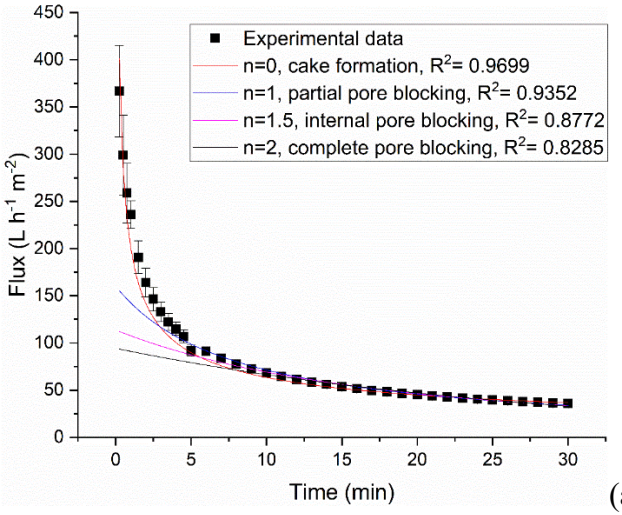

(a)

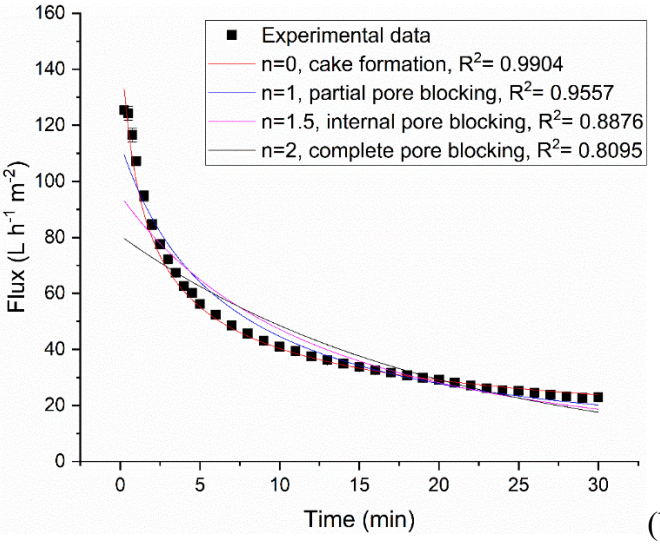

(b)

Figure 10 - Permeate fluxes of *E. coli* bacteria suspensions through (a) pristine and (b) AgNP-impregnated kaolin hollow fibers (n = 0 for cake filtration; n = 1 for partial pore blocking; n = 1.5 for internal pore blocking and n = 2 for complete pore blocking).

The initial fluxes through the pristine membranes in both filtrations were approximately twice greater than through the membranes impregnated with AgNPs. After 30 min of filtration of the *E. cloacae* suspension (Figure 9), the fluxes through pristine and AgNP-impregnated membranes were 35.18±0.24 and 6.78±0.52 L $h^{-1}m^{-2}$, respectively. For the *E. coli* suspension (Figure 10), the stabilized flux was achieved after 30 min of filtration and were of 35.62±0.24 and 22.90±0.42 L $h^{-1}m^{-2}$ for pristine and AgNP-impregnated membranes, respectively. Thus, the impregnation of AgNPs decreased the permeate flux through the membrane. For the experiments with both bacteria, there was a pronounced flux decline during the first minutes of filtration. This decrease was probably due to fouling occurrences during the filtration processes. Figures 9 and 10 present the correlation coefficient (R^2) for the adjustment of each fouling mechanism to experimental flux data for filtrations of *E. cloacae* and *E. coli* aqueous suspensions, respectively.

As presented in Figures 9a and 10a, the best adjustment between calculated and experimental data for filtrating the *E. cloacae* and *E. coli* suspensions through the pristine kaolin hollow fibers was the cake formation. Kaniganti et al. (2014) showed that cake formation was the main fouling occurrence during filtrations of *E. coli* suspensions at initial concentrations of 10^6 CFU/mL through low-cost ceramic membranes. When a bacteriostat layer of silver nanoparticles was deposited on the membrane, cake formation was not more the main fouling occurrence for the filtration of the *E. cloacae* suspension (Figure 9b). Partial and internal pore blocking were the main fouling mechanism during the filtration of the *E. cloacae* suspension through the AgNP-impregnated kaolin hollow fiber. Thus, the AgNP acted to mitigate the cake formation of the membrane surface. However, cake formation was still the main fouling mechanism for the filtration of the *E. coli* suspension through the AgNP- impregnated kaolin hollow fiber (Figure 10b). In this cake, the bacteriostat layer of silver nanoparticles was probably not enough to mitigate the cake formation due to the relatively high initial concentration of the *E. coli* bacteria in the suspension. Kaniganti et al. (2014) also showed the fouling mechanism is changed when the initial bacterial concentration changes from 10^7 to 10^5 CFU/mL.

The detachment of silver nanoparticles from the kaolin hollow fiber is a concern related to the filtration efficiency and to the quality of the produced water. However, none silver detachment was observed after the filtration processes. Silver is water insoluble under normal condition. After filtration, the water samples were centrifuged at 8000 rpm for 30 min and none decanted particles were observed. EDS images (Figure 11) were also verified after filtration of the aqueous solution with *E. coli*, which show that the AgNPs remained in the fiber inner surface and through all the fiber extension at regular distribution. Thus, the AgNPs remained adhered in the fiber after filtrations.

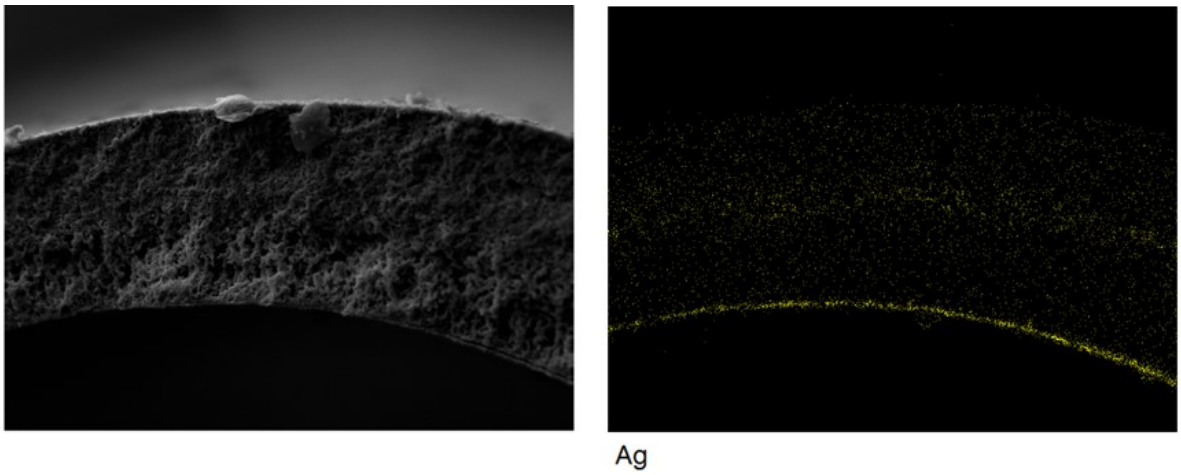

Figure 11 - EDS image of the AgNP kaolin hollow fiber after filtration of the aqueous solution with *E. coli*.

4.4. CONCLUSIONS

Ceramic hollow fiber membranes with asymmetric pore size distribution were produced using kaolin as starting material. Silver nanoparticles were successful synthetized and impregnated in the hollow fiber lumen side by a simple dip-coating filtration assisted method. Both membranes, with and without silver nanoparticles, showed almost 100% of bacterial removal from water suspensions. However, the kaolin hollow fiber impregnated with silver nanoparticles presented higher values of log10 reduction for both E. cloacae and E. coli bacteria than the pristine kaolin hollow fiber membrane. Filtrations of bacteria suspension through the kaolin hollow fiber impregnated with silver nanoparticles presented lower permeate flux than through the pristine kaolin hollow fiber. However, the deposited bacteriostatic layer of silver nanoparticles mitigated the formation of a cake layer on the membrane surface depending on the initial bacterial concentration.

4.5. REFERENCES

BARBHUIYA, R. I. et al. Ultrasound-assisted rapid biological synthesis and characterization of silver nanoparticles using pomelo peel waste. **Food Chemistry**, [s. l.], v. 385, p. 132602, 2022. Disponível em: https://www.sciencedirect.com/science/article/pii/S0308814622005647.

BEHBOUDI, A.; JAFARZADEH, Y.; YEGANI, R. Incorporation of silica grafted silver nanoparticles into polyvinyl chloride/polycarbonate hollow fiber membranes for pharmaceutical wastewater treatment. **Chemical Engineering Research and Design**, [s. l.], v. 135, p. 153–165, 2018. Disponível em: https://www.sciencedirect.com/science/article/pii/S0263876218301333.

BESSA, L. P. et al. Macro-porous dolomite hollow fibers sintered at different temperatures toward widened applications. **Ceramics International**, [s. l.], v. 43, n. 18, p. 16283–16291, 2017. Disponível em: http://dx.doi.org/10.1016/j.ceramint.2017.08.214.

BINDES, M. M. M. et al. Asymmetric Al2O3 and PES/Al2O3 hollow fiber membranes for green tea extract clarification. **Journal of Food Engineering**, [s. l.], v. 277, p. 109889, 2020. Disponível em: http://www.sciencedirect.com/science/article/pii/S0260877419305321.

BOCZEK, L. A.; RICE, E. W.; JOHNSON, C. H. Total Viable Counts: Spread Plate Technique. Second Edied. [S. l.]: Elsevier, 2014. v. 3 E-book. Disponível em: http://dx.doi.org/10.1016/B978-0-12-384730-0.00331-1.

CHAUKURA, N. et al. Development and evaluation of a low-cost ceramic filter for the removal of methyl orange, hexavalent chromium, and Escherichia coli from water. **Materials Chemistry and Physics**, [s. l.], v. 249, p. 122965, 2020. Disponível em: https://www.sciencedirect.com/science/article/pii/S0254058420303412.

COSTA, I. G. F. et al. Photoreduction of chromium(VI) in microstructured ceramic hollow fibers impregnated with titanium dioxide and coated with green algae Chlorella vulgaris. **Journal of Hazardous Materials**, [s. l.], v. 379, n. June, 2019.

DE OLIVEIRA, L. R. et al. Experimental study on the thermal conductivity and viscosity of ethylene glycol-based nanofluid containing diamond-silver hybrid material. **Diamond and Related Materials**, [s. l.], v. 96, n. December 2018, p. 216–230, 2019. Disponível em: https://doi.org/10.1016/j.diamond.2019.05.004.

DIMAPILIS, E. A. S. et al. Zinc oxide nanoparticles for water disinfection. Sustainable **Environment Research**, [s. l.], v. 28, n. 2, p. 47–56, 2018. Disponível em: https://www.sciencedirect.com/science/article/pii/S2468203917300560.

FENG, T. et al. Bactericidal activity and mechanisms of BiOBr-AgBr under both dark and visible light irradiation conditions. **Colloids and Surfaces B: Biointerfaces**, [s. l.], v. 167, p. 275–283, 2018. Disponível em: https://www.sciencedirect.com/science/article/pii/S0927776518302261.

GIL, A. G. et al. A highly permeable hollow fibre substrate for Pd/Al2O3 composite membranes in hydrogen permeation. **International Journal of Hydrogen Energy**, [s. l.], v. 40, n. 8, p. 3249–3258, 2015. Disponível em: https://www.sciencedirect.com/science/article/pii/S0360319915000580.

GOSWAMI, K. P.; PUGAZHENTHI, G. Credibility of polymeric and ceramic membrane filtration in the removal of bacteria and virus from water: A review. **Journal of environmental management**, [s. l.], v. 268, n. March, p. 110583, 2020. Disponível em: https://doi.org/10.1016/j.jenvman.2020.110583.

GUZMÁN, K. et al. Ultrasound-assisted synthesis and antibacterial activity of gallic acid-chitosan modified silver nanoparticles. **Progress in Organic Coatings**, [s. l.], v. 129, p. 229–235, 2019. Disponível em: https://www.sciencedirect.com/science/article/pii/S0300944018307215.

HARABI, A. et al. A new and economic approach to fabricate resistant porous membrane supports using kaolin and CaCO3. **Journal of the European Ceramic Society**, [s. l.], v. 34, n. 5, p. 1329–1340, 2014. Disponível em: https://www.sciencedirect.com/science/article/pii/S095522191300513X.

HERMIA, J. Constant Pressure Blocking Filtration Laws - Application to Power-Law Non-Newtonian Fluids. Icheme, [s. l.], v. 60, p. 183–187, 1982.

HUBADILLAH, S. K. et al. Superhydrophilic, low cost kaolin-based hollow fibre membranes for efficient oily-wastewater separation. **Materials Letters**, [s. l.], v. 191, p. 119–122, 2017. Disponível em: http://dx.doi.org/10.1016/j.matlet.2016.12.099.

KALLMAN, E.; OYANEDEL-CRAVER, V.; SMITH, J. Ceramic Filters Impregnated with Silver Nanoparticles for Point-of-Use Water Treatment in Rural Guatemala. **Journal of Environmental Engineering**, [s. l.], v. 137, p. 407–415, 2011.

KANIGANTI, C. M. et al. Microfiltration of Synthetic Bacteria Solution Using Low Cost Ceramic Membranes. **Separation Science and Technology**, [s. l.], v. 50, n. 1, p. 121–135, 2014. Disponível em: https://doi.org/10.1080/01496395.2014.949772.

KHAN, M. et al. Green synthesis of controlled size gold and silver nanoparticles using antioxidant as capping and reducing agent. **Colloid and Interface Science Communications**, [s. l.], v. 39, p. 100322, 2020. Disponível em: https://www.sciencedirect.com/science/article/pii/S2215038220301023.

KINGSBURY, B. F. K.; LI, K. A morphological study of ceramic hollow fibre membranes. **Journal of Membrane Science**, [s. l.], v. 328, n. 1–2, p. 134–140, 2009.

LEE, M. et al. Formation of micro-channels in ceramic membranes - Spatial structure, simulation, and potential use in water treatment. **Journal of Membrane Science**, [s. l.], v. 483, p. 1–14, 2015.

LUNKOV, A. et al. Synthesis of silver nanoparticles using gallic acid-conjugated chitosan derivatives. **Carbohydrate Polymers**, [s. l.], v. 234, p. 115916, 2020. Disponível em: https://www.sciencedirect.com/science/article/pii/S0144861720300904.

MAGALHÃES, F. de S. et al. Fabrication of kaolin hollow fibre membranes for bacteria removal. **Processing and Application of Ceramics**, [s. l.], v. 14, n. 4, p. 303–313, 2020.

MESTRE, S. et al. Low-cost ceramic membranes: A research opportunity for industrial application. **Journal of the European Ceramic Society**, [s. l.], v. 39, n. 12, p. 3392–3407, 2019. Disponível em: https://www.sciencedirect.com/science/article/pii/S0955221919302134.

MOCANU, A. et al. Antimicrobial properties of polysulfone membranes modified with carbon nanofibers and silver nanoparticles. **Materials Chemistry and Physics**, [s. l.], v. 223, n. October 2018, p. 39–45, 2019.

MUDALIGE, T. et al. Chapter 11 - Characterization of Nanomaterials: Tools and Challenges. In: LÓPEZ RUBIO, A. et al. (org.). **Micro and Nano Technologies**. [S. l.]: Elsevier, 2019. p. 313–353. E-book. Disponível em: https://www.sciencedirect.com/science/article/pii/B9780128141304000117.

MURUGESAN, A. K. et al. Facile green synthesis and characterization of Gloriosa superba L. tuber extract-capped silver nanoparticles (GST-AgNPs) and its potential antibacterial and anticancer activities against A549 human cancer cells. **Environmental Nanotechnology,**

Monitoring & Management, [s. l.], v. 15, p. 100460, 2021. Disponível em: https://www.sciencedirect.com/science/article/pii/S2215153221000350.

MUSICO, Y. L. F. et al. Surface modification of membrane filters using graphene and graphene oxide-based nanomaterials for bacterial inactivation and removal. **ACS Sustainable Chemistry and Engineering**, [s. l.], v. 2, n. 7, p. 1559–1565, 2014.

OWA, F. W. Water Pollution: Sources, Effects, Control and Management. **International Letters of Natural Sciences**, [s. l.], v. 8, p. 1–6, 2014.

PANÁČEK, A. et al. Silver Colloid Nanoparticles: Synthesis, Characterization, and Their Antibacterial Activity. **The Journal of Physical Chemistry B**, [s. l.], v. 110, n. 33, p. 16248–16253, 2006. Disponível em: https://doi.org/10.1021/jp063826h.

PRAVEENA, S. M.; ARIS, A. Z. Application of Low-Cost Materials Coated with Silver Nanoparticle as Water Filter in Escherichia coli Removal. **Water Quality, Exposure and Health**, [s. l.], v. 7, n. 4, p. 617–625, 2015.

PRIHANDANA, G. S. et al. Study Effect of nAg Particle Size on the Properties and Antibacterial Characteristics of Polysulfone Membranes. [S. l.: s. n.], 2022.

QI, L. et al. Facile and efficient in situ synthesis of silver nanoparticles on diverse filtration membrane surfaces for antimicrobial performance. **Applied Surface Science**, [s. l.], v. 456, p. 95–103, 2018. Disponível em: https://www.sciencedirect.com/science/article/pii/S0169433218316313.

SHARMA, V. et al. Integrated adsorption-membrane filtration process for antibiotic removal from aqueous solution. **Powder Technology**, [s. l.], v. 321, p. 259–269, 2017. Disponível em: https://www.sciencedirect.com/science/article/pii/S0032591017306836.

SHEN, Z. et al. Use of cellulose nanofibril (CNF)/silver nanoparticles (AgNPs) composite in salt hydrate phase change material for efficient thermal energy storage**. International Journal of Biological Macromolecules**, [s. l.], v. 174, p. 402–412, 2021. Disponível em: https://doi.org/10.1016/j.ijbiomac.2021.01.183.

SIMONIS, J. J.; BASSON, A. K. Evaluation of a low-cost ceramic micro-porous filter for elimination of common disease microorganisms. **Physics and Chemistry of the Earth**, [s. l.], v. 36, n. 14–15, p. 1129–1134, 2011. Disponível em: http://dx.doi.org/10.1016/j.pce.2011.07.064.

SZERENCSÉS, B. et al. Size-dependent activity of silver nanoparticles on the morphological switch and biofilm formation of opportunistic pathogenic yeasts. **BMC Microbiology**, [s. l.], v. 20, n. 1, p. 1–13, 2020.

TERRA, N. et al. Characterisation of asymmetric alumina hollow fibres: Application for hydrogen permeation in composite membranes. **Brazilian Journal of Chemical Engineering**, [s. l.], v. 33, p. 567–576, 2016.

TERRA, N. M. et al. High Performance of Asymmetric Alumina Hollow Fiber Membranes for the Clarification of Genipap (Genipa americana L.) Fruit Extract. **Food and Bioprocess Technology**, [s. l.], 2018.

UZ, M. et al. Development of AgCl-TiO2 xerogels entrapped antibacterial polyacrylonitrile membranes: The effect of high salinity water on silver release, antibiofouling and antibacterial efficacies. **Desalination**, [s. l.], v. 492, p. 114496, 2020. Disponível em: https://www.sciencedirect.com/science/article/pii/S0011916420301697.

VOHRA, A. et al. Enhanced photocatalytic disinfection of indoor air. Applied Catalysis B: **Environmental**, [s. l.], v. 64, n. 1, p. 57–65, 2006. Disponível em: https://www.sciencedirect.com/science/article/pii/S0926337305003942.

WANG, W. et al. One-step synthesis of biocompatible gold nanoparticles using gallic acid in the presence of poly-(N-vinyl-2-pyrrolidone). Colloids and Surfaces A: **Physicochemical and Engineering Aspects**, [s. l.], v. 301, n. 1, p. 73–79, 2007. Disponível em: https://www.sciencedirect.com/science/article/pii/S0927775706009617.

WHO. World Health Organization. Drinking Water. [S. l.], 2019. Disponível em: https://www.who.int/news-room/fact-sheets/detail/drinking-water. Acesso em: 20 abr. 2021.

XIA, C. et al. Increasing inorganic nanoparticle impregnation efficiency by external pressure for natural fibers. **Industrial Crops and Products**, [s. l.], v. 69, p. 395–399, 2015. Disponível em: https://www.sciencedirect.com/science/article/pii/S0926669015001491.

XIANG, Z. et al. Facile fabrication of AgI/BiVO4 composites with enhanced visible photocatalytic degradation and antibacterial ability. **Journal of Alloys and Compounds**, [s. l.], v. 721, p. 622–627, 2017. Disponível em: https://www.sciencedirect.com/science/article/pii/S0925838817320066.

XU, J.; HE, F. Genomic analysis of two bacterial strains co-isolated from a urinary tract infection: NDM-1-producing Enterobacter cloacae accompanied by extended-spectrum β-lactamase-producing Escherichia coli. **Journal of Global Antimicrobial Resistance**, [s. l.], v. 17, p. 198–200, 2019. Disponível em: https://www.sciencedirect.com/science/article/pii/S2213716519300967.

CHAPTER 5

5. MICROWAVE ASSISTED PECTIN EXTRACTION FROM ORANGE PEELS: MULTIPLE RESPONSE OPTIMIZATION BY THE DESIRABILITY FUNCTION

ABSTRACT

Here we evaluated suitable conditions to extract pectin (a valuable product) from orange peels (an agro-industrial waste) under microwave heating. The microwave-assisted extraction represents a suitable alternative for process intensification with lower energy consumption than conventional heating. The maximum pectin yield of 31.46% was achieved for microwave-assisted extraction at 134°C and 7.5 min, while conventional extractions at 90°C and 180 min resulted in a pectin yield of 26.81%. Also, greater values of galacturonic acid content, degree of esterification, methoxyl content, total polyphenol content, emulsion activity and emulsion stability were observed with the microwave-assisted extraction than under conventional heating. The optimal values of galacturonic acid content, degree of esterification, methoxyl content were achieved for microwave-assisted extractions at 140 °C and 5.6 min. However, the pectin yield was decreased to 22.73% at these conditions. Thus, pectin extractions under microwave heating at 134°C and 7.5 min are suggested to obtain the maximum pectin yield, while optimum pectin quality parameters are achieved at 140 °C and 5.6 min.

Keywords: pectin; food waste; microwave-assisted extraction; conventional extraction

5.1. INTRODUCTION

Orange juice processing processes produce about 50-60% of organic waste composed by peels, seeds and wet pulp (Satari and Karimi, 2018). Waste orange peels account for 11 957 000 t yearly and its discard represents an environmental concern (Pfaltzgraff et al., 2013). Nonetheless, waste orange peels are composed by high value-added chemicals, such as phenolics, flavonoids, essential oils and pectin (Wicker et al., 2014). Pectin is largely used by food industries as stabilizing, thickening and emulsifying agent, in addition to be used as antioxidant agent and in encapsulation of drugs and as additive of cosmetic products. Also, pectin is related to some human health benefits, such as to prevent ulcer, cholesterol and cancer

diseases and also to reduce lipase activity (Rahmani et al., 2020).Thus, pectin extraction from citrus peels represents a lucrative opportunity to obtain a value-added chemical from an industrial waste. Pectin is an acidic polysaccharide with a complex structure, which is composed of a main and linear chain of α-D-galacturonic acid units linked by α-(1,4)-glycosidic bond, and a side chain of neutral sugars at different amounts depending on the pectin source and the extraction method (Christiaens et al., 2016). Pectin is usually extracted from agro-industrial by-products under acid (pH 1.5–3.0) and hot (60–100°C) conditions for long extraction times (up to 6 h) (Colodel and Petkowicz, 2019; Liu et al., 2006). However, the conventional thermal extraction method is time consuming and labor intensive, involves the use of high temperatures and has low extraction efficiency. Application of innovative extraction methods, such as ultrasound and microwave-assisted processes, has been proposed to increase the extraction yield and quality of the extracted pectin yield, besides reducing extraction time and temperature (Bagherian et al., 2011; Marić et al., 2018).

The microwave-assisted extraction process is reported as an eco-friendly alternative to extract pectin from different sources at lower extraction times and with lower energy demand than conventional processes (Solanki et al., 2019). The mass transfer from solid to solvent is intensified under microwave heating mainly due the electric field that generates internal heating within the food matrix (Sucheta et al., 2020). Also, pectin degradation caused by prolonged time exposure at high temperatures is minimized in microwave-assisted processes (Arrutia et al., 2020; Dahmoune et al., 2021; Kaderides et al., 2019). Liew et al. (2019) highlighted microwave-assisted extraction has higher extraction efficiency and lower energy consumption than conventional heating extraction to obtain pectin from pomelo peel. Buratto et al. (2021) successfully applied the microwave-assisted extraction as an intensified process to recover bioactive compounds from açaí pulp residues. Some results are reported in the literature for optimal conditions to extract pectin from different sources under microwave heating. Košťálová et al. Košťálová et al. (2016) evaluated the temperature influence at the range of 80 to 120°C on pectin extraction from pumpkin biomass in a microwave-assisted process. According to Rahmati et al. (2019), the optimal conditions to extract pectin from dragon fruit peels under microwave heating was at pH 2.07, extraction time of 65 s, and solid-to-liquid ratio of 66.57, with the maxima extraction yield of 18.5% at 800 W. Rahmani et al (2020) (Rahmani et al., 2020) evaluated the effect of microwave power, time and pH on pectin yield for pectin extraction from sweet lemon peels and observed the highest pectin yield (25.31%) at microwave power of 700 W, time of 3 min and pH of 1.5. Maran et al. (2013) reported microwave power

of 422 W, time of 169 s, pH of 1.4 and solid–liquid ratio of 1:16.9 g mL^{-1} as optimal conditions for pectin extraction from dried orange peels under microwave hearing, with maximum pectin yield of 19.24%. According to Hosseini et al. (2016), the highest pectin yield (29.1%) was achieved at pH of 1.50, microwave power of 700 W, and time of 3 min for microwave-assisted extractions of pectin from sour orange peel. Su et al. (2019) extracted pectin from orange peels using the microwave-assisted method under optimal conditions (pH 1.2, 7.0 min, and 21.5 v/w liquid-to-solid ratio) with pectin yield of 28.0%. Leão et al. (2018) applied the microwave-assisted process to extract pectin from pequi (*Caryocar brasiliense* Camb.) peels, with pectin yield of 20.76% at extraction time of 3 min, temperature of 108°C and power of 600 W. Xu et al. (2018) combined the ultrasound and microwave processes to extract pectin from jackfruit peel and reported optimum conditions at temperature of 86 °C, time of 29 min, and solid-liquid ratio 1:48 (w/v) with pectin yield of 21.5%. Bagherian et al. (2011) reached a maximum pectin yield of 27.81% (w/w) for microwave-assisted extractions from grapefruit at 900 W for 6 min. However, the relationship between extraction yield and pectin quality with the operation parameters of the microwave-assisted process were not yet systematically presented.

Here we evaluated the influence of temperature and time on pectin yield and quality for microwave-assisted extraction from orange peels and using water as solvent. The pectin quality was analyzed in terms of galacturonic acid content, degree of esterification and methoxyl content. Also, the conventional extraction process was applied for comparison. The main innovation of our research is due to we assessed how pectin yield and quality changed by varying temperature and time, while literature lacks data on the influence of temperature on pectin quality extract from orange peels under microwave heating. Also, the optimal conditions for pectin extraction under microwave irradiation was based on a multi-response function, where galacturonic acid content, degree of esterification and methoxyl content of pectin were considered as responses in addition to extraction yield.

5.2. MATERIAL AND METHODS

5.2.1. Material

Oranges (*Citrus sinensis*) were purchased at a local market in Montreal – Canada and were washed and peeled. The peels were stripped and cut into small pieces with a knife and, then, dried in an oven (40AF, Quincy Lab Inc) with an air circulation at 50 °C to a constant weight. The dried peels were milled and passed through a 40-mesh sieve to obtain powder samples. The orange peel powders were stored in dark bags and kept in a dry environment until use.

Hydrochloric acid (37%, Fisher chemical), ethanol (95%, Commercial alcohols, Greenfield Global), phenol red (Acros organics), sodium chloride (≥ 99.0%, Fisher Scientific), sodium hydroxide (≥ 97.0%, Fisher Scientific), phenolphthalein solution (1% in ethanol, Sigma-Aldrich), m-hidoxydiphenyl (90%, ACROS Organics, Fisher Scientific), sulfamic acid (99%, ACROS Organics, Fisher Scientific), sodium tetraborate (98%, Fisher Scientific), D-(+)-Galacturonic acid monohydrate (analytical standard, Sigma-Aldrich), sulfuric acid (90-100%, Anachemia), folin ciocalteu (2 N, Dinâmica, Brazil), gallic acid (99.5%, Vetec, Brazil), sodium carbonate (Dinâmica, Brazil) and sodium azide (99%, Vetec, Brazil) were used for physico-chemical analyses. Trifluoroacetic acid (99%, Sigma-Aldrich) was used for pectins hydrolysis. D-(+)-Galactose (≥99.0%, Sigma-Aldrich), L-(+)-Rhamnose (≥99.0%, Sigma-Aldrich), L-(+)-Arabinose (≥99.0%, Sigma-Aldrich), D-(+)-Xylose (≥99.0%, Sigma-Aldrich), D-(+)-Glucose (≥ 99.5%, Sigma-Aldrich) and D-(−)-Fructose (≥99.0%, Sigma-Aldrich) were used as standard reagents for chromatographic analyses. Phosphoric acid (85 to 90%, Fluka Analytical) was used as mobile phase in chromatographic analyses.

5.2.2. Extraction process of pectin from orange peels

Conventional extraction of pectin from orange peels was carried out by mixing the dried orange peel powder with acidified water (pH=2) at solid-to-liquid ratio of 1:30 (w/v), temperature of 90°C and time of 180 min, as proposed in the literature (Oliveira et al., 2016, 2015; Patience et al., 2021; Su et al., 2019). The acidified water was prepared by adding hydrochloric acid to distilled water until pH 2, as suggested in the literature (Xu et al., 2018). The extraction vessel was kept inside a water bath for temperature maintenance. Conventional extractions were performed in triplicate and characterization results are reported as mean ± standard deviation.

Microwaved assisted extractions of pectin from orange peels were also carried out with acidified water (pH=2) at solid-to-liquid ratio of 1:30 (v/w), which are the same conditions of the conventional extraction. A central composite design with three replicates at the central point was applied to verify the influence of temperature and irradiation time on pectin yield, galacturonic acid content, degree of esterification and methoxyl content of extracted pectin from orange peels in the microwave assisted process. Axial points of orthogonality were used and the applied variables and ranges are presented in Table 5.1. Values of temperature and time were based on preliminary experiments and also applying the relations presented by Kremsner

& Stadler (2018) to convert the conditions from conventional extraction to equivalent conditions in microwave assisted extraction processes.

Table 5.1 - Levels (real and coded) of temperature and irradiation time of the experimental design for microwave assisted extractions of pectin from orange peels.

Coded level	Temperature (°C)	Time (min)
-1	130	6
0	135	8.5
1	140	11
-1.1474 (-α)	129	5.6
1.1474 (+α)	141	11.4

Analysis of variance (ANOVA) and regression analyses were performed using the STATISTICA 7.1® software in order to evaluate the significance of each term in the fitted equations and to estimate the goodness of fit in each case with a confidence level of 95 % ($p \leq 0.05$). The obtained experimental responses for pectin yield, galacturonic acid content, degree of esterification and methoxyl content were fitted to a quadratic polynomial model. The regression equations were expressed with coded factors, which were calculated according to Equations 5.1 and 5.2. Furthermore, a multi-response optimization study was also performed using the Derringer's desirability approach (Derringer and RR, 1980) in order to simultaneously maximize all the responses. The multi-response optimization analysis was performed by considering all responses (pectin yield, galacturonic acid content, degree of esterification and methoxyl content) to maximize the overall desirability function.

$$X_1 = \frac{(T-135)}{5} \tag{5.1}$$

$$X_2 = \frac{(t-8.5)}{2.5} \tag{5.2}$$

Where X_1 and X_2 are the coded factors for temperature and irradiation time, respectively, T is the temperature (°C) and t is the irradiation time (min).

Microwave assisted extraction processes were carried out in a microwave reactor (Monowave 400, Anton Paar) with a closed 30 mL borosilicate vial under magnetic stirring at 240 rpm. The microwave equipment was operated at the mode "as fast as possible" for the selected values of time and temperature. After the extractions, the liquid medium was first centrifuged (Sigma, MBI Lab Equipment) at 4000 rpm for 40 min to remove insoluble solids. Then, ethanol (95 %, v/v) was added to the aqueous extract fraction to allow pectin

precipitation. The alcoholic solution was kept at 4–6°C for 12 h to complete the pectin precipitation followed by centrifugation (4000 rpm, 40 min). The precipitated pectin was washed with ethanol and dried in an oven with air circulation at 50°C to constant weight (Dranca et al., 2020; Oliveira et al., 2016). The pectin yield was calculated according to Equation 5.3.

$$\text{Pectin yield (\%)} = \frac{m}{m_{OPP}}\ 100 \qquad (5.3)$$

where m is the weight of dried pectin (g) and m_{OPP} is the weight of dried orange peel powder.

5.2.3. Physico-chemical analyses

The precipitated pectin samples were analyzed for galacturonic acid content (GA), degree of esterification (DE), methoxyl content (MC), total phenolic content (TPC), emulsifying activity (EA), emulsion stability (ES) and monosaccharide composition. Physico-chemical analyses were done in triplicate and data are expressed as mean ± standard deviation. The statistical Tukey test was applied for the analysis of variance (ANOVA) and a significance level of 5 % was adopted for rejection of the null hypothesis.

The galacturonic acid content (GA) was determined by the m-hydroxydiphenyl spectrophotometric method (Melton and Smith, 2001). Briefly, 20 mg of pectin were diluted in 50 mL of distilled water at 50°C and then diluted to 100 mL. Thus, 400 µL of the pectin solution were mixed with 40 µL of 4 M sulfamic acid. This solution was then hydrolyzed with 2.4 mL of a solution of sulfuric acid containing 75 mM of sodium tetraborate. The solution was heated in boiling water for 20 min and then cooled down in an ice bath for 10 min. After cooling, 80 µL of 0.15 % (w/v) m-hydroxydiphenyl in 0.5 % (w/v) sodium hydroxide was added and the solution was vigorous mixed in a vortex. Absorbance values were read at 525 nm using a UV-Vis spectrophotometer (Evolution 220 UV-Visible spectrophotometer, Thermo Scientific). The galacturonic acid content was determined by comparison with a standard galacturonic acid curve (0 – 100 µg/ml).

The degree of esterification (DE) of all pectin samples were determined according to the method described in the USP NF 21 (2003). Briefly, 0.1 g of the pectin sample was dissolved in 2 mL of ethanol (95 %) and 20 mL of deionized water. Then, 3 drops of phenolphthalein were added to the solution, which was titrated with a NaOH solution at 0.1 M until the solution color changed to pink. The used volume of NaOH solution in this first titration was recorded as V_1. Afterward, 10 mL of the NaOH solution at 0.1 M was added to the previous mixture, which

was stirred for 20 min for hydrolysis. Then, 10 mL of a HCl solution at 0.1 M was added and the solution was stirred until the disappearance of the pink color. Finally, the solution was titrated again with a NaOH solution at 0.1 M. The used volume of NaOH solution in this second titration was recorded as V_2. The degree of esterification (DE) was calculated according to Equation 5.4.

$$\text{DE}\ (\%) = \frac{V_2}{V_2+V_1}\ 100 \tag{5.4}$$

where DE is the degree of esterification and V_1 and V_2 are the volumes of NaOH solution at 0.1 M in the first and second titrations, respectively.

The methoxyl content (MC) of pectin samples was measured according the method described by Ranggana (1986). Briefly, 0.5 g of pectin was dissolved in 100 mL of distilled water under continuous stirring (300 rpm) for 1 h. Then, 1 g of NaCl was added, followed by the addition of 5 drops of phenol red indicator. The solution was titrated using a NaOH solution at 0.1 N until the solution color changed to pink. The final solution, was mixed with 25 mL of a NaOH solution at 0.25 M under agitation. Then, the solution was allowed to stand for 30 min at room temperature. An equal volume (25 mL) of a HCl solution at 0.25 M was added and the final solution was titrated with a NaOH solution at 0.1 N. The used volume of NaOH solution in this titration was recorded as V_4. Methoxyl content (MC) was calculated according to Equation 5.5.

$$\text{MC}\ (\%) = \frac{3.1\ V_3\ N}{W} \tag{5.5}$$

where MC is the methoxyl content, W is the weight of the pectin sample (g), V_3 is the used volume of the NaOH solution at 0.1 N during titration (mL) and N is the NaOH normality.

The total phenolic content (TPC) of pectin samples were determined according to the Folin-Ciocalteu method. First, 2.5 mL of the Folin-Ciocalteu reagent (10 % v/v) were added to 0.5 mL of the pectin aqueous solution (1 % w/v). After 3 min, 2 mL of a sodium carbonate solution (7.5 % w/v) was added to the previous solution. The prepared solution was then incubated at room temperature. After 1 h of incubation, the absorbance was measured (Shimadzu UV-1280) at 750 nm. Gallic acid was used as a standard for preparing the calibration curve (R^2=99.9 %). Total phenolic content values were expressed as mg of gallic acid equivalents per g of pectin (mg_{GAE}/g_{pectin}).

Values of emulsifying activity (EA) and emulsion stability (ES) were measured according to the methodology described by Hosseini et al. (2016). In a graduated tube, the oil-in-water emulsion was prepared by adding 5 mL of sunflower oil (Caramuru Alimentos, Brazil) to 5 mL of pectin solution (0.5 %, w/w). Also, a sodium azide solution at 0.02 % (w/v) was added as a bactericide. The pre-emulsions were sonicated (Utronique Q9.5/40A, Brazil) for 5 min. Then, the emulsions were centrifuged at 4500 rpm for 5 min. The EA value was calculated according to Equation 5.6.

$$\text{EA}\ (\%) = \frac{V_e}{V_T} 100 \tag{5.6}$$

where V_e is the volume of the formed emulsion and V_T is the total volume in the tube.

The emulsion was then stored for 30 days at 4 °C and the emulsion stability (ES) was calculated according to Equation 5.7.

$$\text{ES}\ (\%) = \frac{V_R}{V_I} 100 \tag{5.7}$$

where V_R was the emulsion volume after storage and V_I was the initial emulsion volume.

Monosaccharide compositions were evaluated by high performance liquid chromatography (HPLC) according to the methodology suggested by Hosseini et al. (2019). Pectin samples were hydrolyzed with a trifluoroacetic acid solution (2 M) at 85°C for 3 h. Afterward, the solution was immediately cooled in an ice-water bath and centrifuged at 4000 rpm for 15 min to separate impurities. The prepared solution was then freeze-dried for acid removal from the hydrolysate samples. Then, the samples were diluted in 2 mL of distillated water and injected to a HPLC (Shimadzu TM model LC-20A Prominence, Supelcogel TM C-610H column) equipped with ultra-violet and refractive detectors (Shimadzu, SPD-20A UV-Vis detector and RID-10A refractive detector). Water with phosphoric acid (pH=2) was applied as mobile phase. Total run time was 35 min. The injection volume for all samples was 20 μL at a flow rate of 0.5 mL min^{-1}. Concentrations were monitored at 210 nm at an oven temperature of 32°C. The monosaccharide composition was calculated by considering the retention time of the standard monosaccharides (galactose, rhamnose, arabinose, xylose, glucose and fructose).

Additionally, structural characteristics of pectin samples were evaluated by Attenuated Total Reflectance-Fourier-transform infrared spectroscopy (ATR-FTIR, Perkin Elmer Spectrum Two, Single Reflection ZnSe/L1600115) at the transmittance mode and

wavenumbers from 4000 to 400 cm^{-1}. The measuring resolution was 2 cm^{-1} and 36 scans were recorded.

5.3. RESULTS AND DISCUSSION

5.3.1. Optimization of pectin yield in microwave assisted extractions

A total number of 11 experimental assays were carried out according to the design of experiments in order to evaluate the influence of the process variables (temperature and irradiation time) on pectin yield (PY), as presented in Table 5.2.

Table 5.2 - Experimental results according to the central composite design to evaluate the influence of temperature and irradiation time on pectin yield (PY) in microwave assisted extractions.

Run	Temperature (X_1)	Irradiation time (min) (X_2)	PY (%)
1	130 (-1)	6 (-1)	25.38
2	130 (-1)	11 (+1)	22.74
3	140 (+1)	6 (-1)	22.31
4	140 (+1)	11 (+1)	10.47
5	129 (-α)	8.5 (0)	26.08
6	141 (+α)	8.5 (0)	22.19
7	135 (0)	5.6 (-α)	29.14
8	135 (0)	11.4 (+α)	24.49
9	135 (0)	8.5 (0)	29.63
10	135 (0)	8.5 (0)	29.86
11	135 (0)	8.5 (0)	29.73

Equation 5.8 was obtained to represent the effects of the independent variables on pectin yield. The effects of the process variables (temperature and irradiation time) on pectin yield are presented by the response surface plot (Figure 5.1).

$$PY = 30.32 - 2.98X_1 - 5.64X_1^2 - 2.98X_2 - 3.61X_2^2 - 2.30X_1X_2 \quad (5.8)$$

where PY is the pectin yield (%) and X_1 and X_2 are the coded factors for temperature and time, respectively.

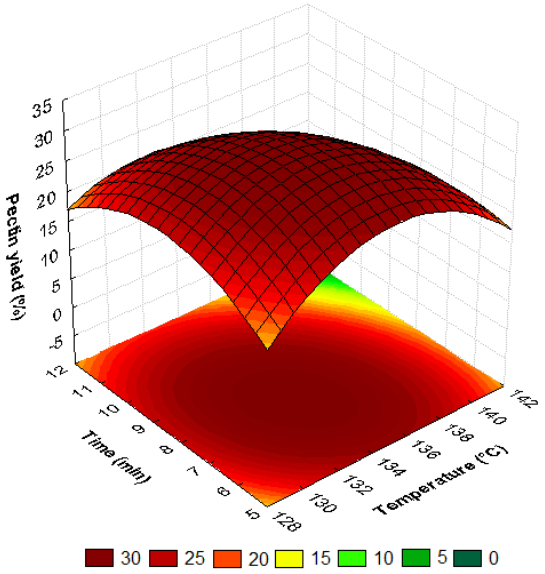

Figure 5.1 - Response surface plot to represent the influence of temperature and irradiation time on pectin yield.

The analysis of variance (ANOVA) was applied to evaluate the significant factors and the model fit (Table 5.3). R^2 value for pectin yield (PY) was 0.9324, which represents the ability of the models to precisely explain the relationship between the variables and response. Thus, the presented second-order equation was sufficient to predict the effects of the two independent variables on the evaluated response.

Table 5.3 - ANOVA results for the proposed model of pectin yield for pectin extraction from orange peels under microwave heating

Source	Sum of Squares	Degrees of freedom	Mean square	F-value	p-value
X_1	59.136	1	59. 137	4867.23	0.000
X_1^2	110.608	1	110.608	8916.47	0.000
X_2	59.279	1	59.279	4778.71	0.000
X_2^2	45.271	1	45.271	3649.46	0.000
X_1X_2	21.168	1	21.168	1706.50	0.001
Lack of fit	21.408	3	7.136	575.28	0.002
Pure error	0.025	2	0.012		
Total SS	316.897	10	-	-	-

According to results presented in Table 5.2, experimental values of pectin yield ranged from 10.47% to 29.86% at the evaluated conditions of temperature and irradiation time in microwave-assisted extractions. The effects of process variables (temperature and irradiation time) on pectin yield are presented by the response surface (Figure 5.1) of the prediction

equation (Equation 5.8). According to the ANOVA results (Table 5.3), linear, quadratic and interaction factors were all significant at $p<0.05$ to predict pectin yield. The critical maximum value for pectin yield was predicted at 134 °C and 7.5 min. Thus, pectin yield was increased for temperature increases up to 134 °C due to the enhance in solvent diffusion into the plant material and the consequent pectin extraction. However, pectin yield was decreased with further temperature increases probably due the hydrolysis of pectin molecules to short-chain sugars (Oliveira et al., 2016). The pectin yield increased with the increase at irradiation time up to 7.5 min. Irradiation time higher than 7.5 min caused a negative effect on pectin yield, since long time exposures in the microwave field probably caused pectin degradation (Guo et al., 2012).

According to Equation 5.8, the predicted maximal pectin yield was 33.31% at the critical values of temperature (134 °C) and time (7.5 min). The predicted maximum value of pectin yield was validated with triplicate experiments at the optimum extraction condition. The observed pectin yield was 31.46% ± 1.35%, which is similar to the predicted value. Maran et al. (2013) reported a maximum pectin yield of 19.24% for microwave-assisted extractions from dried orange peels at an irradiation time of 2.82 min. Su et al. (2019) reported a pectin yield of 28.0% ± 0.5% for microwave-assisted extractions at an irradiation time of 7 min. Hosseini et al. Hosseini et al. (2016) used the microwave-assisted extraction technique to extract pectin from sour orange peel and pectin yield was 29.1% at the optimum irradiation time of 3 min Thus, the extraction conditions used this work enabled to obtain a higher extraction yield.

The extraction temperature is related to the applied power during microwave process. Figure 5.2 presents the temperature and microwave power profiles according to the extraction time at the critical values of temperature (134 °C) and time (7.5 min). Similar profile behavior was observed at the other extraction conditions of temperature and time. The set temperature of 134°C was achieved after 74 s and, at this time, the power reached the maximum value of 533 W. This behavior was expected since the equipment was set at the option of heat as fast as possible. Then, the power decreased since the temperature reached the steady state value. The power was kept at 23.8 ± 1.7 W during the experiment at 134 °C.

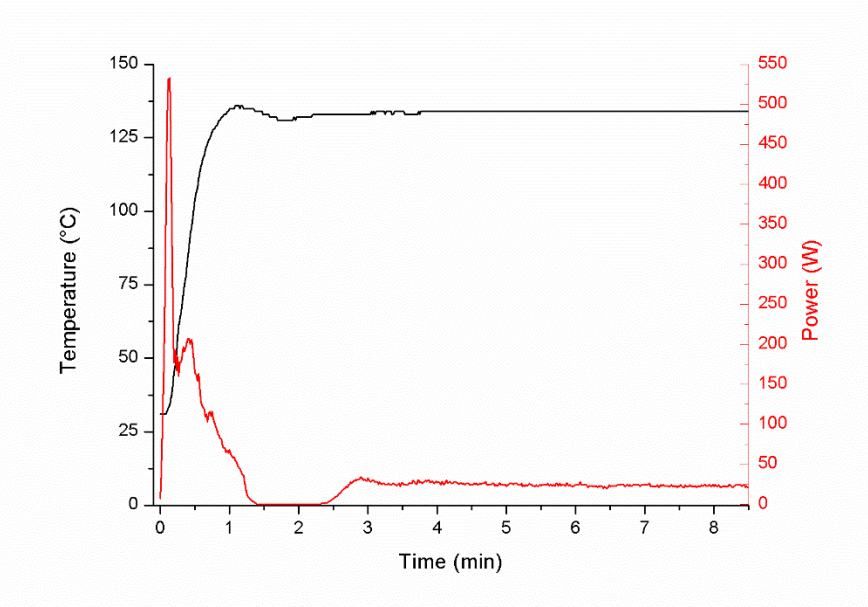

Figure 5.2 – Microwave power and temperature profiles during pectin extraction from orange peels at 134°C for 7.5 min under microwave heating.

5.3.2. Comparison of pectin characteristics for conventional and microwave assisted extractions

The characteristics of pectin extracted in microwaved assisted process at solid: liquid ratio of 1:30 (w/v), pH 2, temperature of 134 °C and extraction time of 7.5 min, which are the optimal conditions of temperature and time to maximize pectin yield, are presented in Table 5.4. Conventional pectin extraction was performed at solid: liquid ratio of 1:30 (w/v), pH 2, temperature of 90 °C and extraction time of 180 min and the characteristics of the conventionally extracted pectin are also presented in Table 5.4.

Table 5.4 - Physico-chemical characteristics of extracted pectin from orange peels in conventional and microwave-assisted extractions.

Characteristics		Microwave-assisted extraction	Conventional extraction
Pectin yield (%)		$31.46^{a} \pm 1.35$	$26.81^{b} \pm 0.92$
Galacturonic acid content (%)		$79.83^{a} \pm 1.41$	$74.92^{b} \pm 0.14$
Degree of esterification (%)		$52.27^{a} \pm 3.21$	$55.95^{a} \pm 1.76$
Methoxyl content (%)		$8.91^{a} \pm 0.56$	$7.35^{b} \pm 0.11$
Total polyphenol content (mg_{GAE}/g of pectin)		$32.81^{a} \pm 0.25$	$26.57^{b} \pm 0.10$
Emulsion activity (%)		$69.00^{a} \pm 2.83$	$58.50^{b} \pm 2.12$
Emulsion stability (%)	1 day	$97.09^{a} \pm 0.11$	$96.62^{a} \pm 2.29$
	30 days	$91.25^{a} \pm 2.41$	$84.65^{b} \pm 1.86$
Monosaccharides (%)	Glucose	$1.14^{a} \pm 0.00$	$1.10^{b} \pm 0.00$
	Rhamnose	$7.23^{a} \pm 0.00$	$6.97^{b} \pm 0.00$
	Galactose	$7.97^{a} \pm 0.00$	$7.69^{b} \pm 0.00$
	Xylose	$4.16^{a} \pm 0.00$	$4.02^{b} \pm 0.00$
	Arabinose	$1.29^{a} \pm 0.00$	$1.24^{b} \pm 0.00$

*Mean values denoted by different letters at the same line are significantly different at $p \leq 0.05$.

The conventional extraction of pectin from orange peels resulted in lower pectin yield than the microwave-assisted extraction, even that longer extraction times were used in the conventional extraction process. Pectin samples extracted from orange peel powder were predominantly constituted of galacturonic acid and the microwave-assisted process resulted in an extract with higher galacturonic acid than the conventional process. Degree of esterification has a significant influence on pectin quality. Although the microwave extracted pectin presented higher methoxyl content than the conventional extracted pectin, conventional and microwave extraction process resulted in equivalent methoxyl content result. Commercial pectins are classified as high methoxyl pectin with degree of esterification greater than 50%, and low methoxyl pectin with degree of esterification lower than 50% (Giacomazza et al., 2018). Both extracted pectins are high-methoxylated pectin with a degree of esterification greater than 50%, pointing out their suitability as gelling agents (Muñoz-Almagro et al., 2017). Also, the pectins obtained with the conventional and microwave-assisted extractions were

categorized as high methoxyl pectin due to the methoxyl content higher than 7% (Rodsamran and Sothornvit, 2019).

Total phenolic functionalities determine important functional properties of pectin samples, such as antioxidant activity. The pectin extracted by the microwave-assisted process presented higher total polyphenol content than by the conventional process. The high temperature used in conventional extractions over a long time may degrade phenolic compounds that are heat sensitive at temperatures higher than 90 °C (Bindes et al., 2019a). Hosseini et al. (2019) reported a total polyphenol content of 39.95 ± 3.13 mg_{GAE}/g pectin for an ultrasound-assisted extraction process from sour orange peels, which is similar to the value obtained in this work for the microwave-assisted process. Sanchez-Reinoso et al. (2020) also reported similar total polyphenol content for extracting bioactive compounds from Sacha Inchi shells under microwave heating at 1500 W for 1.8 min.

The microwave-assisted process resulted in a pectin extract with higher emulsion activity than conventional process. The pectin extract obtained by Hosseini et al. (2019) with the ultrasound-assisted extraction process presented emulsion activity of 58.50% ± 2.12%. Hosseini et al. (2016) applied microwave-assisted extraction process and obtained a pectin extract with an emulsion activity of 40.7%. Also, the pectin extracted by the microwave-assisted process presented higher emulsion stability after 30 days of storage than the pectin extracted by the conventional process. The pectin extracted by both methods presented similar emulsion stability after 1 day of storage. Pectin samples presented similar emulsion stability to the values reported in the literature (Hosseini et al., 2019).

Related to the monosaccharide composition, the main constituents of pectin side chains are neutral sugars, such as galactose, rhamnose, arabinose, xylose and fructose (Hosseini et al., 2019). As presented in Table 5.4, galactose was the most abundant neutral monosaccharide in the extract of microwave process, followed by rhamnose, xylose, arabinose and glucose. Fructose was not detected. The pectin extracted by microwave-assisted extraction resulted in higher amounts of the evaluated neutral sugars than the one extracted by conventional extraction. Higher amounts of galactose, rhamnose and arabinose than others monosaccharides are due to higher amounts of rhamnogalacturonan I regions in pectin structure. Xylose was measured at lower percentage, which may refer to the presence of xylogalactrunan and rhamnogalacturonan II in the pectin structure. Low amounts of glucose could be due to the remnant of non-pectic polysaccharides bonded to the side chains of the pectins (Hosseini et al., 2019). Hosseini et al. (2019) presented similar monosaccharides contents behavior.

The infrared spectra of pectin samples extracted under conventional and microwave-assisted conditions are presented in Figure 5.3. The peaks at 1646 and 1730 cm^{-1} are attributed to the free and esterified carboxyl groups, respectively. The peak at 1225 cm^{-1} was from the cyclic C–C bond in the ring structure of pectin. The bands between 1120 and 990 cm^{-1} were considered the range for the spectral identification of galacturonic acid in pectic polysaccharides (Acikgoz, 2011). The characteristic chemical shifts at 3360, 2930 and 1201 cm^{-1} are due to inter and intramolecular hydrogen of O-H, C-H of CH_2 and CH_3, and C-O-C of glycoside compounds (Dranca et al., 2020; Hosseini et al., 2019).

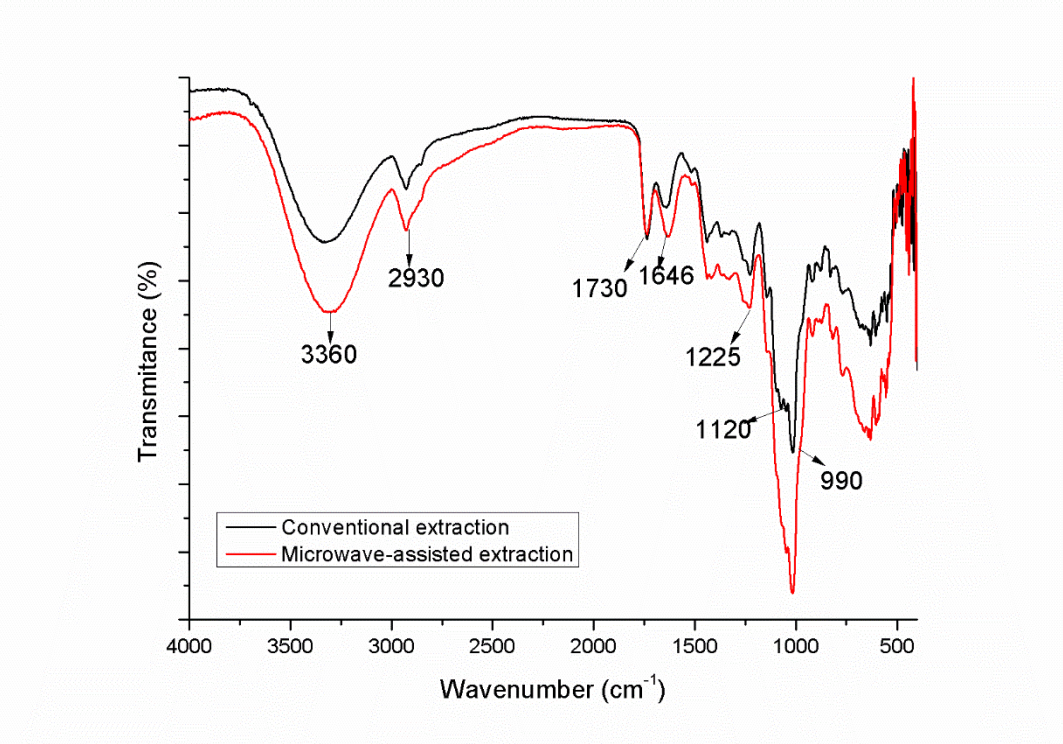

Figure 5.3 - FTIR spectra of pectin samples from conventional and microwave-assisted extraction processes.

5.3.3. Simultaneous optimization of pectin yield, galacturonic acid content, degree of esterification and methoxyl content in microwave assisted extractions

The characteristics of the extracted pectin molecules are critical factors for pectin applications. Thickening, stabilizing and gelling properties of pectin is largely explored by several industries. However, two different pectin gelation mechanisms are possible depending

on the degree of esterification of pectin: gels are formed in acid media if the degree of esterification is greater than 50% and gels are formed with addition of Ca^{2+} ions if the degree of esterification is lower than 50% (Colodel and Petkowicz, 2019; May, 1990). The degree of-esterification represents the percentage of galacturonic acid units possessing the methyl-esterified carboxylic group. Thus, the consideration of galacturonic acid content, degree of esterification and methoxyl content is important for pectin extraction optimization. Table 5.5 presents the results of galacturonic acid content, degree of esterification and methoxyl content according the design of experiment for temperature and time as independent variables. Equations 5.9 to 5.11 were adjusted to represent the effects of the independent variables on galacturonic acid content, degree of esterification and methoxyl content, respectively. The effects of the process variables (temperature and time) on each response are presented by the response surface plot (Figure 5.4).

Table 5.5 - Experimental results according to the central composite design to evaluate the influence of temperature and time on of galacturonic acid content (GA), degree of esterification (DE) and methoxyl content (MC) in microwave-assisted extractions.

Run	Temperature (X_1)	Time (min) (X_2)	GA(%)	DE(%)	MC(%)
1	130 (-1)	6 (-1)	72.89	55.29	9.46
2	130 (-1)	11 (+1)	88.28	55.90	9.90
3	140 (+1)	6 (-1)	80.54	61.67	8.98
4	140 (+1)	11 (+1)	66.671	61.18	9.58
5	129 (-α)	8.5 (0)	85.115	55.90	9.74
6	141 (+α)	8.5 (0)	78.42	60.00	8.88
7	135 (0)	5.6 (-α)	75.33	56.98	9.57
8	135 (0)	11.4 (+α)	67.29	60.37	7.19
9	135 (0)	8.5 (0)	63.04	56.36	6.83
10	135 (0)	8.5 (0)	62.70	55.48	6.82
11	135 (0)	8.5 (0)	62.95	55.84	6.91

$$GA = 63.99 - 3.26X_1 + 11.69X_1^2 - 0.82X_2 + 2.99X_2^2 - 7.32X_1X_2 \quad (5.9)$$

$$DE = 56.07 + 2.47X_1 + 1.14X_1^2 + 0.54X_2 - 1.55X_2^2 - 0.27X_1X_2 \quad (5.10)$$

$$MC = 6.89 - 0.27X_1 + 1.61X_1^2 - 0.26X_2 + 1.04X_2^2 + 0.04X_1X_2 \quad (5.11)$$

where GA is the galacturonic acid content (%) MC is the methoxyl content (%), DE is the degree of esterification (%), and X_1 and X_2 are the coded factors for temperature and time, respectively.

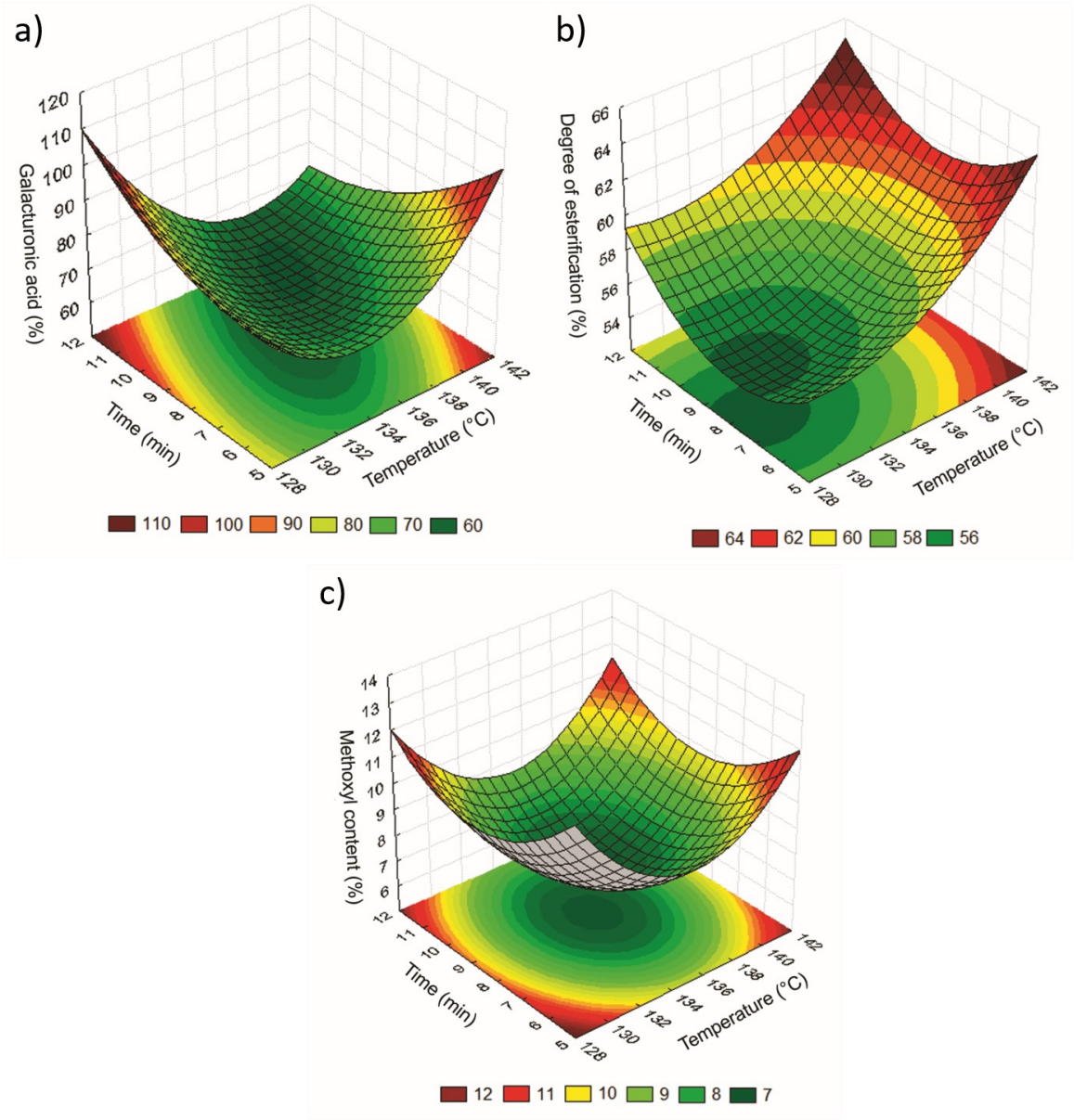

Figure 5.4 - Response surface plot to represent the influence of temperature and time on of galacturonic acid content (a), degree of esterification (b) and methoxyl content (c).

The analysis of variance (ANOVA) was applied to evaluate the significant factors and the model fit (Table 5.6). R^2 values galacturonic acid content (GA), degree of esterification (DE) and methoxyl content (MC) were 0.9534, 0.9031 and 0.8374, respectively. Thus, the presented second-order equations were sufficient to predict the effects of the two independent variables on the evaluated responses.

According to results presented in Table 5.5, experimental values of galacturonic acid content varied from 62.70% to 88.28% at the evaluated conditions of temperature and time in microwave-assisted extractions. According to the FAO and EU regulations, pectin should contain a content of galacturonic acid of at least 65% (Willats et al., 2006). This condition was not achieved at the central point of the experimental design for extractions at 135 °C and 8.5 min. Su et al. (2019) also reported relative low values of galacturonic acid content ranging from 23.4% to 63.5% at different conditions of pH (0.5 to 1.5), time (5 to 7 min), and liquid-to-solid ratio (20 to 30) and showed that low pH values favored the production of pectin with low galacturonic acid content. The effects of process variables (temperature and time) on galacturonic acid content are presented by the response surface (Figure 4a) of the prediction equation (Equation 5.9). As presented in Table 5.6, linear, quadratic and interaction factors were all significant at $p<0.05$ to predict galacturonic acid content. The influence of all factors on the galacturonic acid content is observed in the response surface (Figure 4a), where a minimum point was achieved at 136 °C and 10 min. Thus, the galacturonic acid content is decreased with temperature increase up to 136 °C. The negative effect of temperature on pectin extraction was also observed by Oliveira et al. (2016) for ultrasound assisted pectin extractions from passion fruit peel and this behavior was related to the depolymerization of pectin chain. However, the galacturonic acid content was increased with further temperature increases in short times, as observed in Figure 5.4a. Pereira et al. (2016) also observed that harsh conditions of temperature, pH and time favored galacturonic acid content in pectin extracts from pomegranate peels in a conventional heating process. According to Minjares-Fuentes et al. (2014), galacturonic acid contend is increased with temperature increase due to the extensive hydrolysis of pectin neutral sugars in rhamnogalacturonic regions. Thus, although a maximum point for galacturonic acid content was not achieved, optimal regions are observed in Figure 5.4a at high extraction times or temperatures.

Table 5.6 - ANOVA results for the proposed model galacturonic acid content (GA), degree of esterification (DE) and methoxyl content (MC) for pectin extraction from orange peels under microwave heating.

Response variable	Source	Sum of Squares	Degrees of freedom	Mean square	F-value	p-value
Galacturonic acid content	X_1	462.155	1	70.284	2303.96	0.000
	X_1^2	9.132	1	462.155	15149.75	0.000
	X_2	52.899	1	9.132	299.34	0.003
	X_2^2	214.048	1	52.899	1734.09	0.001
	X_1X_2	56.608	1	214.048	7016.63	0.000
	Lack of fit	0.061	3	18.869	618.54	0.002
	Pure error	462.155	2	0.031		
	Total SS	850.781	10			
Degree of esterification	X_1	40.345	1	40.345	206.36	0.005
	X_1^2	4.483	1	4.483	22.93	0.041
	X_2	1.923	1	1.922	9.83	0.088
	X_2^2	8.337	1	8.337	42.64	0.023
	X_1X_2	0.299	1	0.299	1.52	0.342
	Lack of fit	5.551	3	1.851	9.46	0.097
	Pure error	0.391	2	0.196		
	Total SS	61.330	10			
Methoxyl content	X_1	0.481	1	0.481	197.80	0.005
	X_1^2	9.823	1	9.823	4036.73	0.000
	X_2	0.431	1	0.431	177.12	0.005
	X_2^2	3.308	1	3.308	1359.55	0.001
	X_1X_2	0.006	1	0.006	2.63	0.246
	Lack of fit	2.894	3	0.965	396.40	0.002
	Pure error	0.005	2	0.002		
	Total SS	16.949	10			

According to results presented in Table 5.5, experimental values of degree of esterification varied from 55.29% to 61.67% at the evaluated conditions of temperature and time in microwave-assisted extractions. Based on DE values, all pectins can be classified as high methoxyl pectin as DE was greater than 50%. The effects of process variables (temperature and time) on degree of esterification are presented by the response surface (Figure 5.4b) of the prediction equation (Equation 5.10). According to the ANOVA results (Table 5.6), the linear term of temperature was significant at $p<0.05$ to predict degree of esterification. The critical minimum value for degree of esterification was predicted as 54.62% at 129 °C and 8 min. Figure 5.4b shows that the highest values of degree of esterification are observed at higher temperatures. Minjares-Fuentes et al. (Minjares-Fuentes et al., 2014) also observed the positive and significant effect of temperature on pectin extraction. However, in general, harsh extraction conditions promote the de-esterification of polygalacturonic chains and, thus, low values of degree of esterification are obtained (Mort et al., 1993; Wai et al., 2010). Thus, the extraction conditions in our work were probably the least harsh as compared to other conditions reported in the literature so that the temperature increase did not promote the de-esterification of polygalacturonic chains.

Experimental values of methoxyl content ranged from 6.82% to 9.90% at the evaluated conditions of temperature and time in microwave-assisted extractions (Table 5.5). Rodsamran and Sothornvit (2019) reported methoxyl content values ranging from 8.74% to 10.51% for pectin extracted from lime peel under microwave heating at different conditions. The methoxyl content indicates the dispersibility of pectin in water and its ability for gel formation. Thus, the applied extraction conditions enabled to obtain high methyl pectins that are highly dispersible in water and have a considerable capacity to be sugar bonded (Rodsamran and Sothornvit, 2019). The effects of process variables (temperature and time) on methoxyl content are presented by the response surface (Figure 5.4c) of the prediction equation (Equation 5.11). As presented in Table 5.6, linear and quadratic factors were all significant at $p<0.05$ to predict methoxyl content, while only the interaction factor was not significant at $p<0.05$. The critical minimum value for methoxyl content was at 135 °C and 9 min. Figure 5.4c shows that methoxyl content is higher at extreme conditions of temperature and time.

The four dependent variables (pectin yield, galacturonic acid content, degree of esterification and methoxyl content) presented different optimum regions. The optimum conditions should be those that maximize the pectin yield, the galacturonic content, the degree of esterification and the methoxyl content. The maximization in galacturonic content improves

the pectin quality. Pectin ability to form gels in acid media is enhanced with the improve in the degree of esterification. The improvement in methoxyl content is favorable to improve pectin dispersibility in water and its ability for gel formation. Provided that the optimum regions for these four variables are different, the desirability function technique was applied to simultaneously optimize the extraction conditions (Bindes et al., 2019b), as presented in Figure 5.5. The optimum conditions considering all responses simultaneously were 140 °C and 5.6 min, with R^2 of 0.8800. The results of the predicted responses at these conditions were: 22.73% of pectin yield, 87.73% of galacturonic acid, 61.58% of degree of esterification and 10.01% of methoxyl content, respectively. Thus, the simultaneous optimal condition impaired on pectin yield, since the maximum pectin yield was of 33.31% at the critical values of temperature (134 °C) and time (7.5 min), but the maximization of the other variables was ensured. The simultaneous optimal condition will especially maximize the galacturonic acid content and, thus, pectin quality will be improved.

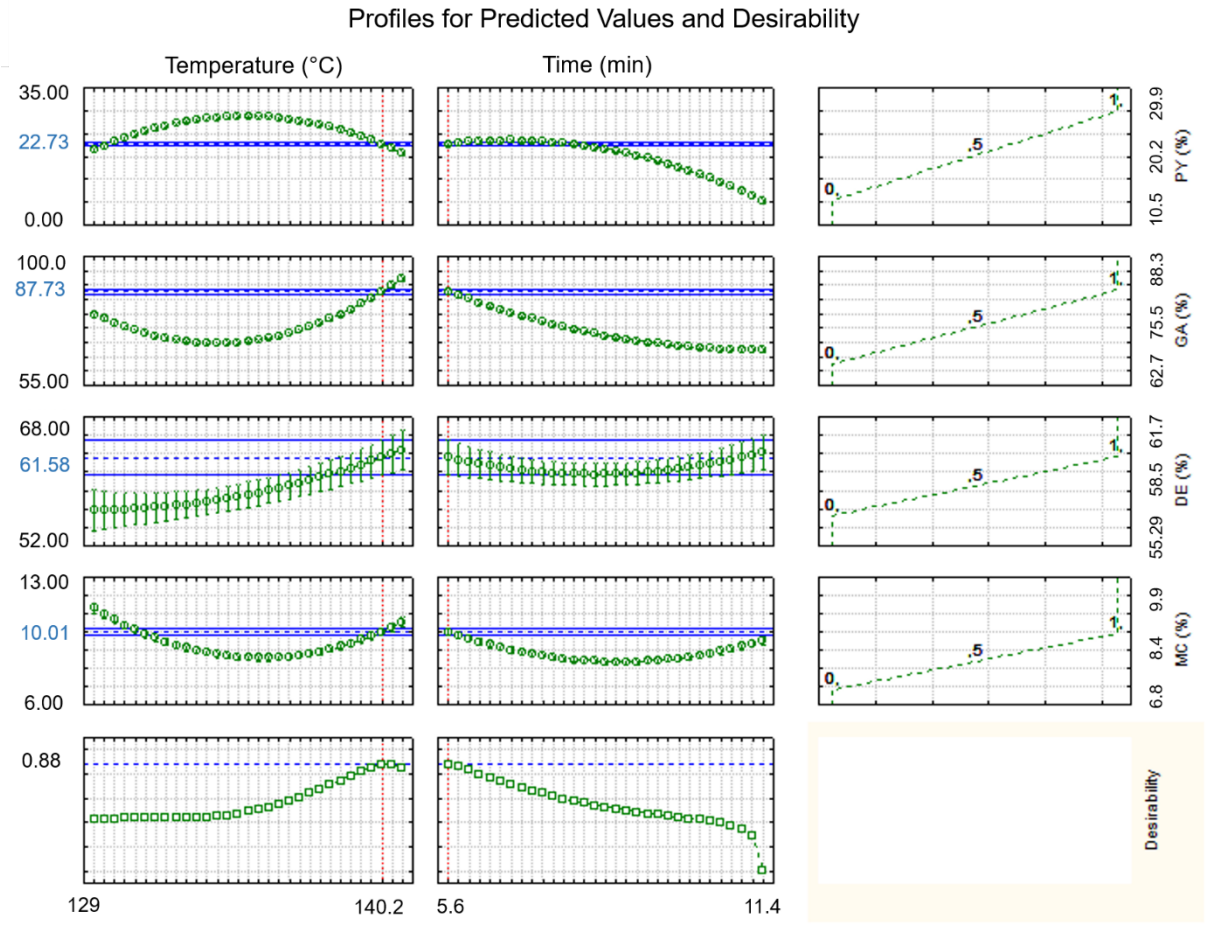

Figure 5.5 - Multi-response optimization chart according to the desirability function methodology for pectin yield, galacturonic acid content, degree of esterification and methoxyl content.

5.4. CONCLUSION

The analysis of the influence of temperature and time on pectin yield and quality in microwave-assisted process is important to find optimal extraction conditions. Within the evaluated range of temperature and time, mild extraction conditions are suggested to enhance the pectin yield extraction from orange peels under microwave heating. Temperature and time extractions up to 134°C and 7.5 min, respectively, improved pectin yield probably due to the enhancement in solvent diffusion through the orange peels. However, further increases in temperature and time caused a decrease in pectin yield, which is related to the hydrolysis of pectin molecules to short-chain sugars and pectin degradation. Conventional heating extraction was performed at 90 °C and extraction time of 180 min, but even at such longer extraction time, pectin yield in the conventional extraction was 1.2 times lower than in the microwave-assisted extraction at 134°C and 7.5 min. Also, the microwave-assisted process enabled to obtain a pectin extract with superior quality in terms of galacturonic acid content, degree of esterification, methoxyl content, total polyphenol content, emulsion activity and emulsion stability if compared to the conventional heating extraction. According to the desirability function technique, the extraction conditions that simultaneously optimize pectin yield, galacturonic acid content, degree of esterification and methoxyl content were at temperature of 140 °C and time of 5.6 min. However, this simultaneous optimal condition resulted in a pectin yield lower than at the critical point for pectin yield. Thus, an increase in temperature from 134 to 140 °C and a decrease in extraction time from 7.5 to 5.6 min in the microwave-assisted process ensured to obtain a high-quality pectin, although a decrease in pectin yield from 31.46 to 22.76% have been predicted. Thus, the microwave-assisted process is suggested to extract pectin from orange peels at energy saver conditions than the conventional heating process and optimal values of temperature and time are suggested to enhance pectin yield, galacturonic acid content, degree of esterification and methoxyl content.

5.5. REFERENCES

ACIKGOZ, C. Extraction and characterization of pectin obtained from quince fruits (Cydonia vulgaris pers) grown in Turkey. **Asian Journal of Chemistry**, [s. l.], v. 23, n. 1, p. 149–152, 2011.

ARRUTIA, F. et al. Development of a continuous-flow system for microwave-assisted extraction of pectin-derived oligosaccharides from food waste. **Chemical Engineering Journal**, [s. l.], v. 395, n. April, p. 125056, 2020. Disponível em: https://doi.org/10.1016/j.cej.2020.125056.

BAGHERIAN, H. et al. Comparisons between conventional, microwave- and ultrasound-assisted methods for extraction of pectin from grapefruit. **Chemical Engineering and Processing: Process Intensification**, [s. l.], v. 50, n. 11–12, p. 1237–1243, 2011. Disponível em: http://dx.doi.org/10.1016/j.cep.2011.08.002.

BINDES, M. M. M. et al. Maximisation of the polyphenols extraction yield from green tea leaves and sequential clarification. **Journal of Food Engineering**, [s. l.], v. 241, n. August 2018, p. 97–104, 2019.

BINDES, M. M. M. et al. Ultrasound-assisted extraction of bioactive compounds from green tea leaves and clarification with natural coagulants (chitosan and Moringa oleífera seeds). **Ultrasonics Sonochemistry**, [s. l.], v. 51, n. October 2018, p. 111–119, 2019.

BURATTO, R. T.; COCERO, M. J.; MARTÍN, Á. Characterization of industrial açaí pulp residues and valorization by microwave-assisted extraction. **Chemical Engineering and Processing - Process Intensification**, [s. l.], v. 160, p. 108269, 2021. Disponível em: https://www.sciencedirect.com/science/article/pii/S0255270120307315.

CHRISTIAENS, S. et al. Process–Structure–Function Relations of Pectin in Food. **Critical Reviews in Food Science and Nutrition**, [s. l.], v. 56, n. 6, p. 1021–1042, 2016. Disponível em: https://doi.org/10.1080/10408398.2012.753029.

COLODEL, C.; PETKOWICZ, C. L. de O. Acid extraction and physicochemical characterization of pectin from cubiu (Solanum sessiliflorum D.) fruit peel. **Food Hydrocolloids**, [s. l.], v. 86, n. September 2017, p. 193–200, 2019. Disponível em: https://doi.org/10.1016/j.foodhyd.2018.06.013.

DAHMOUNE, B. et al. Microwave assisted extraction of bioactive saponins from the starfish Echinaster sepositus: Optimization by response surface methodology and comparison with ultrasound and conventional solvent extraction. **Chemical Engineering and Processing - Process Intensification**, [s. l.], v. 163, p. 108359, 2021. Disponível em: https://www.sciencedirect.com/science/article/pii/S0255270121000635.

DERRINGER, G.; RR, S. Simultaneous Optimization of Several Response Variable. [s. l.], v. 12, 1980.

DRANCA, F.; VARGAS, M.; OROIAN, M. Physicochemical properties of pectin from Malus domestica ‘ F ă lticeni ’ apple pomace as a ff ected by non-conventional extraction techniques. **Food Hydrocolloids**, [s. l.], v. 100, n. May 2019, p. 105383, 2020. Disponível em: https://doi.org/10.1016/j.foodhyd.2019.105383.

GIACOMAZZA, D. et al. The role of sucrose concentration in self-assembly kinetics of high methoxyl pectin. **International Journal of Biological Macromolecules**, [s. l.], v. 112, p. 1183–1190, 2018. Disponível em: http://www.sciencedirect.com/science/article/pii/S0141813017341752.

GUO, X. et al. Extraction of pectin from navel orange peel assisted by ultra-high pressure, microwave or traditional heating: A comparison. **Carbohydrate Polymers**, [s. l.], v. 88, n. 2, p. 441–448, 2012. Disponível em: http://dx.doi.org/10.1016/j.carbpol.2011.12.026.

HOSSEINI, S. S. et al. Optimization and characterization of pectin extracted from sour orange peel by ultrasound assisted method. **International Journal of Biological Macromolecules**, [s. l.], v. 125, p. 621–629, 2019. Disponível em: https://doi.org/10.1016/j.ijbiomac.2018.12.096.

HOSSEINI, S. S.; KHODAIYAN, F.; YARMAND, M. S. Optimization of microwave assisted extraction of pectin from sour orange peel and its physicochemical properties. **Carbohydrate Polymers**, [s. l.], v. 140, p. 59–65, 2016. Disponível em: http://www.sciencedirect.com/science/article/pii/S0144861715012291.

KADERIDES, K. et al. Microwave-assisted extraction of phenolics from pomegranate peels: Optimization, kinetics, and comparison with ultrasounds extraction. **Chemical Engineering and Processing - Process Intensification**, [s. l.], v. 137, p. 1–11, 2019. Disponível em: https://linkinghub.elsevier.com/retrieve/pii/S0255270118314363.

KOŠŤÁLOVÁ, Z.; AGUEDO, M.; HROMÁDKOVÁ, Z. Microwave-assisted extraction of pectin from unutilized pumpkin biomass. Chemical Engineering and Processing: **Process Intensification**, [s. l.], v. 102, p. 9–15, 2016.

KREMSNER, J. M.; STADLER, A. A Chemist’s Guide to Microwave Synthesis. 3. ed. Austria: Anton Paar GmbH, 2018.

LIEW, S. Q. et al. Comparisons of process intensifying methods in the extraction of pectin from pomelo peel. Chemical Engineering and Processing **- Process Intensification**, [s. l.], v. 143, p. 107586, 2019. Disponível em: https://www.sciencedirect.com/science/article/pii/S0255270119303514.

LIU, Y.; SHI, J.; LANGRISH, T. A. G. Water-based extraction of pectin from flavedo and albedo of orange peels. **Chemical Engineering Journal**, [s. l.], v. 120, n. 3, p. 203–209, 2006.

MARAN, J. P. et al. Optimization of microwave assisted extraction of pectin from orange peel. **Carbohydrate Polymers**, [s. l.], v. 97, n. 2, p. 703–709, 2013. Disponível em: http://www.sciencedirect.com/science/article/pii/S0144861713005274.

MARIĆ, M. et al. An overview of the traditional and innovative approaches for pectin extraction from plant food wastes and by-products: Ultrasound-, microwaves-, and enzyme-assisted extraction. **Trends in Food Science & Technology**, [s. l.], v. 76, p. 28–37, 2018. Disponível em: http://www.sciencedirect.com/science/article/pii/S0924224418300220.

MAY, C. D. Industrial pectins: Sources, production and applications. **Carbohydrate Polymers**, [s. l.], v. 12, n. 1, p. 79–99, 1990. Disponível em: https://www.sciencedirect.com/science/article/pii/0144861790901052.

MELTON, L. D.; SMITH, B. G. Determination of the Uronic Acid Content of Plant Cell Walls Using a Colorimetric Assay. **Current Protocols in Food Analytical Chemistry**, [s. l.], v. 00, n. 1, p. E3.3.1-E3.3.4, 2001. Disponível em: https://doi.org/10.1002/0471142913.fae0303s00.

MINJARES-FUENTES, R. et al. Ultrasound-assisted extraction of pectins from grape pomace using citric acid: A response surface methodology approach. **Carbohydrate Polymers**, [s. l.], v. 106, p. 179–189, 2014. Disponível em: https://www.sciencedirect.com/science/article/pii/S0144861714001349.

MORT, A. J.; QIU, F.; MANESS, N. O. Determination of the pattern of methyl esterification in pectin. Distribution of contiguous nonesterified residues. **Carbohydrate Research**, [s. l.], v. 247, p. 21–35, 1993. Disponível em: https://www.sciencedirect.com/science/article/pii/0008621593842382.

MUÑOZ-ALMAGRO, N. et al. Modification of citrus and apple pectin by power ultrasound: Effects of acid and enzymatic treatment. **Ultrasonics Sonochemistry**, [s. l.], v. 38, p. 807–819, 2017.

OLIVEIRA, C. F. de et al. Extraction of pectin from passion fruit peel assisted by ultrasound. **LWT - Food Science and Technology**, [s. l.], v. 71, p. 110–115, 2016. Disponível em: http://dx.doi.org/10.1016/j.lwt.2016.03.027.

OLIVEIRA, C. F. De et al. Extraction of pectin from passion fruit peel using moderate electric field and conventional heating extraction methods. **Innovative Food Science and Emerging Technologies**, [s. l.], v. 29, p. 201–208, 2015. Disponível em: http://dx.doi.org/10.1016/j.ifset.2015.02.005.

PATIENCE, N. A.; SCHIEPPATI, D.; BOFFITO, D. C. Continuous and Pulsed Ultrasound Pectin Extraction from Navel Orange Peels. **Ultrasonics Sonochemistry**, [s. l.], v. 73, p. 105480, 2021. Disponível em: https://doi.org/10.1016/j.ultsonch.2021.105480.

PEREIRA, P. H. F. et al. Pectin extraction from pomegranate peels with citric acid. **International Journal of Biological Macromolecules**, [s. l.], v. 88, p. 373–379, 2016. Disponível em: https://www.sciencedirect.com/science/article/pii/S0141813016303087.

PFALTZGRAFF, L. A. et al. Food waste biomass: A resource for high-value chemicals. **Green Chemistry**, [s. l.], v. 15, n. 2, p. 307–314, 2013.

RAHMANI, Z. et al. Optimization of microwave-assisted extraction and structural characterization of pectin from sweet lemon peel. **International Journal of Biological Macromolecules**, [s. l.], v. 147, p. 1107–1115, 2020. Disponível em: https://doi.org/10.1016/j.ijbiomac.2019.10.079.

RANGGANA, S. Handbook of analysis and quality control for fruit and vegetable products. [S. l.: s. n.], 1986. E-book. Disponível em: https://books.google.com/books?hl=ro&lr=&id=jQN8Kpj0UOMC&oi=fnd&pg=PR7&ots=fcYnTUpHCM&sig=q2qvOlI76IvU60kv_FqTegnYo7g.

RODSAMRAN, P.; SOTHORNVIT, R. Microwave heating extraction of pectin from lime peel: Characterization and properties compared with the conventional heating method. **Food Chemistry**, [s. l.], v. 278, n. November 2018, p. 364–372, 2019. Disponível em: https://doi.org/10.1016/j.foodchem.2018.11.067.

SANCHEZ-REINOSO, Z. et al. Microwave-assisted extraction of phenolic compounds from Sacha Inchi shell: Optimization, physicochemical properties and evaluation of their antioxidant activity. Chemical Engineering and Processing - **Process Intensification**, [s. l.], v. 153, p. 107922, 2020. Disponível em: https://www.sciencedirect.com/science/article/pii/S0255270120303792.

SATARI, B.; KARIMI, K. Citrus processing wastes: Environmental impacts, recent advances, and future perspectives in total valorization. **Resources, Conservation and Recycling**, [s. l.], v. 129, n. September 2017, p. 153–167, 2018. Disponível em: http://dx.doi.org/10.1016/j.resconrec.2017.10.032.

SOLANKI, K. P.; DESAI, M. A.; PARIKH, J. K. Microwave intensified extraction: A holistic approach for extraction of citronella oil and phenolic compounds. **Chemical Engineering and Processing - Process Intensification**, [s. l.], v. 146, p. 107694, 2019. Disponível em: https://www.sciencedirect.com/science/article/pii/S0255270119302661.

SU, D. L. et al. Efficient extraction and characterization of pectin from orange peel by a combined surfactant and microwave assisted process. **Food Chemistry**, [s. l.], v. 286, n. February, p. 1–7, 2019. Disponível em: https://doi.org/10.1016/j.foodchem.2019.01.200.

SUCHETA; MISRA, N. N.; YADAV, S. K. Extraction of pectin from black carrot pomace using intermittent microwave, ultrasound and conventional heating: Kinetics, characterization and process economics. **Food Hydrocolloids**, [s. l.], v. 102, p. 105592, 2020. Disponível em: http://www.sciencedirect.com/science/article/pii/S0268005X19323720.

USP NF 21. THE UNITED STATES PHARMACOPEIA – THE NATIONAL FORMULARY. In: , 2003, Rockville. United States Pharmacopeial Convention. Rockville: [s. n.], 2003. p. 1401–1402.

WAI, W. W.; ALKARKHI, A. F. M.; EASA, A. M. Effect of extraction conditions on yield and degree of esterification of durian rind pectin: An experimental design. **Food and Bioproducts Processing**, [s. l.], v. 88, n. 2–3, p. 209–214, 2010. Disponível em: http://dx.doi.org/10.1016/j.fbp.2010.01.010.

WICKER, L. et al. Pectin as a bioactive polysaccharide - Extracting tailored function from less. **Food Hydrocolloids**, [s. l.], v. 42, n. P2, p. 251–259, 2014. Disponível em: http://dx.doi.org/10.1016/j.foodhyd.2014.01.002.

WILLATS, W. G. T.; KNOX, J. P.; MIKKELSEN, J. D. Pectin: New insights into an old polymer are starting to gel. **Trends in Food Science and Technology**, [s. l.], v. 17, n. 3, p. 97–104, 2006.

XU, S. Y. et al. Ultrasonic-microwave assisted extraction, characterization and biological activity of pectin from jackfruit peel. **LWT - Food Science and Technology**, [s. l.], v. 90, n. September 2017, p. 577–582, 2018. Disponível em: https://doi.org/10.1016/j.lwt.2018.01.007.

CHAPTER 6

6. GRAPHENE OXIDE MEMBRANES FOR PECTIN PURIFICATION

ABSTRACT

Purification of pectin solution extracted from orange peels was carried out by using pristine and graphene oxide coated hollow fiber membranes. The produced kaolin hollow fibers presented a finger like region at the lumen side with pore sizes between 7.86 and 9.17 μm and a sponge like layer in the fiber outer layer with pore sizes between 1.14 and 2.16 μm. The water permeability of the pristine kaolin fiber was 8.46 ± 0.17 L $h^{-1} \cdot m^{-2} \cdot kPa^{-1}$ and the bending strength of the membrane was 103.58 ± 14.41 MPa, indicating that the kaolin fibers have suitable mechanical resistance for pressure driven filtrations. After graphene oxide (GO) deposition, the GO-coated membrane presented a GO layer with thickness of 143 nm. The pectin sample extracted from orange peels was predominantly constituted of galacturonic acid (68.69 ± 1.75%). The extracted pectin presented a degree of esterification lower than 50% and, thus, can be considered low-methoxylated pectin. Purification of this extract using the kaolin hollow fiber and the GO-coated membrane increases galacturonic acid values (75.91 ± 0.43% and 82.12 ± 0.47%) respectively. Thus, this study evidenced the potential application of crossflow filtration processes to the purification of pectin using pristine and GO-coated kaolin hollow fiber membranes. Both membranes, pristine and GO-coated kaolin hollow fiber membrane, showed be able to purify pectin (higher amount of galacturonic acid content).

Keywords: Pectin; Purification; Graphene oxide; Kaolin; Ceramic membranes.

6.1. INTRODUCTION

Pectins are complex polysaccharides that consist of a linear chain of α-1,4-linked D-galacturonic acid with neutral sugar side chains composed by arabinans, galactans and arabinogalactans (Marić et al., 2018). Due their thickening, emulsifying and gelling properties, pectins are used by the food industry for formulations of sauces, jellies and jams (Marić et al., 2018; Naqash et al., 2017). More recently, pectin has been related to some antibacterial activity and the literature suggests prospective uses of pectin as a healthy biomolecule (Ciriminna et al., 2020; Muhidinov et al., 2021). However, especially for medicinal purposes, suitable pectin extraction and purification methods should be proposed. Citrus peels and apple pomace are prime sources of pectin for commercial usage (Zhang et al., 2015). Waste orange peels represent

a promising low cost alternative for pectin extraction, in addition to the minimization of waste disposals (Wicker et al., 2014).

High temperatures (80–90 °C), acidified water pH values (2–3), long extraction times (1–5 h) and high solid-to-liquid ratios (1:30–1:50) are commonly employed for pectin extraction. Mineral or organic acids were used to break the plant cell wall fibers and release pectin chains. High temperatures are applied to accelerate molecular motion and to facilitate pectin dissolution in aqueous solution (Kang et al., 2015). After pectin extraction, the most commonly method used for purification is the precipitation with ethanol (Yapo, Robert, et al., 2007). Although alcohol precipitation is ready-to-operate, this method presents low selectivity in addition to the disadvantage of high alcohol consumption, especially in scale-up production (Kang et al., 2015; Yapo, Robert, et al., 2007). Also, valuable neutral sugars and pectin oligosaccharides are usually not precipitated by alcohol and are difficult to recover from alcohol solution (Muhidinov et al., 2021).

Membrane separation processes are an environmental-friendly alternative for pectin purification, since the membranes are able to effectively remove the contaminants and to obtain pectin samples with improved properties. Hoagland et al. (1993) showed that pectin solutions can be concentrated by the ultrafiltration process. Cho et al. (2003) applied the microfiltration process to concentrate and purify soluble citrus peel pectin. Yapo et al. (2007b) showed that membrane filtration enabled to obtain a pectin sample with more galacturonic acids than the alcohol precipitation. Xie et al. (2008) applied a zirconia ceramic membrane for pectin purification and observed that cake formation is a limiting factor to improve permeate fluxes. Qiu et al. (2009) applied ultrafiltration membranes of different cut-off molecular weights to purify pectin molecules from apple pectin solutions. Kang et al. (2015) showed that, compared to the alcohol precipitation process, the ultrafiltration process enabled to obtain a pectin solution with superior quality, mainly related to the degree of amidation. Muñoz-Almagro et al. (2020) showed that the ultrafiltration process was the best pectin purification method compared to alcohol precipitation and microfiltration. Muhidinov et al. (2021) demonstrated that the diaultrafiltration process is a suitable alternative to produce pectin at high purity at a pilot scale. Li et al. (2022) showed that at least 3 different pectin fractions, including neutral and acid polysaccharides, can be separated by a cellulose chromatographic column from crude pectin extract of citrus fruit. Actually, pectin is a macromolecule with average molecular weight of about 50,000–180,000 Da, which may form agglomerates. These characteristics contribute to fouling occurrences during membrane filtrations of pectin solutions. Moresi and Sebastiani

(2008) highlighted the use of ceramic membranes to improve the permeate flux of pectin solutions. Also, other non-conventional devices, such as pulsatile flow and external electric field, in addition to enzymatic hydrolysis, are reported in the literature to prevent fouling occurrences during membrane filtrations of pectin solutions (Muhidinov et al., 2021).

Ceramic membranes present remarkable stability at extreme conditions of temperature and pH and are also recommended to minimize fouling occurrences (Dashti & Asghari, 2015). Some alternative ceramic materials have been proposed in order to decrease the membrane cost (Bessa et al., 2019; Mestre et al., 2019). Magalhães et al. (2020) proposed the use of kaolin as the starting ceramic material to produce microfiltration hollow fiber membranes for water disinfection. Asymmetric ceramic membranes can be produced by the single step phase inversion method followed by sintering (Wei et al., 2008). These ceramic membranes usually present pore sizes greater than 0.2 μm (Terra et al., 2016). Bindes et al. (2020) proposed the addition of a polymeric layer on the ceramic hollow fiber surface to improve the membrane selectivity. Graphene oxide (GO) is a derivative of graphene and has been considered as a promising material to realize functional thin films due to its two-dimensional structure. GO-coated membranes have demonstrated great potential in liquid filtrations (Aba et al., 2015; Han et al., 2013; Hu & Mi, 2013). Wu et al. (2022) deposited a thin GO layer on a ceramic substrate and the composite GO membrane was able to retain dye molecules in the molecular weights range between 200 and 900 g mol^{-1}.

Herein, we report for the first time the application of ceramic GO-coated membranes for orange peel pectin concentration. The pristine ceramic hollow fiber membranes were produced using kaolin as the starting ceramic material in order to use a low-cost substrate. The proper conditions to deposit a uniform, stable and selective GO layer on the substrate were presented. Experimental flux decay data were adjusted to mathematical models to better understand fouling occurrences during pectin filtrations though pristine and GO-coated kaolin hollow fiber membranes.

6.2. MATERIAL AND METHODS

6.2.1. Material

Oranges (*Citrus sinensis*) were purchased at a local market in Uberlandia - Brazil and were washed and peeled. The peels were cut into small pieces and dried in an oven (Biomact, Brazil) with an air circulation at 50 °C until a constant weight. After drying, the peels were

milled and passed through a 40-mesh sieve to obtain powder samples. The orange peel powders were stored in dark bags and kept in a dry environment until use.

Hydrochloric acid (36.5%, Êxodo Científica, Brazil), ethanol (95%, Alphatec, Brazil), phenol red (Sigma-Aldrich), sodium chloride (99.0%, Dinâmica, Brazil), sodium hydroxide (98%, Dinâmica, Brazil), phenolphthalein (Isofar, Brazil), m-hydoxydiphenyl (85%, Sigma-Aldrich), sulfamic acid (99%, Sigma-Aldrich), sodium tetraborate (99.5%, Labsynth), D-(+)-Galacturonic acid (97%, Sigma-Aldrich), sulfuric acid (H_2SO_4, 98%, Dinâmica, Brazil), folin ciocalteu (2 N, Dinâmica, Brazil), gallic acid (99.5%, Vetec, Brazil), sodium carbonate (Dinâmica, Brazil) and sodium azide (99%, Vetec, Brazil) were used for physico-chemical analyses. Kaolin (Kalamazon Estudos Geológicos LTDA, Brazil), n-methyl-2-prirolidone (NMP, Vetec, Brazil), PEG-30 Dipolyhydroxy stearate (Arlacel^{TM} P135, Croda) and polyethersulfone (PES, Veradel 3000P, Solvay) were used for membrane production. Commercial graphite powder (Vonder, Brazil), sulfuric acid (H_2SO_4, 98%, Dinâmica, Brazil), sodium nitrate ($NaNO_3$, 85%, Dinamica, Brazil), potassium permanganate ($KMnO_4$, PA, Vetec, Brazil) and hydrogen peroxide (H_2O_2, 30 vol%, Vetec, Brazil) were used for graphene oxide synthesis. Dopamine hydrochloride (98%, Sigma-Aldrich), Tris buffer (99%, Dinâmica, Brazil), Ethylenediamine (EDA, 99% Sigma-Aldrich) were used to increase the deposition of graphene oxide on the ceramic membranes surface.

6.2.2. Production of hollow fiber ceramic membranes

The ceramic suspension was prepared by first dissolving 1 wt% of the additive (Arlacel™ P135 (PEG-30 Di polyhydroxy stearate), in 57 wt % of solvent (n-methyl-2-prirolidone (NMP)), followed by the addition of 36 wt% of the kaolin powder. This ceramic suspension was stirred in a ball mill for 48 h. Afterward, 6 wt% of the polymer (PES) were added to the suspension, which was stirred for another 48 h (Hubadillah et al., 2017).

Phase inversion/sintering technique was used to produce the hollow fibers by following the methodology described by Kingsbury and Li (2009). First, the ceramic suspension was degassed using a vacuum pump at 850 mmHg for approximately 2 h for air removal. Then, the ceramic suspension was extruded through a spinneret (outer diameter of 3 mm, inner diameter of 1.2 mm), falling into a water bath. An air gap distance of 5 cm was used. Flow rates of 15 mL min^{-1} for ceramic suspension and 25 mL min^{-1} for the internal coagulant were used and were controlled using two individual pumps (Harvard Apparatus, model XHF). The precursor

hollow fibers were left in the coagulating bath for 48 h to complete the phase inversion, and were then manually cut to the desired length. After straightened and dried at room temperature (approximately 25 °C), the fiber precursors were sintered in a furnace (Carbolite, model TZF 15) at the temperature of 1150 °C (Magalhães et al., 2020).

6.2.3. Synthesis of graphene oxide

Graphene oxide was prepared by oxidation and exfoliation of graphite powder by the method suggested by Hummers and Offeman (1958) with some modifications (Hummers & Offeman, 1958; Silva et al., 2020). Briefly, 140 mL of sulfuric acid were mixed with 6 g of commercial graphite powder. Then, 3 g of sodium nitrate were added under mechanical stirring (300 rpm) to complete the oxidative process. Afterward, potassium permanganate (18 g) was slowly added to the dispersion and the temperature was controlled below 20 °C using an ice bath. After 1 h at 20 °C of stirring, the mixture was removed from the ice bath and 250 mL of distilled water were slowly added to the dispersion. This step caused effervescence and temperature increase to approximately 95 °C. After 20 min under magnetic stirring, the dispersion temperature decreased to room temperature (approximately 25 °C) and 500 mL of cold distilled water (5°C) at were added. Finally, 50 mL of hydrogen peroxide were slowly added to the dispersion under stirring for more 30 min. The final solution was then allowed to settle for 12 h and, after that, the supernatant was removed and mixed with 1 L of hydrochloric acid. Twice additional steps of settling for 12 h followed by the addition of 1 L of distilled water were then repeated. After that, the dispersion presented a dark brown color. Subsequently, the dispersion was left in a bath-sonicator (Sonic Mill, 1790 W and 20 kHz) for 1 h for the chemical exfoliation process.

The synthetized GO powder was characterized by Attenuated Total Reflectance-Fourier-transform infrared spectroscopy (ATR-FTIR, Perkin Elmer Spectrum Two, Single Reflection ZnSe/L1600115) to confirm the presence of all functional groups. The FTIR spectrum was recorded at the transmittance mode and wavenumbers from 4000 to 400 cm^{-1}. The measuring resolution was 2 cm^{-1} and with 36 scans. Additional GO characterizations were already reported in by Ribeiro et al. (2022).

6.2.4. Deposition of graphene oxide on the ceramic membranes

To enhance the adhesion between GO layer and the hollow fiber membrane, A length of 15 cm extension of the kaolin hollow fiber was first immersed in the dopamine hydrochloride solution (0.01 mol L^{-1} buffered with Tris buffer solution with pH of 8.5) for 4 h to ensure self-polymerization of dopamine. The membrane was then taken out from the aqueous solution and drained off with deionized water to remove the loosely adhered dopamine. Then the dopamine coated membrane was used for vacuum filtration. One end of the fiber was sealed and the other end was kept open. Graphene oxide was deposited on the fiber outer surface by a vacuum assisted process, as suggested by Aba et al. (2015) with modifications. As suggest by Kong et al. (2020), a solution with aqueous graphene oxide (0.1 g L^{-1}) and EDA (ratio 200:1) was used for depositions. This concentration of GO solution was based on the literature (Aba et al., 2015) and on preliminary tests, since greater concentrations resulted on thick graphene oxide layers, which caused further peel off of the GO layer in the presence of water. The opened end of the ceramic fiber was connected to a vacuum line and fiber was then immersed in the graphene oxide/EDA dispersion for 5 s without vacuum. After that, the vacuum pump (Prismatec, Brazil) was turned on at 50 mmHg and the fiber was kept immersed in the graphene oxide dispersion under vacuum for 10 min. After this time, the GO-coated hollow fibers were removed from the graphene oxide/EDA dispersion and the vacuum was kept turned on for 1 min to ensure the full adherence of the GO to the fiber. The GO-coated hollow fibers were then dried overnight at 80 °C (Silva et al., 2020).

Morphologies of prepared membranes were analyzed by scanning electron microscopy (SEM, Carl Zeiss, model EVO MA10, Carl Zeiss). The samples were previously coated with gold using a sputtering equipment (LEICA Metallizer EM SCD 050) under vacuum for 120 s at 50 mA. The qualitative composition of the membrane samples was verified by energy dispersive spectroscopy analyses (EDS, Oxford, model 51 - ADD0048). The pore structure of the kaolin hollow fiber was investigated by mercury intrusion porosimetry (MIP, Autopore IV 9500, Micrometrics) at a pressure range between 1.41 and 225,221.51 kPa. Morphological characterizations of the hollow fiber membranes were verified in an atomic force microscope (AFM, Shimadzu, model SPM-9600). Water fluxes through the pristine and GO-coated membranes were measured at different transmembrane pressures and at room temperature (25 °C) in order to determine the water permeability of each membrane sample.

6.2.5. Membrane filtrations of pectin extract

Conventional pectin extraction was carried out by mixing the dried orange peel powder at a solid-to-liquid ratio of 1:30 (v/w) with HCl acidified water at pH=2, as suggested by (Xu et al., 2018). The solution was maintained under continuous stirring (240 rpm) for 180 min at 90 °C Oliveira et al. (2016) and Su et al. (2019). After extractions, the extract was centrifuged (Thermo Scientific, Megafuge 8) at 4000 rpm for 40 min and filtered through a Büchner funnel with a paper filter (Unifil, Brazil, 6 μm) to remove insoluble solids.

The produced pectin extract was filtered through pristine and GO-coated hollow fiber membranes. The hollow fibers with a filtration area of 1.01×10^{-3} m^2 were connected to a cross-flow filtration module. The pectin solution was fed from the membrane lumen side and the permeate was collected from the membrane shell side. The filtrations were conducted at a transmembrane pressure of 300 kPa and cross-flow velocity $1.33x10^{-2}$ m s^{-1}. For all filtrations, the membranes were previously compacted by deionized water filtration for at least 30 min. Filtrations of pectin solution were carried out at 50 °C until a concentration factor of 1.5. Permeate samples were collected for further analyses and experimental flux data were recorded according to the filtration time.

The differential equations of the mathematical model proposed by Field et al. (1995) (Equation 1) were used to adjust the experimental flux decay data according to filtration time. Equation 1 was computationally solved by the fourth order Runge-Kutta method. Values of coefficient of determination (adjusted R^2) were considered to analyze the adjustment of experimental data to the proposed equations for each fouling mechanism.

$$-\frac{dJ}{dt} = K_n \; A^{2-n} \; J^{3-n} \qquad (1)$$

where t is the filtration time (h), k is an empirical constant, J (L h^{-1} m^{-2}) is the permeate flux, J_s is the steady-state flux (L h^{-1} m^{-2}) and the parameter "n" represents each fouling occurrence (n = 0 for cake formation; n = 2 for complete pore blocking; n = 1 for partial pore blocking and n = 1.5 for internal pore blocking).

Pectin was precipitated by adding ethanol (95%, v/v) (1:1 v/v) to crude and concentrate aqueous extracts. After ethanol addition, the extract was kept at 4–6°C overnight to complete the pectin precipitation and after that, the pectin was separate by centrifugation (4000 rpm, 40 min). Then, the precipitated pectin was dried in an oven with air circulation at 50 °C to constant weight (Dranca et al., 2020; Oliveira et al., 2016). Pectin yield was calculated according to Equation 2.

$$\text{Pectin yield (\%)} = \frac{M_p}{M_{OPP}}\ 100 \quad (2)$$

where M_p is the weight of dried pectin (g) and M_{OPP} is the weight of dried orange peel powder.

6.2.6. Physico-chemical analyses of pectin extracts

The pectin samples were analyzed for galacturonic acid content (GA), degree of esterification (DE), methoxyl content (MC), total phenolic content (TPC), emulsifying activity, emulsion stability and total phenolic content (TPC). All physical-chemical analyses were done in triplicate and were statically analyzed according to the Tukey test at a significance level of 5%.

The galacturonic acid content (GA) was determined by the m-hydroxydiphenyl spectrophotometric method suggested by Melton and Smith (2001). Briefly, 20 mg of pectin were diluted in 100 mL of distilled water at 50°C. In sequence, 400 µL of the pectin solution were mixed with 40 µL of sulfamic acid 4 M. This solution was hydrolyzed with 2.4 mL of a solution of sulfuric acid containing sodium tetraborate 75 mM. The solution was heated in boiling water for 20 min and then cooled in an ice bath for 10 min. After cooling, 80 µL of m-hydroxydiphenyl 0.15% (w/v) in sodium hydroxide 0.5% (w/v) was added and the solution was mixed in a vortex. Absorbance values were read at 525 nm using a UV-Vis spectrophotometer (Shimadzu UV-1280). The galacturonic acid content was determined by comparison with a standard galacturonic acid curve (0 – 100 µg/mL).

Degree of esterification (DE) of pectin samples were determined according to the method described in the USP NF 21 (USP NF 21. The United States pharmacopeia – The national formulary, 2003). Briefly, 100 mg of the pectin sample was dissolved in 20 mL of deionized water and 2 mL of ethanol (95%). Then, 3 drops of phenolphthalein were added to the solution, that was titrated with a NaOH 0.1 M solution until the solution color. The volume of NaOH solution in this first titration was recorded as V_1. In sequence, 10 mL of the NaOH 0.1 M solution at was added to the previous mixture. The solution was stirred for 20 min for hydrolysis. Then, 10 mL of a HCl 0.1 M solution was added and the solution was stirred until the disappearance of the pink color. Afterward, the solution was titrated again with a NaOH 0.1 M solution. The second volume of NaOH solution in this titration was recorded as V_2. The degree of esterification (DE) was calculated according to Equation 3.

$$\text{DE}\ (\%) = \frac{V_2}{V_2+V_1}\ 100 \quad (3)$$

where DE is the degree of esterification and V_1 and V_2 are the volumes of NaOH 0.1 M solution in the first and second titrations, respectively.

Methoxyl content (MC) of pectin samples was measured according to Ranggana, (1986). Briefly, 500 mg of pectin was dissolved in 100 mL of distilled water under continuous stirring (300 rpm) for 1 h. Then, 1 g of NaCl was added in the solution, followed by the addition of 5 drops of phenol red indicator. The solution was then titrated using a NaOH 0.1 M solution until color changed to red. The final solution, was mixed with 25 mL of a NaOH 0.25 M solution under agitation. After 30 min, an equal volume (25 mL) of a HCl 0.25 M solution was added and the final solution was titrated with a NaOH 0.1 M solution. The used volume of NaOH solution in this titration was recorded as V_{NaOH}. Methoxyl content (MC) was calculated according to Equation 4.

$$\text{MC}\ (\%) = \frac{3.1\ V_{NaOH}\ N}{W} \quad (4)$$

where MC is the methoxyl content, W is the weight of the pectin sample (g), V_{NaOH} is the volume of the NaOH solution at 0.1 N during titration (mL) and N is the NaOH normality.

The total phenolic content (TPC) of pectin samples were determined according to the Folin-Ciocalteu method. Briefly, 2.5 mL of the Folin-Ciocalteu reagent (10% v/v) were added to 0.5 mL of the pectin aqueous solution (1% w/v). After 3 min, 2 mL of a sodium carbonate solution (7.5% w/v) was added to the previous solution. The prepared solution was then incubated at room temperature. After 1 h, the absorbance was measured (Shimadzu UV-1280) at 750 nm. Gallic acid was used as a standard for preparing the calibration curve (R^2=99.9%). Total phenolic content values were expressed as mg of gallic acid equivalents per g of pectin (mg_{GAE}/g_{pectin}).

Values of emulsifying activity and emulsion stability were measured according to the methodology described by Hosseini et al. (2016). In a graduated tube, the oil-in-water emulsion was prepared by adding 5 mL of sunflower oil (Caramuru Alimentos, Brazil) to 5 mL of pectin solution (0.5 %, w/w). Also, a sodium azide solution at 0.02 % (w/v) was added as a bactericide. The pre-emulsions were sonicated (Utronique Q9.5/40A, Brazil) for 5 min. Then, the emulsions were centrifuged at 4500 rpm for 5 min. The emulsifying activity value was calculated according to Equation 5.

$$\text{Emulsifying activity (\%)} = \frac{V_e}{V_T} 100 \quad (6)$$

where V_e is the volume of the formed emulsion and V_T is the total volume in the tube.

The emulsion was then stored for 30 days at 4 °C and the emulsion stability was calculated according to Equation 6.

$$\text{Emulsion stability (\%)} = \frac{V_R}{V_I} 100 \quad (6)$$

where V_R was the emulsion volume after storage and V_I was the initial emulsion volume.

Structural characteristics of pectin samples were evaluated by Attenuated Total Reflectance-Fourier-transform infrared spectroscopy (ATR-FTIR, Perkin Elmer Spectrum Two, Single Reflection ZnSe/L1600115) at the transmittance mode and wavenumbers from 4000 to 400 cm^{-1}. The measuring resolution was 2 cm^{-1} and 36 scans were recorded.

6.3. RESULTS AND DISCUSSION

6.3.1. Characteristics of the produced membranes

The FTIR spectra of synthetized GO sample (Figure 6.1) shows all expected oxygen moieties: a O-H stretching vibration band at 3340 cm^{-1}, a carboxyl C=O stretching band at 1762 cm^{-1}, O-H deformation vibration band at 1404 cm^{-1} and C-O stretching vibration at 1087 cm^{-1} and a C-H bond at a 840 cm^{-1} (Ribeiro et al., 2022; Wu et al., 2022). Additional GO characterizations were reported in a study of GO membrane for gas separations (Ribeiro et al., 2022). Briefly, the morphological structure of the synthetized GO is at the nanosheeted scale and the oxidation reaction achieved the desired conversion so that the GO samples presented significant structural defects.

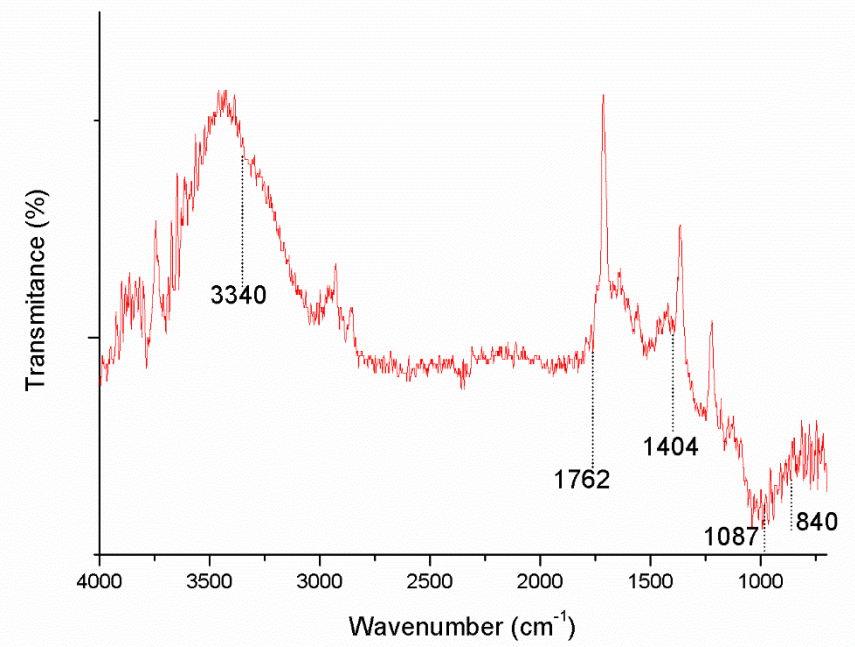

Figure 6.1 - FTIR spectra of synthesized graphene oxide.

As presented in the cross-section SEM image (Figure 6.2c), the kaolin hollow fiber presented an asymmetric pore size distribution, with a dense outer sponge like layer which accounts for approximately 60% of the fiber thickness. The air gap of 50 mm between the spinneret and the external coagulation bath promoted a quick densification of the ceramic suspension and the formation of a sponge like layer in the fiber outer surface. According to mercury intrusion analyses, the sponge like layer presents pores with sizes between 1.14 and 2.16 μm. During extrusion, the inner side of the hollow fiber was at direct contact with the coagulant fluid, which favored the formation of micro-voids, as evidenced in Figure 6.2c. The formation of micro-voids is caused by interfacial instabilities due to the density, viscosity and composition differences between the ceramic suspension and the internal coagulant fluid (Lee et al., 2015). According to mercury intrusion analyses, the pore sizes of the opened micro-

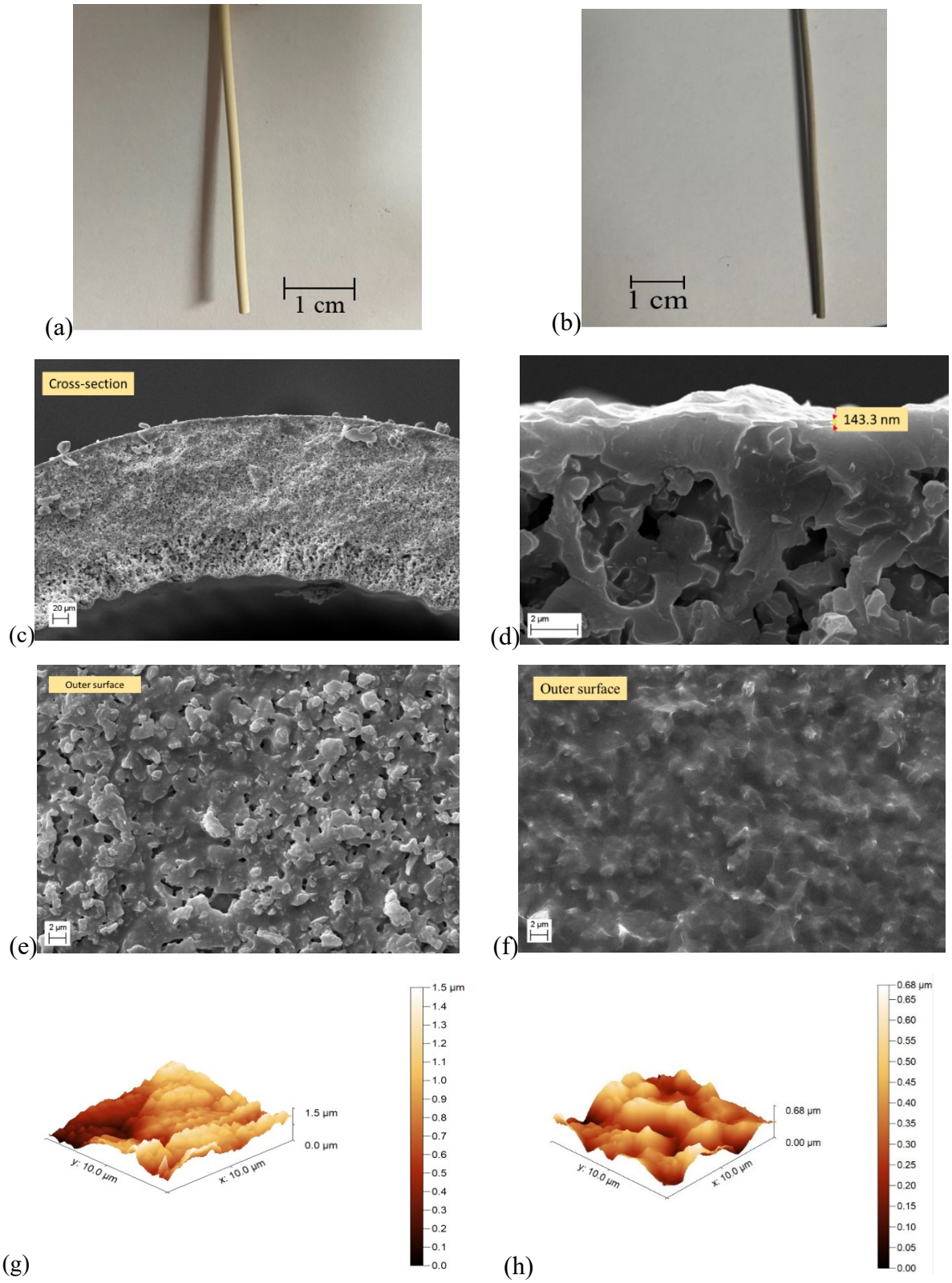

Figure 6.2 - Images of the (a) pristine kaolin hollow fiber, (b) GO-coated kaolin hollow fiber membrane, (c) SEM image of cross section of pristine membrane, (d) SEM image of cross section of GO-coated kaolin hollow fiber, (e) outer surface of pristine kaolin hollow fiber, (f) outer surface of GO-coated kaolin hollow fiber, (g) AFM image of the hollow fiber and (h) AFM image of the GO-coated kaolin hollow fiber.

channels were from 7.86 to 9.17 μm. The dense outer sponge-like layer is ideal to the deposition of a selective layer, while the micro-voids minimize the resistance to the permeation though the composite membrane.

After GO deposition, the color of the fiber surface changed from white to brown, as presented in Figure 6.2a and 6.2b. According to the cross-section SEM image (Figure 6.2d), the deposited GO layer presented a thickness of 143.3 nm. The literature presents different values of GO thickness depending on the applied substrate, deposition methods and the desired application. The GO thickness impacts on the membrane stability, selectivity and permeance. Aba et al. (2015) showed that a GO membrane of approximately 10 μm thick are easily peeled off from the PES substrate and, thus, applied GO membranes with thicknesses of 1.5 and 3.2 μm for solvent filtrations. Also, Yang et al. (2017) indicated that GO membranes with thickness above 100 nm presents low water permeance. Akbari et al. (2018) evaluated the permeation of several solvents through a composite GO/PVDF membrane with a thickness of approximately 100 ± 20 nm. Kong et al. (2020) deposited a GO layer of thickness between 50 and 70 nm on a PVDF substrate for pharmaceutical concentrations. Wu et al. (2022) deposited a GO layer of approximately 380 nm on the top of alumina hollow fibers and the composite GO membranes were applied for the retention of dye molecules.

The outer surface of the pristine hollow fiber (Figure 6.2e) presents several pinholes that contribute to the fiber porosity. After GO deposition (Figure 6.2f) the outer surface of the substrate was covered by a dense layer of GO with thickness of 1.43 nm. Kong et al. (2020) suggested the use of ethylenediamine as a crosslinker to improve the membrane stability of the d-spacing between the GO layers. Also, the substrate was covered by dopamine layer to enhance the adhesion between GO layer and the substrate (Kong et al., 2020). The surface average roughness of kaolin hollow fiber before GO deposition (Figure 6.2g) was 207.19 ± 9.45 nm and after GO deposition (Figure 6.2h) the roughness decrease to 187.82 ± 32.02 nm. Thus, the GO layer was able to reduce the roughness and reduce the pores on the membrane surface. Similar results on GO deposition was reported by (Ribeiro et al., 2022).

The bending strength of the pristine kaolin hollow fiber was 103.58 ± 14.41 MPa, indicating that the fibers have suitable mechanical resistance for pressure driven filtrations. The water permeability of the pristine and GO-coated kaolin hollow fiber membranes were 8.46 ± 0.17 and 0.52 ± 0.03 L $h^{-1} \cdot m^{-2} \cdot kPa^{-1}$, respectively. Thus, the water permeability of the pristine kaolin hollow fiber was reduced in 93% after GO deposition. This reduction was related to the

formation of a layer of graphene oxide on the surface of the membrane and the entering of some particles into the pores of the membrane causing the decrease in the fiber porosity. This result is similar to the water permeability showed by Huang et al. (2013) for a polymeric membrane with a GO layer of 3-5 nm (6.95 L $h^{-1}m^{-2}$ kPa^{-1}). However, the water permeability of the GO composite membrane is higher than some values reported in the literature. Aba et al. (2015) found results to water permeability of 0.01 L $h^{-1}m^{-2}$ kPa^{-1} for a ceramic hollow fiber with a GO layer of 1.5 μm thickness and 0.0058 L $h^{-1}m^{-2}$ kPa^{-1} for a ceramic hollow fiber with a GO layer of 3.2 μm thickness, probably due thickness of GO layer.

6.3.2. Flux behavior during pectin purification using kaolin hollow fiber membranes

Figure 6.3a and 6.3b presents the flux decays through pristine and GO-coated kaolin hollow fibers for filtrations of pectin solution respectively. Experimental flux values were also adjusted to the model proposed by Field et al. (1995) in order to investigate the fouling mechanisms.

The initial flux for pectin solution filtration using the pristine kaolin hollow fiber membrane was approximately 190 ± 12.60 L h^{-1} m^{-2}, which is almost 9 times lower than water flux through the membrane at the same transmembrane pressure. Experimental data showed a pronounced flux decay during the first 50 min of filtration and after 180 min of filtration, the concentration factor of 1.5 was achieved and the flux was stabilized at approximately 56 ± 2.93 L h^{-1} m^{-2}. For the filtration using GO-coated membrane, the initial flux was 78.80 ± 3.84 L h^{-1} m^{-2}, which is almost 2.5 times lower than water flux through the membrane at the same transmembrane pressure and almost 60% lower than the flux using the pristine kaolin hollow fiber membrane. The concentration factor of 1.5 was achieved with the GO-coated membrane after 270 min of operation and the steady state flux was 20.5 ± 3.7 L h^{-1} m^{-2}. Xie et al. (2008) applied a crossflow ultrafiltration module with a ZrO_2 ceramic membrane to concentrate a solution of pectin extracted from citrus peels and observed a permeate flux of approximately 25 L h^{-1} m^{-2} after 60 min of operation.

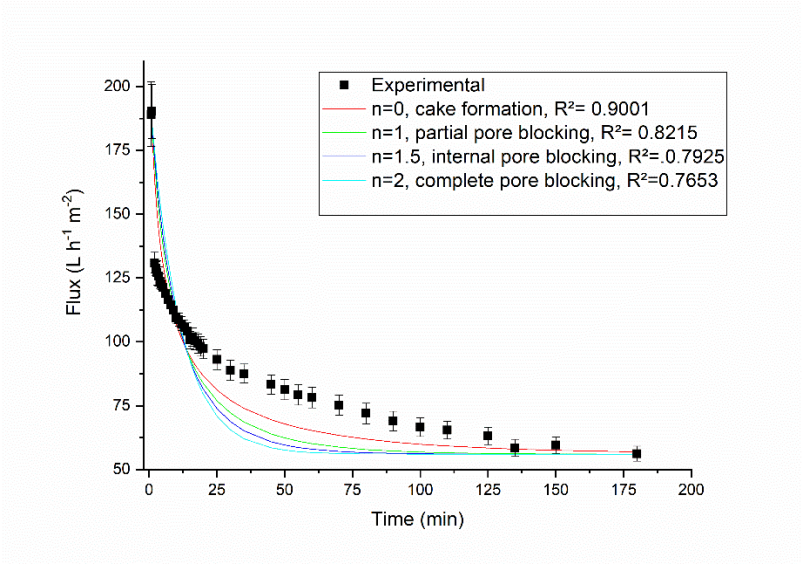

(a)

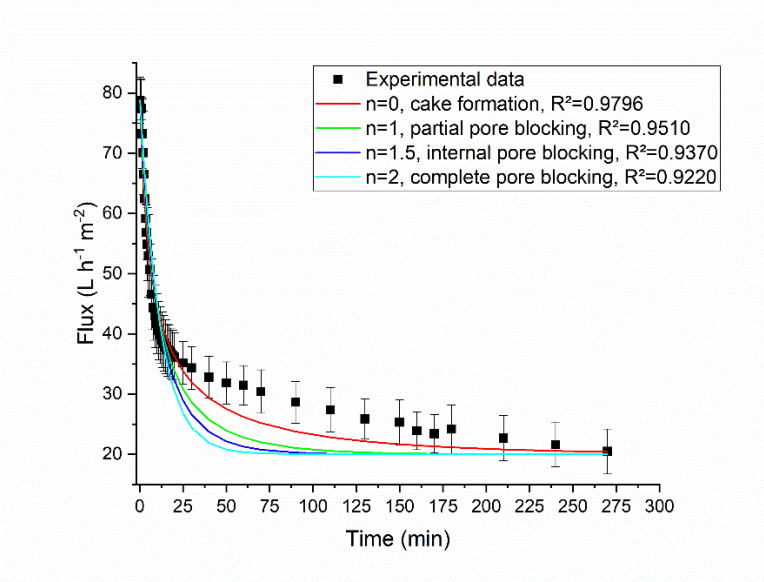

(b)

Figure 6.3- Permeate fluxes of pectin solutions through (a) pristine and (b) GO-coated kaolin hollow fibers.

The best adjustment between experimental and calculated data for both membranes was cake formation. Thus, cake formation was the main fouling occurrence during filtrations of pectin solution. This behavior was already expected, because pectin is a long macromolecule. The linear and branched structure of the pectin molecules allow, for deformation and mobility of the pectin chain under the action of a pressure, their insertion into the membrane pores and their passage through them. However, the increase of the concentration and the interactions

between the molecules in solution, which results gelling properties to pectin in the presence of sugars, favors to gel-like fouling of the pectin on the membrane surface (Gimenes et al., 2014).

6.3.3. Characterizations of pectin from orange peel powder before and after filtration

Both pectin extract and the concentrates from membrane filtrations were precipitated with ethanol for further characterizations. Table 6.1 shows the results for pectin yields, GA content, degree of esterification, methoxyl weight, total polyphenol content, emulsion activity and emulsion stability.

Table 6.1 - Parameters (galacturonic acid content, degree of esterification, methoxyl content and total of polyphenol content), emulsion activity and emulsion stability of orange peel pectin of feed stream and concentrated stream of both filtrations.

Characteristics		Feed stream	Concentrate stream	
			Kaolin hollow fiber	GO-coated kaolin hollow fiber
Pectin yield (%)		$21.98^{b} \pm 3.12$	$25.36^{a} \pm 2.51$	$33.80^{b} \pm 0.69$
Galacturonic acid content (%)		$68.69^{b} \pm 1.75$	$75.91^{a} \pm 0.43$	$82.12^{a} \pm 0.47$
Degree of esterification (%)		$39.09^{a} \pm 2.05$	$40.25^{a} \pm 1.09$	$42.32^{a} \pm 0.56$
Methoxyl content (%)		$6.74^{b} \pm 0.42$	$7.5^{a} \pm 0.75$	$7.91^{a} \pm 0.55$
Total polyphenol content (mg_{GAE}/g of pectin)		$24.13^{c} \pm 0.06$	$26.86^{b} \pm 0.53$	$30.58^{a} \pm 1.15$
Emulsion activity (%)		$53.00^{b} \pm 2.83$	$60.51^{a} \pm 0.70$	$68.50^{a} \pm 0.71$
Emulsion stability (%)	1 day	$97.20^{a} \pm 1.18$	$98.34^{a} \pm 0.02$	$98.54^{a} \pm 0.01$
	30 days	$88.73^{a} \pm 2.07$	$89.25^{a} \pm 1.29$	$92.72^{a} \pm 4.05$

*Mean values denoted by different letters at the same line are significantly different at $p \leq 0.05$.

After conventional extraction (90°C and 180 min) and alcohol precipitation, pectin yield was 21.98 ± 3.12 %. This value is higher than the results presented by Güzel and Akpınar (2019) for pectin extracted from orange peels (11.46%). The authors used a citric acid solution (pH 1)

to acidified water and a solid-to-liquid ratio of 1:10 and the extraction was carried out at 80 °C for 60 min. After filtration through the pristine hollow fiber, the pectin yield related to the concentrate stream increased to 25.36 ± 2.51%. However, pectin yield values of feed stream and concentrate stream with pristine hollow fiber are statistically equivalent since some pectin may have passed to the permeate stream. During filtration using the GO-coated kaolin hollow fiber, the impurities were isolated while all pectin was remained in retentate stream, thus the result of pectin yield increased to 33.80 ± 0.69 %. These results are in accordance with Muñoz-Almagro et al. (2020) that presented an increase of 8.8 ± 0.3% to 12.3 ± 0.4% when pectin from sunflower was purified using ultrafiltration followed by diafiltration to a concentration factor of 2.

Results showed that the pectin sample extracted from orange peel powder by conventional extraction were predominantly constituted of galacturonic acid (68.69 ± 1.75%). Hosseini et al. (2016) showed that the galacturonic acid content was 71.0 ± 0.8%. Galacturonic acid showed values higher than 65% for pectin extracted from sour orange peel under ultrasound irradiation. Pectin samples should not contain less than 65% of galacturonic acid to be consider pectin (Dranca et al., 2020). The galacturonic acid content for further increased by considering the retentate streams from filtrations with both pristine and GO-coated kaolin hollow fibers (Table 6.1). Muñoz-Almagro et al. (2020) also reported an increased in galacturonic acid content when the pectin extract from sunflower was purified using ultrafiltration followed by diafiltration (from 81.3% to 90.2%). Yapo et al. (2007) also presented increases on galacturonic acid content with ultrafiltration purification (from 55.9% to 72.1%).

Commercially pectins can be classified as high methoxy pectin (>50% esterified, degree of esterification greater than 50 %) and low methoxy pectin (<50% esterified, degree of esterification lower 50%) (Muñoz-Almagro et al., 2017). Pectins extracted from orange peel powder in this study can be considered low-methoxylated pectin with a degree of esterification lower than 50%. This kind of pectin forms gels in a wide pH range from 3.0 to 7.0 (Alba et al., 2015; X. Yang et al., 2018). Also, the pectin obtained with the conventional extraction was categorized as high low methoxyl pectin due to the methoxyl content lower than 7% (Rodsamran & Sothornvit, 2019).

Total polyphenol concentration of pectin extract (Table 6.1) is lower than the result showed for pectin extracted from sour orange peel by ultrasound assisted method (39.95 ± 3.13 mg GAE/g pectin) (Hosseini et al., 2019). According Sousa et al. (2016), temperatures greater

than 80°C can degrade the phenolic compounds and, thus, the applied extraction temperature of 90°C for 180 min may have contributes for the degradation of the phenolic compounds. The membrane purifications with pristine and GO-coated hollow fibers significantly increase the total polyphenol concentration. The purified pectins present higher emulsion activity than pectin without purification. Among the factors that affect the emulsifying properties of pectin, some factors like the degree of esterification, molecular weight or monosaccharide composition could be the most important. For example, for higher DE values, there is greater content of hydrophobic groups (methyl ester and acetyl groups) in the pectin structure providing the polysaccharide with the ability to be placed at the oil-water interphase (Verkempinck et al., 2018). Also, the pectin purified using both membranes (pristine and GO-coated) presented higher emulsion stability after 1 and 30 days of storage than the pectin without purification. Pectin purified samples presented similar emulsion stability to the values reported by Hosseini et al. (2019).

The infrared spectral patterns (Figure 6.4) when we compare pectin before and after purification using both membranes. These results suggested, that the pectin did not suffer important modifications after purification using pristine and GO-coated kaolin hollow fiber membrane. Pectin samples presented chemical shifts at 3387, 2924 and 1148 cm^{-1}, which were attributed to inter and intramolecular hydrogen stretching of O–H, C–H, CH_2 and CH_3, and C–O–C of glycoside compounds (Dranca et al., 2020; Hosseini et al., 2019). The band around 1734 cm^{-1} is related to the tension of esters of the carbonyl groups and increased its intensity when pectin was purified with both membranes, the signal at 1633cm^{-1}, belongs to the tension of the carboxylate ions. The bands at 1462, 1097 and 1020 cm^{-1} were attributed to –C-O-C glycoside ring bond as well as C-O stretching in COOH (Muñoz-Almagro et al., 2020). These results are similar to results presented by Muñoz-Almagro et al. (2020) for pectin extracted from sunflower and purified using ultrafiltration followed diafiltration.

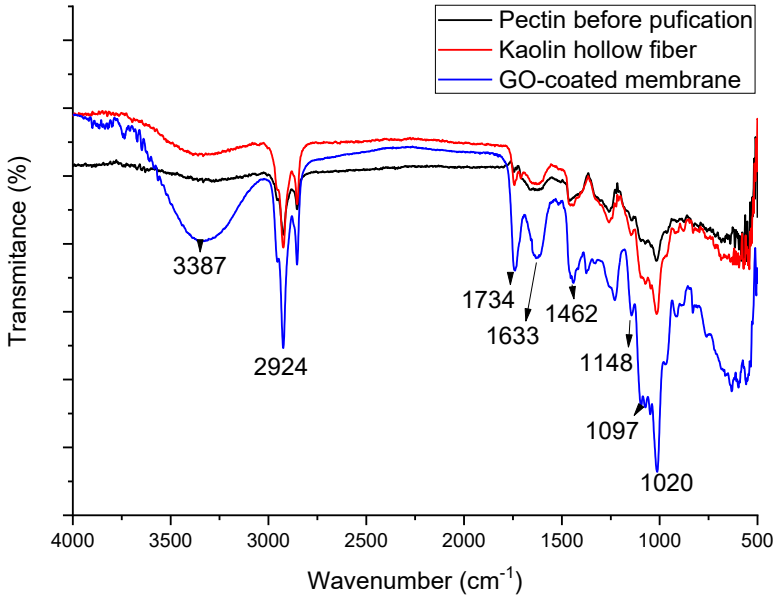

Figure 6.4 - FTIR spectra of pectin samples before and after purification using pristine and GO-coated kaolin hollow fiber membrane.

6.4. CONCLUSIONS

This study evidenced the potential application of crossflow filtration processes to the purification of pectin using pristine and GO-coated kaolin hollow fiber membranes. Ceramic hollow fiber membranes with asymmetric pore size distribution were produced using kaolin as starting material. Graphene oxide was successful deposited on the hollow fiber outer surface. However, some pinholes were visualized on the GO layer, which impacted on the permeate flux and on the membrane selectivity. Both membranes, pristine and GO-coated kaolin hollow fiber membranes, showed to be able for pectin purification (increased amount of galacturonic acid content). The steady-state permeate flux obtained for the pristine kaolin hollow fiber membrane was 56 ± 2.93 L h^{-1} m^{-2} and for the GO-coated membranes was 20.5 ± 3.7 L h-1 m-2 for filtrations at a temperature of 50 °C and at 400 kPa. From the analysis of the blocking models, we can conclude that the dominant restriction mechanisms for both membranes, notably is the cake filtration due the formation of gel layer on the membrane surface.

6.5. REFERENCES

ABA, N. F. D. et al. Graphene oxide membranes on ceramic hollow fibers – Microstructural stability and nanofiltration performance. **Journal of Membrane Science**, [s. l.], v. 484, p. 87–94, 2015. Disponível em: https://www.sciencedirect.com/science/article/pii/S0376738815001672.

AKBARI, A. et al. Solvent Transport Behavior of Shear Aligned Graphene Oxide Membranes and Implications in Organic Solvent Nanofiltration. **ACS Applied Materials & Interfaces**, [s. l.], v. 10, n. 2, p. 2067–2074, 2018. Disponível em: https://doi.org/10.1021/acsami.7b11777.

ALBA, K.; KASAPIS, S.; KONTOGIORGOS, V. Influence of pH on mechanical relaxations in high solids LM-pectin preparations. **Carbohydrate Polymers**, [s. l.], v. 127, p. 182–188, 2015. Disponível em: https://www.sciencedirect.com/science/article/pii/S0144861715002647.

BESSA, L. P. et al. Micro-structured and reinforced spinel hollow fiber membranes: Influence of sintering temperature and ceramic powder composition. **Ceramics International**, [s. l.], v. 45, n. 17, Part B, p. 23632–23642, 2019. Disponível em: https://www.sciencedirect.com/science/article/pii/S0272884219322722.

BINDES, M. M. M. et al. Asymmetric Al2O3 and PES/Al2O3 hollow fiber membranes for green tea extract clarification. **Journal of Food Engineering**, [s. l.], v. 277, p. 109889, 2020. Disponível em: http://www.sciencedirect.com/science/article/pii/S0260877419305321.

CHO, C. W.; LEE, D. Y.; KIM, C. W. Concentration and purification of soluble pectin from mandarin peels using crossflow microfiltration system. **Carbohydrate Polymers**, [s. l.], v. 54, n. 1, p. 21–26, 2003.

CIRIMINNA, R. et al. Pectin: A Long-Neglected Broad-Spectrum Antibacterial. **ChemMedChem**, [s. l.], v. 15, n. 23, p. 2228–2235, 2020. Disponível em: https://doi.org/10.1002/cmdc.202000518.

DASHTI, A.; ASGHARI, M. Recent Progresses in Ceramic Hollow-Fiber Membranes. **ChemBioEng Reviews**, [s. l.], v. 2, n. 1, p. 54–70, 2015. Disponível em: https://doi.org/10.1002/cben.201400014.

DRANCA, F.; VARGAS, M.; OROIAN, M. Physicochemical properties of pectin from Malus domestica ‘ F ă lticeni ’ apple pomace as a ff ected by non-conventional extraction techniques. **Food Hydrocolloids**, [s. l.], v. 100, n. May 2019, p. 105383, 2020. Disponível em: https://doi.org/10.1016/j.foodhyd.2019.105383.

FIELD, R. W. et al. Critical flux concept for microfiltration fouling. **Journal of Membrane Science**, [s. l.], v. 100, n. 3, p. 259–272, 1995. Disponível em: https://www.sciencedirect.com/science/article/pii/037673889400265Z.

GIMENES, M. L. et al. Pretreatment of Aqueous Pectin Solution by Cross-Flow Microfiltration: Study on Fouling Mechanism. **International Journal of Chemical Engineering and Application**s, [s. l.], v. 5, n. 3, p. 281–286, 2014.

GÜZEL, M.; AKPINAR, Ö. Valorisation of fruit by-products: Production characterization of pectins from fruit peels**. Food and Bioproducts Processing**, [s. l.], v. 115, p. 126–133, 2019. Disponível em: https://www.sciencedirect.com/science/article/pii/S0960308518308927.

HAN, Y.; XU, Z.; GAO, C. Ultrathin graphene nanofiltration membrane for water purification. **Advanced Functional Materials**, [s. l.], v. 23, n. 29, p. 3693–3700, 2013.

HOAGLAND, P. D.; KONJA, G.; FISHMAN, M. L. Component Analysis of Disaggregation of Pectin During Plate Module Ultrafiltration. **Journal of Food Science**, [s. l.], v. 58, n. 3, p. 680–687, 1993. Disponível em: https://doi.org/10.1111/j.1365-2621.1993.tb04355.x.

HOSSEINI, S. S. et al. Optimization and characterization of pectin extracted from sour orange peel by ultrasound assisted method. **International Journal of Biological Macromolecules**, [s. l.], v. 125, p. 621–629, 2019. Disponível em: https://doi.org/10.1016/j.ijbiomac.2018.12.096.

HOSSEINI, S. S.; KHODAIYAN, F.; YARMAND, M. S. Optimization of microwave assisted extraction of pectin from sour orange peel and its physicochemical properties. **Carbohydrate Polymers**, [s. l.], v. 140, p. 59–65, 2016. Disponível em: http://www.sciencedirect.com/science/article/pii/S0144861715012291.

HU, M.; MI, B. Enabling graphene oxide nanosheets as water separation membranes. **Environmental Science and Technology**, [s. l.], v. 47, n. 8, p. 3715–3723, 2013.

HUANG, H. et al. Ultrafast viscous water flow through nanostrand-channelled graphene oxide membranes. **Nature Communications**, [s. l.], 2013.

HUBADILLAH, S. K. et al. Superhydrophilic, low cost kaolin-based hollow fibre membranes for efficient oily-wastewater separation. **Materials Letters**, [s. l.], v. 191, p. 119–122, 2017. Disponível em: http://dx.doi.org/10.1016/j.matlet.2016.12.099.

HUMMERS, W. S.; OFFEMAN, R. E. Preparation of Graphitic Oxide. **Journal of the American Chemical Society**, [s. l.], v. 80, n. 6, p. 1339, 1958. Disponível em: https://doi.org/10.1021/ja01539a017.

KANG, J. et al. Characterization of natural low-methoxyl pectin from sunflower head extracted by sodium citrate and purified by ultrafiltration. **Food Chemistry**, [s. l.], v. 180, p. 98–105, 2015. Disponível em: https://www.sciencedirect.com/science/article/pii/S0308814615002071.

KINGSBURY, B. F. K.; LI, K. A morphological study of ceramic hollow fibre membranes. **Journal of Membrane Science**, [s. l.], v. 328, n. 1–2, p. 134–140, 2009.

KONG, F. et al. Rejection of pharmaceuticals by graphene oxide membranes: Role of crosslinker and rejection mechanism. **Journal of Membrane Science**, [s. l.], v. 612, p. 118338, 2020. Disponível em: https://www.sciencedirect.com/science/article/pii/S0376738820309169.

LEE, M. et al. Formation of micro-channels in ceramic membranes - Spatial structure, simulation, and potential use in water treatment**. Journal of Membrane Science**, [s. l.], v. 483, p. 1–14, 2015.

LI, G. et al. Physicochemical, structural and rheological properties of pectin isolated from citrus canning processing water. **International Journal of Biological Macromolecules**, [s. l.], v. 195, p. 12–21, 2022. Disponível em: https://www.sciencedirect.com/science/article/pii/S0141813021026088.

MAGALHÃES, F. de S. et al. Fabrication of kaolin hollow fibre membranes for bacteria removal. **Processing and Application of Ceramics**, [s. l.], v. 14, n. 4, p. 303–313, 2020.

MARIĆ, M. et al. An overview of the traditional and innovative approaches for pectin extraction from plant food wastes and by-products: Ultrasound-, microwaves-, and enzyme-assisted extraction. **Trends in Food Science & Technology**, [s. l.], v. 76, p. 28–37, 2018. Disponível em: http://www.sciencedirect.com/science/article/pii/S0924224418300220.

MELTON, L. D.; SMITH, B. G. Determination of the Uronic Acid Content of Plant Cell Walls Using a Colorimetric Assay. **Current Protocols in Food Analytical Chemistry**, [s. l.], v. 00, n. 1, p. E3.3.1-E3.3.4, 2001. Disponível em: https://doi.org/10.1002/0471142913.fae0303s00.

MESTRE, S. et al. Low-cost ceramic membranes: A research opportunity for industrial application. **Journal of the European Ceramic Society**, [s. l.], v. 39, n. 12, p. 3392–3407, 2019. Disponível em: https://www.sciencedirect.com/science/article/pii/S0955221919302134.

MORESI, M.; SEBASTIANI, I. Pectin recovery from model solutions using a laboratory-scale ceramic tubular UF membrane module. **Journal of Membrane Science**, [s. l.], v. 322, n. 2, p. 349–359, 2008. Disponível em: https://www.sciencedirect.com/science/article/pii/S0376738808005267.

MUHIDINOV, Z. K. et al. Structural characterization of pectin obtained by different purification methods**. International Journal of Biological Macromolecules**, [s. l.], v. 183, p. 2227–2237, 2021. Disponível em: https://www.sciencedirect.com/science/article/pii/S0141813021010692.

MUÑOZ-ALMAGRO, N. et al. Modification of citrus and apple pectin by power ultrasound: Effects of acid and enzymatic treatment. **Ultrasonics Sonochemistry**, [s. l.], v. 38, p. 807–819, 2017.

MUÑOZ-ALMAGRO, N. et al. Obtainment and characterisation of pectin from sunflower heads purified by membrane separation techniques. **Food Chemistry**, [s. l.], v. 318, p. 126476, 2020. Disponível em: https://www.sciencedirect.com/science/article/pii/S0308814620303381.

NAQASH, F. et al. Emerging concepts in the nutraceutical and functional properties of pectin—A Review. **Carbohydrate Polymers**, [s. l.], v. 168, p. 227–239, 2017. Disponível em: https://www.sciencedirect.com/science/article/pii/S0144861717303144.

OLIVEIRA, C. F. de et al. Extraction of pectin from passion fruit peel assisted by ultrasound. LWT - **Food Science and Technology**, [s. l.], v. 71, p. 110–115, 2016. Disponível em: http://dx.doi.org/10.1016/j.lwt.2016.03.027.

QIU, N. xue et al. Apple Pectin Behavior Separated by Ultrafiltration. **Agricultural Sciences in China**, [s. l.], v. 8, n. 10, p. 1193–1202, 2009. Disponível em: http://dx.doi.org/10.1016/S1671-2927(08)60329-6.

RANGGANA, S. Handbook of analysis and quality control for fruit and vegetable products. [S. l.: s. n.], 1986. E-book. Disponível em: https://books.google.com/books?hl=ro&lr=&id=jQN8Kpj0UOMC&oi=fnd&pg=PR7&ots=fcYnTUpHCM&sig=q2qvOlI76IvU60kv_FqTegnYo7g.

RIBEIRO, S. R. F. L. et al. Enhanced hydrogen permeance through graphene oxide membrane deposited on asymmetric spinel hollow fiber substrate. International **Journal of Hydrogen Energy**, [s. l.], 2022. Disponível em: https://www.sciencedirect.com/science/article/pii/S0360319922001094.

RODSAMRAN, P.; SOTHORNVIT, R. Microwave heating extraction of pectin from lime peel: Characterization and properties compared with the conventional heating method. **Food Chemistry**, [s. l.], v. 278, n. November 2018, p. 364–372, 2019. Disponível em: https://doi.org/10.1016/j.foodchem.2018.11.067.

SILVA, C. L. de M. et al. Improved hydrogen permeation through thin Pd/Al2O3 composite membranes with graphene oxide as intermediate layer. **International Journal of Hydrogen Energy**, [s. l.], v. 45, n. 43, p. 22990–23005, 2020. Disponível em: https://www.sciencedirect.com/science/article/pii/S0360319920322552.

SOUSA, L. dos S. et al. Purification of polyphenols from green tea leaves by ultrasound assisted ultrafiltration process. **Separation and Purification Technology**, [s. l.], v. 168, p. 188–198, 2016.

SU, D. L. et al. Efficient extraction and characterization of pectin from orange peel by a combined surfactant and microwave assisted process. **Food Chemistry**, [s. l.], v. 286, n. February, p. 1–7, 2019. Disponível em: https://doi.org/10.1016/j.foodchem.2019.01.200.

TERRA, N. et al. Characterisation of asymmetric alumina hollow fibres: Application for hydrogen permeation in composite membranes. **Brazilian Journal of Chemical Engineering**, [s. l.], v. 33, p. 567–576, 2016.

USP NF 21. THE UNITED STATES PHARMACOPEIA – THE NATIONAL FORMULARY. In: , 2003, Rockville. **United States Pharmacopeial Convention**. Rockville: [s. n.], 2003. p. 1401–1402.

VERKEMPINCK, S. H. E. et al. Emulsion stabilizing properties of citrus pectin and its interactions with conventional emulsifiers in oil-in-water emulsions. **Food Hydrocolloids**, [s. l.], v. 85, p. 144–157, 2018. Disponível em: https://www.sciencedirect.com/science/article/pii/S0268005X18305903.

WEI, C. C. et al. Ceramic asymmetric hollow fibre membranes—One step fabrication process. **Journal of Membrane Science**, [s. l.], v. 320, n. 1, p. 191–197, 2008. Disponível em: https://www.sciencedirect.com/science/article/pii/S0376738808003062.

WICKER, L. et al. Pectin as a bioactive polysaccharide - Extracting tailored function from less. **Food Hydrocolloids**, [s. l.], v. 42, n. P2, p. 251–259, 2014. Disponível em: http://dx.doi.org/10.1016/j.foodhyd.2014.01.002.

WU, T.; MOGHADAM, F.; LI, K. High-performance porous graphene oxide hollow fiber membranes with tailored pore sizes for water purification. **Journal of Membrane Science**, [s. l.], v. 645, p. 120216, 2022. Disponível em: https://www.sciencedirect.com/science/article/pii/S037673882101156X.

XIE, L.; LI, X.; GUO, Y. Ultrafiltration behaviors of pectin-containing solution extracted from citrus peel on a ZrO2 ceramic membrane pilot unit. **Korean Journal of Chemical Engineering**, [s. l.], v. 25, n. 1, p. 149–153, 2008.

XU, S. Y. et al. Ultrasonic-microwave assisted extraction, characterization and biological activity of pectin from jackfruit peel. **LWT - Food Science and Technology**, [s. l.], v. 90, n. September 2017, p. 577–582, 2018. Disponível em: https://doi.org/10.1016/j.lwt.2018.01.007.

YANG, X. et al. Low methoxyl pectin gelation under alkaline conditions and its rheological properties: Using NaOH as a pH regulator. **Food Hydrocolloids**, [s. l.], v. 79, p. 560–571, 2018. Disponível em: https://www.sciencedirect.com/science/article/pii/S0268005X17311773.

YANG, Q. et al. Ultrathin graphene-based membrane with precise molecular sieving and ultrafast solvent permeation. [s. l.], v. 16, n. December, 2017.

YAPO, B. M. et al. Effect of extraction conditions on the yield, purity and surface properties of sugar beet pulp pectin extracts. **Food Chemistry**, [s. l.], v. 100, n. 4, p. 1356–1364, 2007.

YAPO, B. M.; WATHELET, B.; PAQUOT, M. Comparison of alcohol precipitation and membrane filtration effects on sugar beet pulp pectin chemical features and surface properties. **Food Hydrocolloids**, [s. l.], v. 21, n. 2, p. 245–255, 2007.

ZHANG, L. et al. Effect of degradation methods on the structural properties of citrus pectin. **LWT - Food Science and Technology**, [s. l.], v. 61, n. 2, p. 630–637, 2015. Disponível em: https://www.sciencedirect.com/science/article/pii/S0023643814007051.

CHAPTER 7

7. GENERAL CONCLUSIONS

In this thesis, kaolin was successfully used as a low-cost ceramic material for producing hollow fiber membranes by the phase-inversion and sintering technique towards different applications: bacterial removal and pectin purification. Besides, the study of pectin extraction was successfully done using conventional and microwave assisted extraction. Kaolin hollow fiber membranes with different morphology, pore size distribution, bending strength and water permeability were produced depending on the applied extrusion rates, ceramic particle size and used solvent (NMP or DMSO) in the ceramic suspension. The milling of the as received kaolin powder from 8.7 to 5.1 μm is suggested to produce membranes with the hollow fiber geometry. Also, the hollow fiber geometry is guaranteed if using higher extrusion rates (15 and 25 mL min^{-1} instead of 7 and 15 mL min^{-1} for the ceramic suspension and internal coagulant, respectively). Kaolin hollow fibers should be sintered at 1150°C to guarantee the necessary mechanical resistance in pressurized filtration process, even that at lower transmembrane pressures (lower than 2 bar). The kaolin hollow fiber membranes were efficient in retaining the *Enterobacter* bacteria from the feed solution at 4.0×10^{8} CFU mL^{-1}. The bacterial retention values were of 99.8 and 99.9% for the hollow fibers sintered at 1200 and 1250 C°, respectively.

Silver nanoparticles were successful synthetized and impregnated in a kaolin hollow fiber. The membranes, with and without AgNPs, showed potential for bacteria removal from water with rejection values of almost 100%. However, the kaolin hollow fiber impregnated with silver nanoparticles presented higher values of log10 reduction for both *E. cloacae* and *E. coli* bacteria than the pristine kaolin hollow fiber membrane.

Within the evaluated range of temperature and time, mild extraction conditions are suggested to enhance the pectin yield extraction from orange peels under microwave heating. Temperature and time extractions up to 134°C and 7.5 min, respectively, improved pectin yield probably due to the enhancement in solvent diffusion through the orange peels. Also, the microwave-assisted process enabled to obtain a pectin extract with superior quality in terms of galacturonic acid content, degree of esterification, methoxyl content, total polyphenol content, emulsion activity and emulsion stability if compared to the conventional extraction.

Graphene oxide was successful deposited on the kaolin hollow fiber outer surface and aimed to purify pectin solution. Both membranes, pristine and GO-coated kaolin hollow fiber

membranes, showed to be able for pectin purification (increased amount of galacturonic acid content).

7.1. FUTURE WORK

Different tests, and experiments have been left for the future due to lack of. Future work concerns deeper analysis of new proposals to try different methods. Here, there are some ideas that can be developed to increase the thesis value. This thesis has been mainly focused on production of kaolin hollow fiber to bacteria removal and pectin purification, therefore, the following ideas could be tested:

- Evaluate the application of hollow fiber membranes impregnated with AgNPs in gran positive microorganisms' sterilization;
- Study the application of diamine monomers (i.e., ethylenediamine, butylenediamine and p-phenylenediamine) as crosslinker of GO nanosheets to prepare stable GO-coated membranes through vacuum;
- Apply the GO-coated kaolin hollow fiber membranes with crosslinkers in purification of pectin solution;
- Evaluate the filtration of pectin solution followed a diafiltration.